## Title

Analyzing and Predicting Effects of Approximated Space Exploration Atmospheres on Flame Spread Rate across Various Types of Electrical Wires and Dripping of Molten Insulation



## Author

Gagnon, Lauren

## Publication Date

2021

Peer reviewed|Thesis/dissertation

# Analyzing and Predicting Effects of Approximated Space Exploration Atmospheres on Flame Spread Rate across Various Types of Electrical Wires and Dripping of Molten Insulation

by

Lauren Bergin Gagnon

A dissertation submitted in partial satisfaction of the

requirements for the degree of

Doctor of Philosophy

in

Engineering - Mechanical Engineering

and the Designated Emphasis

in

Energy, Science, and Technology

in the

Graduate Division

of the

University of California, Berkeley

Committee in Charge:

Professor Carlos Fernandez-Pello, Co-Chair
Professor Van P. Carey, Co-Chair
Associate Professor Duncan Callaway
Professor Ömer Savaş

Summer 2021

Analyzing and Predicting Effects of Approximated Space Exploration Atmospheres on Flame Spread Rate across Various Types of Electrical Wires and Dripping of Molten Insulation

# Abstract

Analyzing and Predicting Effects of Approximated Space Exploration Atmospheres on Flame Spread Rate across Various Types of Electrical Wires and Dripping of Molten Insulation

by

Lauren Bergin Gagnon

Doctor of Philosophy in Engineering - Mechanical Engineering

Designated Emphasis in Energy, Science, and Technology

University of California, Berkeley

Professor Carlos Fernandez-Pello, Co-Chair

Professor Van P. Carey, Co-Chair

Electrical wires are potential sources of fire safety issues and fire ignition in electrical systems for structural, transportation, and space applications. Electrical wires acting as fire hazards become especially important when considering the current global-scale transition from fossil fuel energy technologies towards increasing use of electrically driven energy technologies, especially transportation and heating, fueled by renewable energy sources. Additionally, NASA's next generation of spacecrafts are planned to operate with reduced pressure and elevated oxygen concentrations within the cabins, causing an increased risk for fire hazards in such environments. In combination, these factors make fire safety in electrically powered systems increasingly important. Thus, it is of interest to understand the burning behavior of electrical wires in different environments, particularly in space exploration atmospheres. This understanding can be improved by obtaining results which provide further insight into the complex mechanisms present in flame spread along electrical wiring. Future analogous experiments planned to take place on the International Space Station (ISS) can also be compared to this work for increased understanding of this problem and improved predictive capabilities of models of wire burning in spacecraft.

In this work, simulated electrical wires were burned horizontally subject to various forced flow, ignition, ambient pressure, and oxygen concentration conditions. The wire samples consisted of cores 125 mm in length surrounded by insulation sheaths 100 mm in length, with these lengths being determined by the available experimental apparatus. The cores were made of either solid copper rods with diameters of 0.64 mm, 1.8 mm, or 2.5 mm, nichrome rods with diameters of 0.64 mm, or stainless-steel tubes with outer diameters of 2.4 mm. The surrounding insulation was composed of low-density polyethylene (LDPE) with an outer diameter of 3 mm for wires with core diameters of 1.8 mm or an outer diameter of 4 mm for all other wire sample types. The cores and insulation geometries were selected to match those of experiments to be conducted in the ISS.

Each of the environmental variables were tested in different combinations, but the overall ranges of each parameter were as follows. The flow varied from a no forced flow condition up to 0.3 m/s in either an opposed or concurrent configuration relative to the direction of flame spread. The ignition time was increased as a means to test the effect of excess heat in the wire. The ambient pressure ranged from 40 kPa to 100 kPa. Finally, the oxygen concentration was varied from 18%

to 27%. For each combination of conditions tested, the flame spread rate over the surfaces of these wires was measured to characterize their burning behavior. Dripping of molten insulation was also observed, and both the frequency and the total mass loss by dripping were tracked and reported as well.

Results showed that in experiments with variation in flow velocity, the flame spread rate was found to increase linearly with the flow velocity for concurrent flame spread but to decrease for opposed flame spread. The mass loss due to dripping was found to remain approximately constant for all airflow velocities. These trends were observed for all tested wire types, except for thick copper wire samples, which showed no spread in the opposed flow regime due to the core's heat sink effect on the flame in such an environment.

When varying the ignition condition, in a 100 kPa environment, it was found that for wire samples with either thin copper rod cores or other less conductive cores, the length of igniter exposure had very little effect on the flame spread rate. For more conductive wire samples, a slight effect was observed in which longer lengths of exposure to the igniter produced faster flame spread along the wires. For the highly conductive, thick copper wire samples, a much more exaggerated form of the same trend was observed. Repeating these igniter exposure experiments in a low-pressure environment caused delays in ignition and enhanced the effect of igniter exposure length on flame spread rate. As with the atmospheric-pressure environment, tests in a low-pressure, 60 kPa, environment showed samples with low-conductivity cores had negligible changes in flame spread rate as the length of igniter exposure increased. The more conductive wire samples showed similar trends to one another which included a drastic increase in flame spread rate with increased exposure to the igniter.

Results from experiments which kept the igniter exposure time constant and varied pressure showed that flame spread rate increases with pressure. Melted and burning insulation left behind by flame dripped with a frequency that increased with pressure, and the total mass of insulation dripped decreased with pressure. Coincidingly, as the mass of dripped insulation increased, the flame spread rate decreased. Comparison of present results with those from previous analogous studies with different wire samples show that the effect of environmental parameters on flame spread and insulation dripping depends strongly on core conductivity and core and insulation diameters.

Results from further experiments which varied both ambient pressure and oxygen concentration as well as forced flow velocity showed that the flame spread rate along these horizontal simulated electrical wires tends to increase with increasing oxygen concentration. It was also found that this increase in flame spread rate for increasing oxygen concentration occurred for all tested forced flow velocities and pressures. The limiting oxygen concentration for the tested wires was identified to be either slightly below or between the range of 18 to 21% oxygen concentration. Finally, the possible observation of elevated oxygen concentrations allowing for increased flame spread rates even at lower pressures compared to atmospheric, sea-level conditions was unable to be confirmed due to disruptions in testing due to the COVID-19 pandemic and a resulting incomplete dataset.

In additional to the experimental work completed for this analysis, further understanding of the flame spread over electrical wire problem was achieved through use of an artificial neural network (ANN). This ANN was trained to predict the flame spread rate along simulated electrical wires of different sizes and compositions while exposed to different ambient conditions. The wire core materials used to train the ANN included solid copper, nichrome, and iron and stainless-steel tubing. The wire insulation material used to train the ANN included high-density polyethylene

(HDPE), LDPE, and ethylene tetrafluoroethylene (ETFE). Finally, the conditions used to train the ANN included varying forced flows, ambient pressure, oxygen concentration, wire orientation, and gravitational strength.

To facilitate the training of the ANN which allowed it to make flame spread rate predictions, a comprehensive data base of 1200 data points was created by incorporating flame spread rate results from both the data presented in this work as well external experiments from other sources. After this training, predictions from the ANN show that it is possible to merge together various data sets, including results from horizontal, inclined, vertical, and microgravity experiments, and obtain unified results. While these initial results are very encouraging with an overall average error rate of 14%, they also show that future improvements to the ANN could still be made to increase prediction accuracy.

ANN predictions in the form of parametric trends were also compared with experimental flame spread rate results both from the present work and from the literature. These predictions alongside experimental results confirmed that the effect of environmental parameters on flame spread rate depends strongly on core conductivity, insulation diameters, and insulation dripping. Consequently, care should be taken in extending results obtained from specific wire tests to other wires without justification, especially if there was variation in gravitational strength across the experiments.

To my family and friends who have supported me throughout this journey,

Thank you for all your encouragement over the years. I can't believe I am finally at the end of the student era of my life. I wouldn't be here without my parents, especially my mom, believing from the very beginning that I was capable of so much more than I could have ever imagined. I appreciate everyone for never losing faith in my abilities even when I wasn't always so sure. Thank you all for providing me with shoulders to lean on, bright smiles, and open arms in the good times and the bad. I am truly grateful for your presence in my life.

Love,
Lauren

# Contents

# List of Figures

# List of Tables

# List of Symbols

| | |
|---|---|
| $A$ | Cross-sectional area (subscripts of i and c appear, indicating insulation and core, respectively) |
| $a$ | ANN node outputs (subscripts *i* and *j*, appear, indicating node position) |
| $b$ | ANN biases (subscripts *i* and *j* appear, indicating node location) |
| $c_{\mathrm{p}}$ | Specific heat (subscripts of i and c appear, indicating insulation and core, respectively) |
| $d_{\mathrm{c}}$ | Wire core diameter |
| $g$ | Gravitational strength vector component (subscripts *x* and *y* appear, indicating direction) |
| $\vec{g}$ | Gravitational strength vector |
| $h$ | Convection coefficient |
| $k$ | Thermal conductivity (subscripts of i and c appear, indicating insulation and core, respectively) |
| $L$ | Length of wire insulation sheath |
| $l$ | Heated length (subscripts of f, c, m, and h appear, indicating flame, core, melted insulation, and maximum heated length, respectively) |
| $Nu_{\mathrm{L}}$ | Length dependent Nusselt number |
| $P$ | Ambient pressure (subscript of $O_2$ appears, indicating partial pressure of oxygen) |
| $\dot{Q}_{\mathrm{f}\rightarrow\mathrm{i}}$ | Heat conduction from the flame to the insulation |
| $\dot{Q}_{\mathrm{c}\rightarrow\mathrm{i}}$ | Heat conduction from the core to the insulation |
| $\dot{q}"$ | Heat flux (subscripts of surf, conv, rad, ext, f, c, m, and s,r, sometimes written as rerad, appear, indicating fuel surface, convection, radiation, external heat, flame, core, melted insulation, and surface re-radiation, respectively) |
| $r$ | Wire sample radius |
| $T$ | Temperature (subscripts of flame, surf, py and ∞ appear indicating flame, surface, pyrolysis, and ambient, respectively) |

| | |
|---|---|
| $t_{\mathrm{ig}}$ | Ignition time of fuel |
| $v$ | Flow velocity vector component (subscripts *x*, *y*, and *z* appear, indicating direction) |
| $\vec{v}$ | Flow velocity vector, sometimes written as $V_{\mathrm{air}}$ |
| $v_{\mathrm{f}}$ | Flame spread rate, sometimes written as $V_{\mathrm{f}}$ or $V_{\mathrm{flame}}$ |
| $w$ | ANN weights (subscripts *i* and *j* appear, indicating node location; subscript *k* appears, indicating the number weights) |
| $x$ | ANN node inputs (subscripts *i* and *j* appear, indicating node location; subscript *k* appears, indicating the number inputs) |
| $z$ | ANN intermediate calculation (subscripts *i* and *j* appear, indicating node location) |
| $\delta_{\mathrm{i}}$ | Insulation thickness |
| $\nu_{\mathrm{air}}$ | Kinematic viscosity of air |
| $\rho$ | Density (subscripts of i and c appear, indicating insulation and core, respectively) |
| $\sigma$ | ANN activation function, defined as tanh for the current study |
| $\tau$ | Insulation thickness |
| $\%O_2$ | Percent oxygen concentration by volume |

## Acknowledgements

My deepest gratitude to my advisors, lab mates, and peers who helped guide me through the Mechanical Engineering PhD program. Both Professor Van P. Carey and Professor Carlos Fernandez-Pello provided me with their complete support overs the years as members of their labs, and I would not be here without them. I will never forget my time working with both former and current EMT lab mates Dre, Zach, Emma, Paige, Sam, Alanna, Ursan, and Claire and former and current CFP lab mates Mari, James, Charles, Christina, Luca, Franz, and Andy. I had such an amazing time working with you all, and you taught me so much over the years. In the CFP lab, both my past lab mates Mari Thomsen and James Urban provided me with such genuine mentorship, and I wouldn't have succeeded without their help. Thank you as well to all the members of the Berkeley Fire Research Lab who I also worked very closely with and came to know over the last year. I also have the utmost respect for fellow former resident of Hesse Hall, Eric Ibarra, who was a great tutor and friend since my very first heat transfer class at Berkeley. Additionally, thank you to NASA, who supported this work with Grant 80NSSC19K0331. Thank you also to Maria Thomsen, who provided advice with the experiments and the video post-processing script, and Francisco Martin, who helped with the construction of Figure 5.3 and Figure 5.4. Finally, much gratitude to all of the undergraduate researchers who worked with me during my PhD including Aram Cariaga, Christina Liveretou, Benson Peng, Tony Wu, Nicholas Te, Migueljose Baeza, and Hammad Ali.

# Chapter 1. Introduction

## 1.1 Background

For NASA, it is desired to improve the designs of their Space Exploration Vehicles (SEVs) to address several issues. These issues include decompression sickness that is experienced by astronauts during extravehicular activities, such as spacewalks, which are conducted in low-pressure space suits, the long preparation time for these extravehicular activities, and high structural demands on the craft itself [1]. One solution that will improve all these problems is to decrease the pressure within the cabin environments, or Space Exploration Atmospheres (SEAs). Therefore, NASA's next generation of SEVs, such as those pictured in Figure 1.1 and Figure 1.2, are planned to operate under reduced pressure [2, 3].

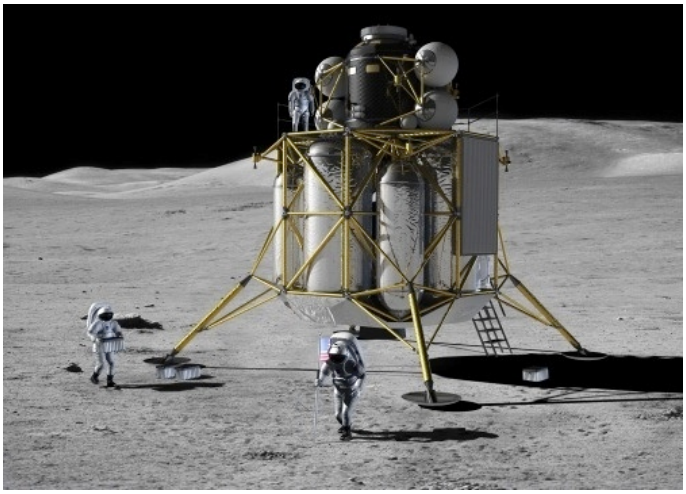

Figure 1.1 Artist's rendition of the Altair Lunar Lander on the Moon [4].

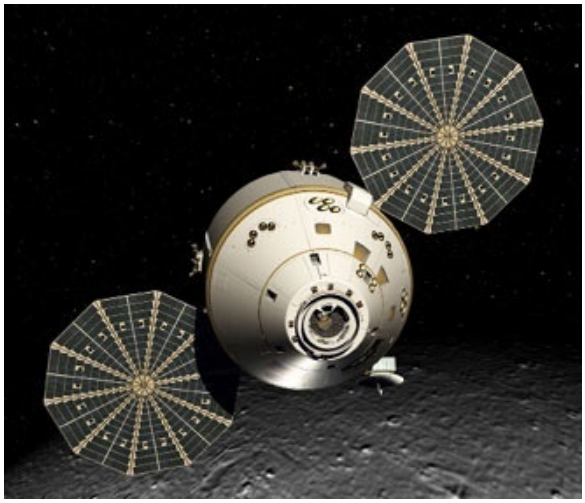

Figure 1.2 Artist's rendition of the Orion Crew Exploration Vehicle in lunar orbit [5].

## 1.2 Motivation

While there are many benefits to reducing the pressure within SEV cabins, there are also drawbacks. As the pressure is decreased in the cabin, the amount of oxygen in the cabin will decrease as well, similar to how the air thins as elevation increases, corresponding to a decrease in pressure, here on Earth. If the amount of oxygen in the air is decreased to too great a degree, this can lead to hypoxia in the astronauts. Hypoxia is a serious condition where not enough oxygen is available to the cells and tissues in the body. To counteract this effect, the percent of oxygen in the SEA must be increased. Therefore, it is desirable to use a combination of ambient pressure and oxygen concentration which results in a partial pressure of oxygen equal to that of a normal atmospheric environment at sea level, as calculated in Equation 1.

$$P_{O_2} = \%O_2 \cdot P = 21 \text{ kPa} \quad (1$$

**Error! Bookmark not defined.**)

This constant partial pressure of oxygen, also known as the normoxic condition, is illustrated visually in Figure 1.3. Following this constant partial pressure along the normoxic condition will keep the oxygen supply at a comfortable breathing level for astronauts.

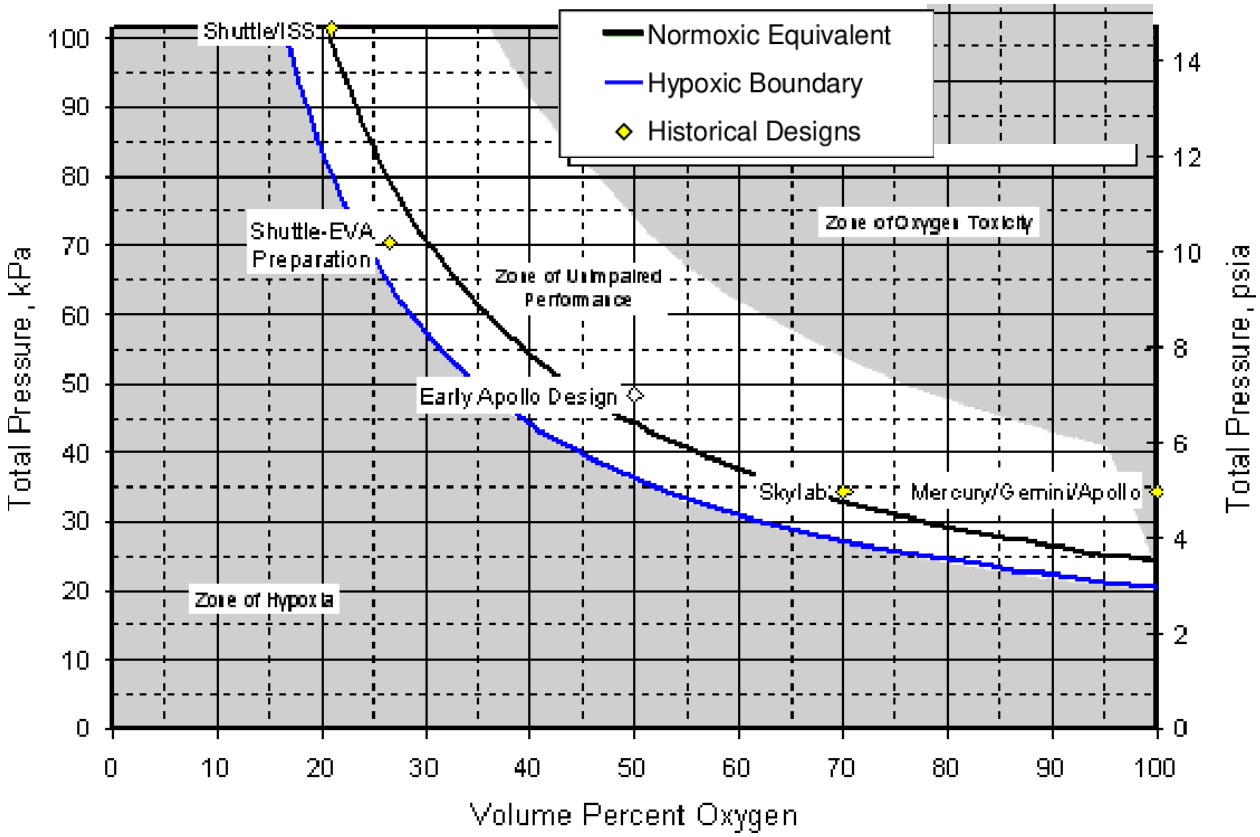


Figure 1.3 Definition of normoxic equivalent, hypoxic boundary, zone of oxygen toxicity, zone of hypoxia, and zone of unimpacted performance alongside historic designs for atmospheric conditions of spacecrafts [3].

Unfortunately, there are increased flammability risks associated with increasing the oxygen concentration percentage in the SEA, as this can cause materials to ignite more readily and burn hotter. In addition, other complexities exist for this problem when accounting for all the variables that are present within the SEA. Considering these increased flammability risks and the complexities present, the Japan Aerospace Exploration Agency (JAXA) in cooperation with

NASA, ESA; Centre national d'e´tudes spatiales, and university researchers from Japan, the United States, and Europe created a joint fire safety project, Flammability Limits At Reduced-g Experiments (FLARE) to research this problem [6, 7]. The FLARE logo is shown in Figure 1.4.


Figure 1.4 NASA and JAXA's joint Flammability Limits at Reduced-g Experiments project logo.

The goal of FLARE is to estimate material flammability characteristics in SEAs from data obtained on the ground [6, 7]. In other words, it is desired to be able to test material flammability here on Earth under conditions that will produce results most similar to those that would occur in a spacecraft cabin in microgravity. As mentioned, this research is to be facilitated by comparison of results to microgravity experiments to be conducted in the Kibo laboratory module of the ISS [6, 7]. The crafts shown in Figure 1.1 and Figure 1.2 are designed to operate within the "Zone of Unimpacted Performance" shown in Figure 1.3 to balance the benefits obtained from the lower pressure with the flammability risks associated with an increased oxygen concentration. These operating conditions consists of cabin pressures ranging from 55 kPa to 103 kPa and oxygen concentrations ranging from 30 to 34% [1], thus determining the range of conditions of interest for FLARE.

## 1.3 Complexity of Flames in Space Exploration Atmospheres

Aside from the complexities added to the problem by reducing ambient pressure and increasing oxygen concentration, there are also several other variables to consider that are present within SEAs that are not present on Earth. Thus, it becomes harder to replicate an SEA environment on Earth and produce similar result to those expected to be found in such an environment.

The first, most obvious, variable that is present in an SEA but not on Earth is microgravity. Considering this variable from a fire safety point of view, it is important to realize that flames behave much differently in microgravity environments than in environments with the gravitational strength experienced on Earth. Figure 1.5 displays this difference in flame behavior. As seen in the figure, the flame exposed to 1g gravitational strength takes on a much sharper shape than the flame exposed to microgravity. This flame elongation occurs in 1g environments because the heat from the flame transfers to the air around it, producing density gradients within the air which then causes the hotter air to rise and induce buoyant flows. Because these buoyancy-induced flows do not form in microgravity, the rounder flame shape from Figure 1.5 is observed.

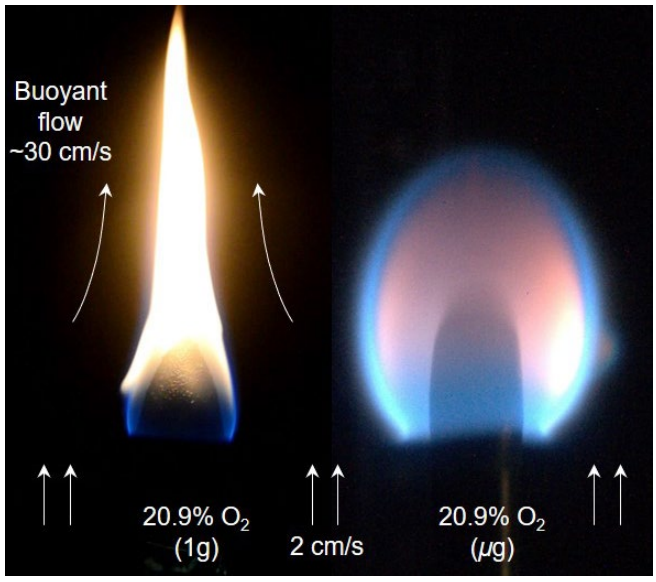

Figure 1.5 Difference in flame behavior in 1g (left) versus in microgravity (right) [9].

The absence of a stronger gravitational force in an SEA makes it difficult to replicate experiments on Earth for several reasons. The first is that the flame behaves differently because of these buoyancy-induced flows experienced on Earth. The second reason is because another variable in these SEAs are low HVAC flows, which are typically on the order of 6 – 20 cm/s, to provide air circulation [8]. As noted in Figure 1.5, the magnitude of the buoyancy-induced flows is on the order of 30 to 50 cm/s [9], which is greater than the HVAC flows present in SEAs. Therefore, it becomes difficult to see the effect of these HVAC flows on flames exposed to 1g gravitational strength as opposed to flames exposed to microgravity.

One way the work presented here will attempt to deal with these issues is to focus on flames burning on fuels that are oriented horizontally, thus allowing the flame to spread perpendicular to the buoyant flows, as shown in Figure 1.6. While this solution does not fully address the buoyant flow issue, it does somewhat isolate the effects of buoyant flows versus forced flows on the flame spread rate. However, also seen in Figure 1.6 is the leaning effect that this horizontal forced flow has on the flame, which can affect the flame spread rate, as discussed in subsequent chapters.

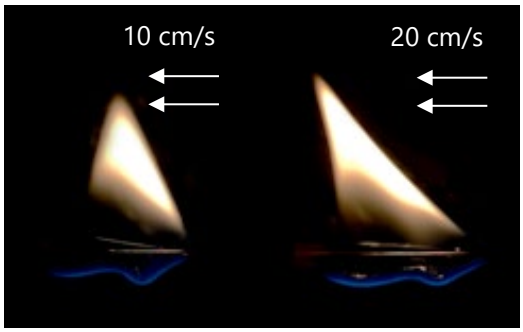

Figure 1.6 Example of horizontal forced flow effect on a flame.

Another way to counteract the effect of these buoyancy-induced flows is to reduce the ambient pressure surrounding the flame. Such a pressure reduction in turn reduces the buoyancy effect and thus diminishes the strength of the buoyancy-induced flows, as seen in Figure 1.7. As has been previously found [10, 11, 12], reducing the pressure to achieve lower buoyancy-induced flows can be a successful way to begin mimicking a microgravity environment. Using reduced pressures is

especially advantageous to the FLARE project as well because lower ambient pressure is one of the main components needed to replicate the SEAs of interest.

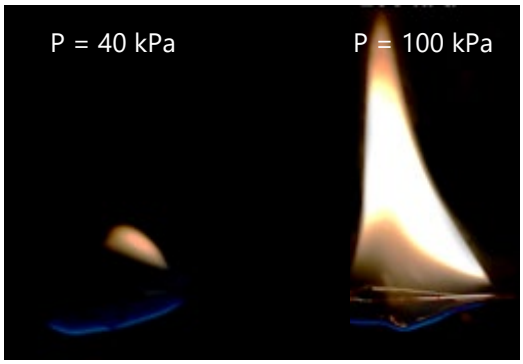


Figure 1.7 Example of reduced pressure effect on buoyancy induced flows produced by a flame.

# 1.4 Material of Interest

Within the FLARE project, there are many different materials being explored by the collaborators. The focus of the research presented here is on the burning behavior of electrical wires. Electrical wires were selected as a material of interest because they are potential sources of fire ignition and spread in spacecrafts, aircrafts, vehicles, and structures [13, 14, 15, 16], which can have disastrous consequences. As discussed previously, this problem becomes highly complex when considering the presence of microgravity and low velocity HVAC flows in addition to the reduced pressure and increased oxygen concentration conditions planned for the cabin environments of NASA's next generation of spacecrafts [2]. This together with the possibility of molten insulation dripping in 1g gravity, since there would be no insulation dripping in microgravity, makes the characteristics of wire burning on Earth or a spacecraft very different. Thus, there is a need for further study on the effect of such environments on electrical wire flammability.

Additionally, there is currently a global-scale transition from fossil fuel energy technologies towards increasing use of electrically driven energy technologies, especially transportation and heating, fueled by renewable energy sources [17]. Figure 1.8 [17] shows the required increase in electricity consumption for a renewable energy roadmap (REmap) from the present through 2050 that seeks to keep carbon emissions low enough such that the increase in global temperature is limited to 2°C. This REmap map shows that there should be a doubling of electricity-produced energy consumption by 2050. Figure 1.9 [17] breaks this requirement down even further, showing that, for the REmap case, electricity-produced energy should account for one third to one half of consumption in industry and buildings and approximately one third in transportation by the year 2050.

Such an expansion in the demand for electricity is making fire safety in electrically powered systems increasingly important. Electrically initiated fires account for nearly 7% of home structure fires [14], the cause of which can be poor contact, short circuiting, external heating, or ground faults [16]. Consequently, it is of even more interest to study the flammability of electrical wires.

While the main focus of this work is the potential for fires in spacecrafts, considering the potential increase in demand for electricity on Earth, it is important to understand the burning behavior of electrical wires in their many different operating environments. Therefore, this work

not only considers varying pressure, oxygen concentration, and gravitational strength, but also varying flow speed, wire orientation, and wire composition, which are import parameters in nearly every different operating environment, including the aforementioned spacecraft, vehicle, and structural applications.

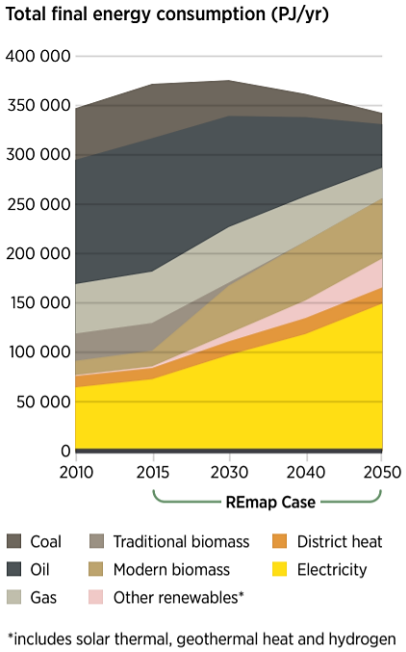


Figure 1.8 Figure 1. © IRENA 2018 The rising importance of electricity derived from renewable energy - share of electricity in total final energy consumption (PJ/yr) [17].

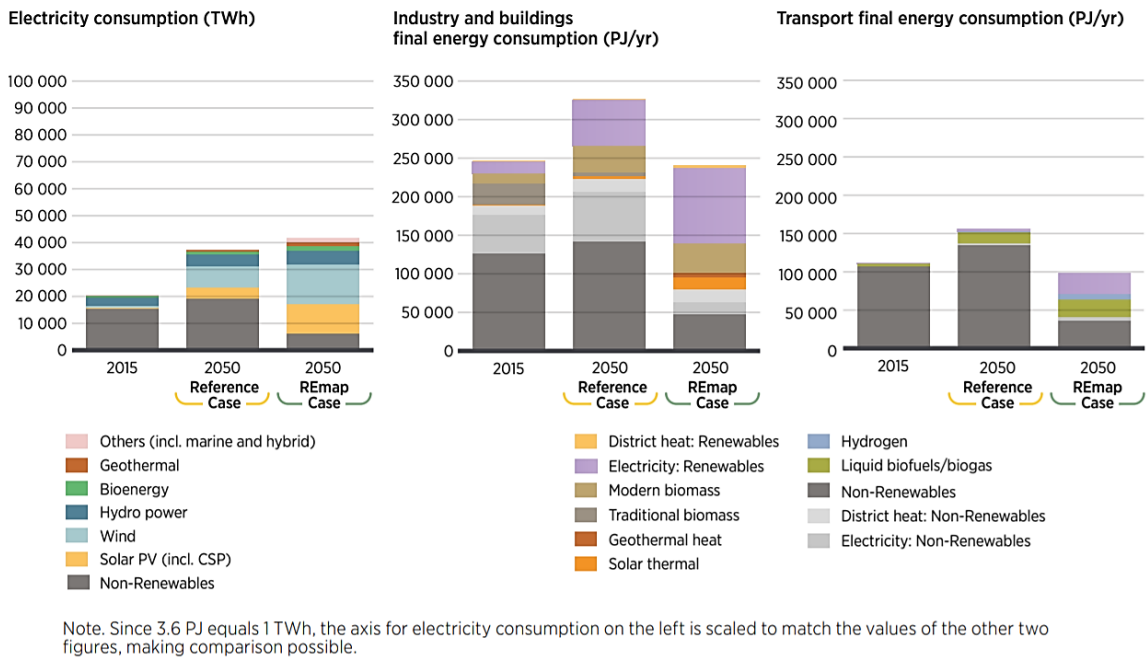


Note. Since 3.6 PJ equals 1 TWh, the axis for electricity consumption on the left is scaled to match the values of the other two figures, making comparison possible.

Figure 1.9 Figure 2. © IRENA 2018 Renewable energy should be scaled up to meet power, heat and transport needs - (left) use of renewable and fossil energy in electricity generation, (middle) buildings and industry, and (right) transport – reference and REmap cases, 2015-2050 (TWh/yr or PJ/yr) [17].

## 1.5 Selecting Experimental Variables

In wire combustion, the relevant parameters can be loosely grouped into three categories: the characteristics of the wire, environmental conditions, and geometric parameters. The characteristics of the wire include the dimensions and makeup of the metal core and insulation. The environmental conditions can include forced flow speed, ambient pressure, oxygen concentration, external radiant heating, strength of gravity, and even electro-magnetic fields. Finally, geometric parameters can include the direction and inclination of flame spread relative to forced flow speed and gravity.

Typically, experimental studies have considered the effect of at least one environmental variable. Some of the environmental variables which have been investigated by studies thus far include gravitational strength, oxygen concentration, dilution gas, flow speed, external radiant heating, and electric fields. However, many studies have also varied multiple parameters, including wire characteristics, environmental variables, and geometric parameters, within their experiments. For example, the investigations initiated by Fujita *et al.* [18, 19, 20, 21] conducted a series of tests using thin wires to determine the influence of wire temperature as well as core size, ambient oxygen concentration, and opposed flow on wire combustion. Another investigator, Leung *et al.* [22], studied the effect of the wire core under both external heating and non-flaming pyrolysis. Nakamura *et al.* [23, 24] looked at the effect of pressure, core size, and thermal conductivity on wire combustion, and Miyamoto *et al.* [25] investigated the effect of varying external radiation and core conductance for the combustion of thick electrical wires.

The work presented here also aims to study the effect of a combination of environmental variables on the flame spread along electrical wires. While there are many parameters that are important to the wire burning problem, as previously studied by so many in the field, considering the variables described to be present in SEAs, the environmental conditions that are the focus of this study are forced flow speed, ambient pressure, oxygen concentration, and gravitational strength. However, because of the limitations of the Earth-based experimental setup, variations in gravitational strength were only examined through modeling rather than experimental means. It should be noted that the FLARE project plans to include experiments performed in microgravity in the Kibo laboratory module of the ISS, the results from which will be compared to the normal gravity data to further understand the flammability of materials in SEAs. For detailed analyses of the effects of further environmental conditions that were not considered in this work, studies focusing on dilution gas [18], external radiant heating [24, 26, 27, 28, 29, 30], electric fields [31, 32, 33, 34] and microgravity [18, 20, 21, 26, 33, 34, 35] can be referenced.

For the geometric parameters, as mentioned previously, this work focuses on horizontally oriented wires. This orientation was selected because horizontal forced flow is perpendicular to the buoyancy-induced flows produced by flames. Thus, the effects of the forced flow on horizontal flame spread rate can be somewhat isolated for analysis. In all experiments, the horizontal forced flow was examined in one of two configurations. The first configuration was opposed flow, where the forced flow was in the opposite direction of the flame spread. The second configuration was concurrent flow, where the forced flow was in the same direction as the flame spread. For in-depth analyses of flame spread rate along wires of other orientations, studies utilizing either vertical [26, 28, 36, 37, 38] or inclined [32, 39, 40, 41] wires can be referenced, and for further information on the effects of other flow conditions, studies examining the effects of transverse flow can be referenced [42].

Finally, regarding the wire characteristics, several different wire types were explored throughout this work to facilitate comparison to previous results from the literature as well as future results to be obtained from experiments performed on the ISS. For the experiments presented here, different metals were tested for the wire core, and variations in the metal core diameter and insulation thickness were also tested. However, the insulation material was kept constant for simplicity. It should be noted that, as was done in this work, most studies use polyethylene (PE) in either the high density (HDPE) or low density (LDPE) variety. For further information on the effects of different insulation types, other studies which have looked at the effect of PE with or without coloring additives [26, 43] or the effect of fire-resistant insulation materials which exhibit different behavior [30, 44] can be referenced.

## 1.6 Evaluating Material Flammability

Considering all the variables that are relevant to the wire burning problem makes the study of wire flammability very complicated. In this work, the spread rate of the flame along the wire was the main parameter used to characterize wire flammability. Flame spread rate was chosen because it is a classic burning mechanism used to assess material flammability. This metric is commonly used because after a material is ignited, the rate of heat released by the fire is dependent on its rate of spread.

Additionally, although not normally considered as a material flammability parameter, another consideration that must be accounted for when performing combustion experiments which include the burning of PE insulated wires is the dripping phenomena of the molten PE insulation. The dripping insulation is typically burning as it falls and has been shown to be capable of igniting thin fuels [45]. Kobayashi *et al.* [43] also found that the dripping, whether in a horizontal or vertical configuration, corresponded to portions of the wire core that act as a heat sink. Furthermore, since dripping is caused by gravity, there is a fundamental difference in the propensity for a molten burning material to spread a fire in normal gravity, in the absence of gravity, or in reduced gravity, as in a spacecraft or space habitat. Thus, dripping is relevant in the study of wire flammability, particularly when assessing their fire hazard potential in spacecraft environments as compared to Earth-based environments.

# Chapter 2. Methodology

## 2.1 Wire Samples

All the experiments performed for this work were conducted with simulated electrical wires. These wires consisted of 125mm-long metal cores made of either copper rods, nichrome rods, or stainless-steel tubes and 100mm-long LDPE insulation sheaths, as shown in the left half of Figure 2.1. Also shown in this figure is that the arrangement of the insulation along the metal core for the experiments was such that their tips were aligned at one end and the bare metal core was exposed on the other. Constructing the samples in this way allowed for the bare end of the wire to be secured by the sample holder. The different diameter dimensions of the wire sample types used in the experiments are pictured in the right half of Figure 2.1. These dimensions as well as the different core materials that were used are summarized in Table 2.1. Moving forward, each different sample type will be referred to as their corresponding sample type identifier as presented in this table. The material properties of each of the different metal cores as well as the insulation are given in Table 2.2.

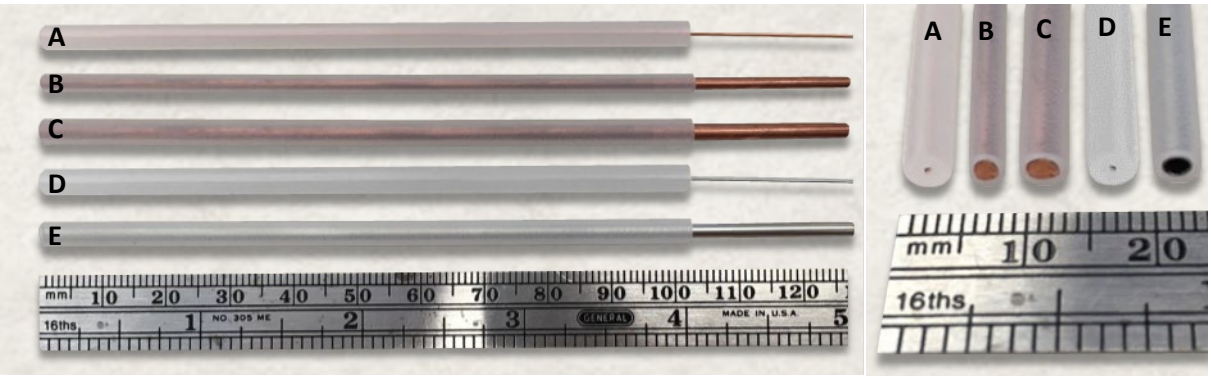


Figure 2.1 Wire samples used throughout flame spread rate and dripping experiments labelled with identifier by sample type.

Table 2.1 Wire sample configurations.

| Sample Type Identifier | Core Material | Core Diameters (OD/ID) [mm] | LDPE Insulation Diameters (OD/ID) [mm] | Thickness [mm] (τ) |
|---|---|---|---|---|
| A | Copper | 0.64/- | 4.0/0.70 | 1.7 |
| B | Copper | 1.8/- | 3.0/1.8 | 0.60 |
| C | Copper | 2.5/- | 4.0/2.5 | 0.75 |
| D | Nichrome | 0.64/- | 4.0/0.70 | 1.7 |
| E | Stainless Steel | 2.4/2.2 | 4.0/2.5 | 0.75 |

It should also be noted that the relatively large size of these simulated wires, while not intended to necessarily reproduce actual electrical wires, were selected to facilitate the interpretation of the experimental results. It is for this reason that wire flammability studies often use these simulated wires which are assembled from a metal rod for the core and plastic tubes for the insulation, which is the case in this study. Additionally, these sample types were utilized to compare results with the previously mentioned future experiments to be conducted on the ISS which will use the same type of wires.

Table 2.2 Wire sample core and insulation properties.

| Wire Part | Material | Density [kg/m$^3$] | Specific Heat [J/kg·K] | Thermal Conductivity [W/m·K] |
|---|---|---|---|---|
| Core | Copper | 8,880 | 390 | 398 |
| Core | Nickel-Chrome | 7,800 | 440 | 21.5 |
| Core | Stainless Steel | 8,650 | 500 | 17.4 |
| Insulation | LDPE | 920 | 0.27 | 1990 |

# 2.2 Experimental Setup

The two experimental apparatus used to complete this research are shown in Figure 2.2 through Figure 2.5. These setups were used to facilitate flame spread tests of LDPE-insulated wire samples with different core materials under various environmental conditions, including variable flow velocity, ambient pressure, and oxygen concentration. As shown in these figures, different experimental setups were used throughout experimentation. These different setups allowed for implementation of the different environmental conditions of interest.

## External Flow Duct

The setup in Figure 2.2 was used for forced flow conditions with the wire sample exposed to atmospheric pressure. This setup consisted of an external flow duct open to the atmosphere on one end and connected to a wind tunnel on the other end. This set up, however, was eventually only used for quiescent conditions, and the wind tunnel was only used for venting after each experiment. Here, the sample was suspended in the middle of the flow duct, which had a cross sectional area of 152x121 mm$^2$ and a total length of 368 mm, with the sample tip located approximately 155 mm from the upwind end of the duct.

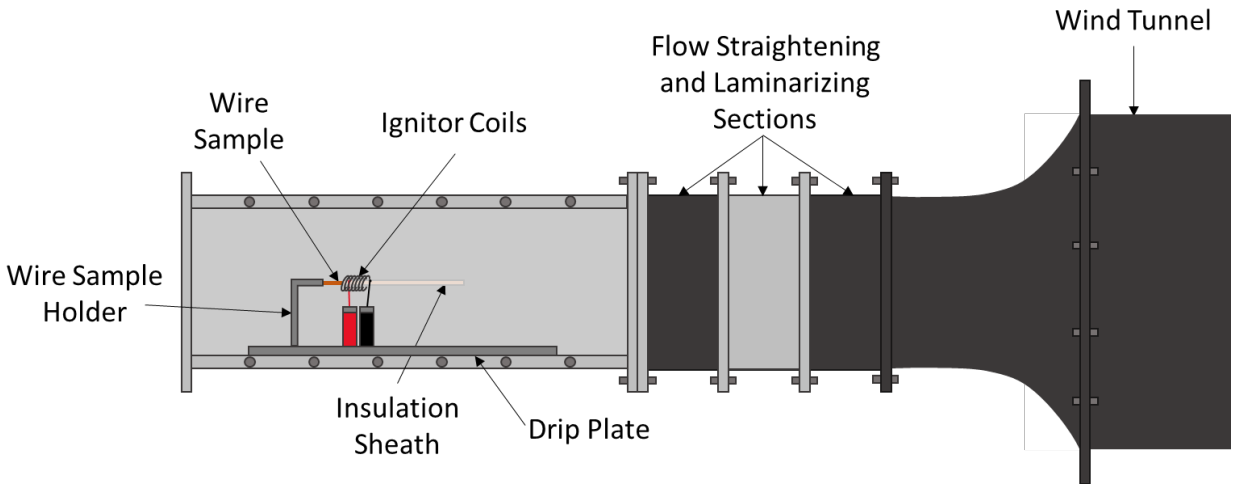


Figure 2.2 Experimental setup for limited experiments subject to atmospheric pressure.

## Pressure Chamber

All other experiments were performed using the setup depicted in Figure 2.3 through Figure 2.5, which show an apparatus, now oriented horizontally, that was previously developed to

study the flammability of solid combustible materials under various SEA-like ambient conditions [46]. Figure 2.3 shows the external view of this experimental setup, and Figure 2.4 and Figure 2.5 show various internal views. As seen in these figures, this setup consisted of a flow duct open at one end and connected to an oxidizing gas source at the other end, all contained within an airtight pressure chamber. This flow duct had a cross sectional area of 128x128 $mm^2$ and a total length of 255 mm. The wire sample was suspended horizontally in the middle of the duct with the sample tip located approximately 95 mm from the upwind end of the flow duct, where uniform air entered the duct from a flow laminarizing and straightening section.

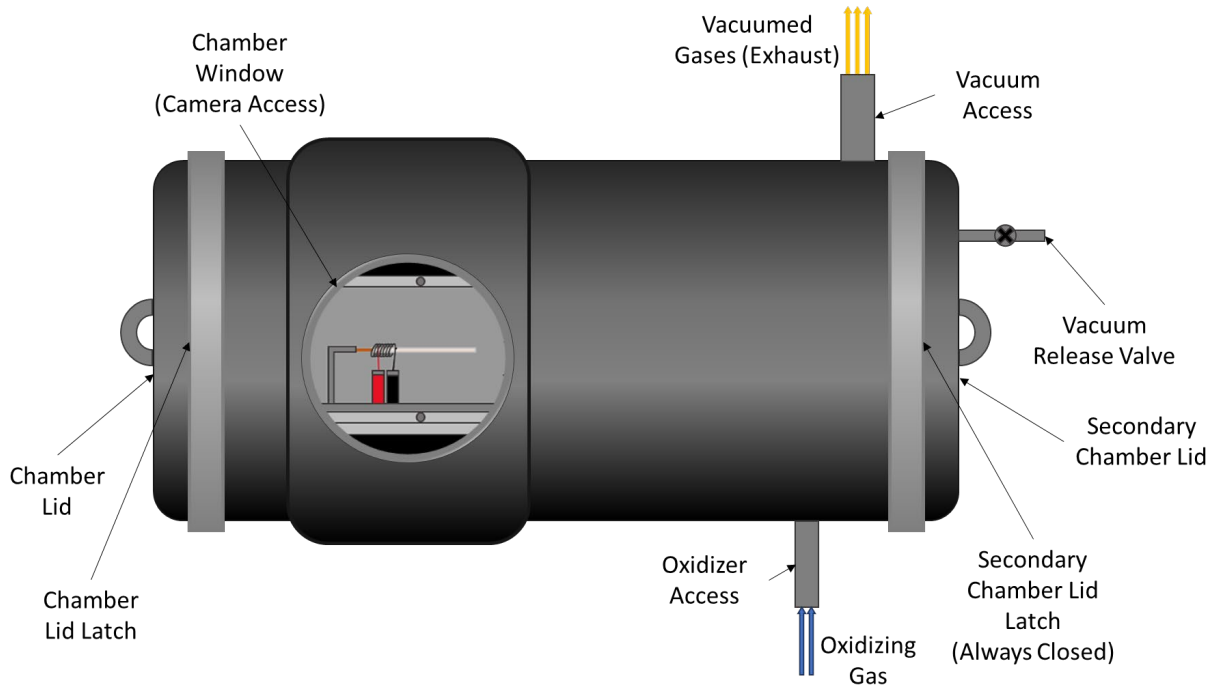


Figure 2.3 External view of pressure chamber experimental setup.

The environment within the flow duct had access to an oxidizing gas source through the hose attached to one end. This hose received the oxidizing gas as either air provided by a pressurized tank fed by a compressor or a mixture of oxygen and nitrogen from pressurized canisters, which allowed for experimentation with different oxygen concentrations. The compressed house air as well as the compressed oxygen and nitrogen were supplied through critical nozzles (O'Keefe Controls), with pressure measured immediately ahead of the nozzles by mechanical gauges. After metering, in the case of using nitrogen and oxygen, the gases were mixed in the line. All oxidizing gasses then passed through a bulkhead in the vacuum chamber to be delivered through the hose attached to the flow duct.

At the same time, a high-capacity vacuum generator (Vaccon JS-300) attached to the pressure chamber and controlled through a mechanical vacuum regulator allowed for maintaining a constant pressure, at or below atmospheric, inside the chamber. Thus, the experimental environment, with the pressure monitored constantly with an electronic pressure transducer (Omega Engineering, Inc. PX303-015A5V), remained consistent throughout the length of each test. The presence of this vacuum, while not attached directly to the duct, is what necessitated the use of the setup shown in Figure 2.2 for no forced flow condition experiments.

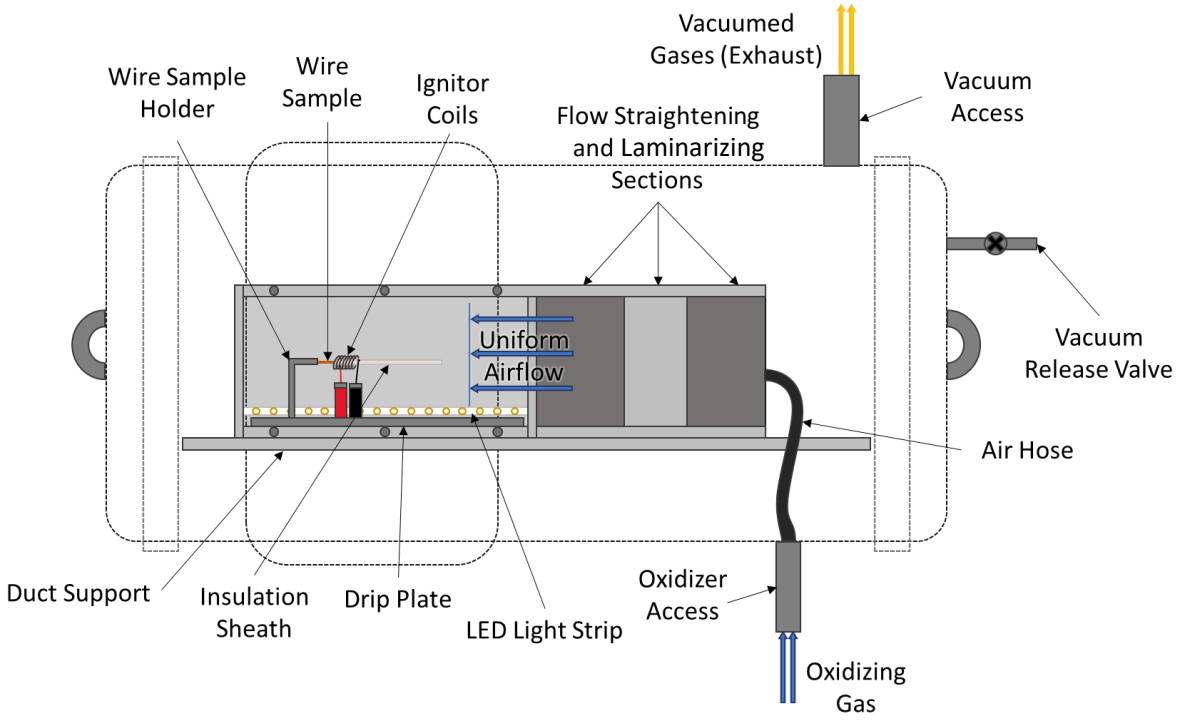


Figure 2.4 Internal view of pressure chamber experimental setup with wire sample oriented for opposed flow flame spread.

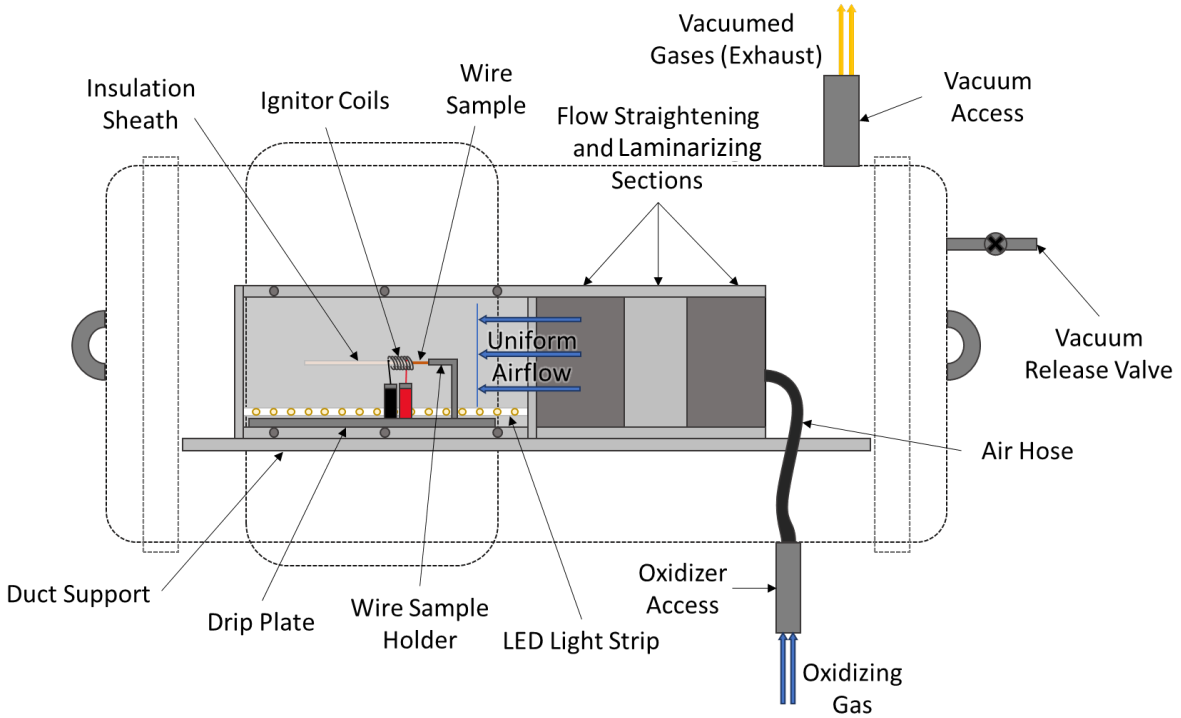


Figure 2.5 Internal view of pressure chamber experimental setup with wire sample oriented for concurrent flow flame spread.

Accounting for the desired pressure and oxygen concentration within the chamber, calibrations of the flow nozzles could be used to determine the correct pressure at which the gases should be inputted into the chamber to maintain a constant chosen flow rate. Thus, facilitating experiments

with exposure to various flow speeds. These calibrations were verified by measuring the flow rate manually using a hot-wire anemometer under atmospheric conditions with the pressure chamber open to the ambient surroundings.

The difference between the two internal setups shown in Figure 2.4 and Figure 2.5 is the orientation of the wire sample within the flow duct. The wire sample holder and igniter were able to be installed in the duct in different orientations to allow for ignition at one end of the wire or the other. If the igniter were positioned on the downwind end of the wire, as shown in Figure 2.4, once the wire was ignited, the flame would travel upwind, opposed to the direction of flow, toward the unburned part of the insulation fuel. Therefore, this positioning of wire and igniter was used for opposed flow experiments. If the igniter were positioned on the upwind end of the wire, as shown in Figure 2.5, once the wire was ignited, the flame would travel downwind, concurrent to the direction of flow, toward the unburned part of the insulation fuel. Therefore, this positioning of wire and igniter was used for concurrent flow experiments.

### Common to All Experimental Setups

For all the different setups, the igniter consisted of a 0.64mm-diameter nichrome wire that was coiled into a diameter of about 8 mm with 6 loops. It was powered by a Variac power source which was set to provide an RMS voltage of approximately 15 V, resulting in a power output of approximately 155 W. Additionally, to characterize the dripping, a drip plate was placed beneath the length of the wire to collect fallen material that dropped from the burning sample for later mass analysis.

Windows on the sides of the flow ducts and chamber provided optical access, which allowed for video recording using a Nikon D3200 camera with a DX AF-S NIKKOR 18 55 mm 1:3.5-5.6G lens. The recordings were taken at 30 fps with an incandescent white balance, ISO of 200, exposure time of 1/60, and aperture setting of F6.3. Subsequent video analysis allowed for measurement of the flame spread rate across each sample as well as the frequency of insulation dripping that was observed to occur.

## 2.3 Experimental Procedure

While the conditions and parameters that were being tested varied throughout the experiments, the main procedure remained the same as follows. The wire sample and clean drip plate were first weighed. Next, the sample was installed in the duct with the drip plate below it. As part of the installation, the sample was oriented in such a way as to either facilitate opposed or concurrent flame spread. If the experiment was performed in the pressure chamber, the lid was sealed. Next, the environmental conditions of interest were set to the desired values.

Once the sample and experimental conditions were set, the video recording was started on the camera. An LED light strip was then used to illuminate the wire sample for approximately 3 s at the start of the experiment, so the insulation on the sample, which provided a length scale, could be more easily measured during post image-processing of the videos. Then, the Variac power source was turned on for the desired amount of time. While this ignition time was varied for some experiments, for most experiments, an ignition time of 35 s was used. Such a lengthy ignition time was required due to the thickness of the insulation on the sample.

Once the power source was switched off, the test was allowed to continue until the flame propagated along the entire length of the wire or until burning along the wire naturally

extinguished. After the flame extinguished, the camera recording was stopped, and air was passed through the flow duct for several minutes to remove any remaining combustion products in the duct as well as to bring the temperature in the duct back down to room temperature. With the duct cooled down, the sample and drip plate were both safe to remove and weigh again. The drip plate was then cleaned, and the process could repeat. For most experiments, six tests were conducted for each wire type and combination of environmental conditions.

## 2.4 Measurement of Dependent Variables

### Flame Spread Rate

After the experiments were conducted, the recorded videos were analyzed using an interactive image processing script, which had been developed previously by Thomsen *et al.* [10, 11], to extract geometric information about the flame at regular intervals during its spread. The intervals, examples of which are shown in Figure 2.6, were chosen such that 50 to 80 of the recorded frames of the flame spread were examined. In each of the analyzed frames, the leading edges of the base of the flame were recorded. With further analysis, the locations of the leading edges were fit with a linear regression, as shown in Figure 2.7. The flame spread rate was calculated as the slope of the regression, which, after ignoring end effects, was found to be linear in all cases. Using the length of the insulation sheath on the sample as a length scale, a conversion from pixel coordinates to lab scale (mm) was made, and the final flame spread, $V_f$, rate was determined.

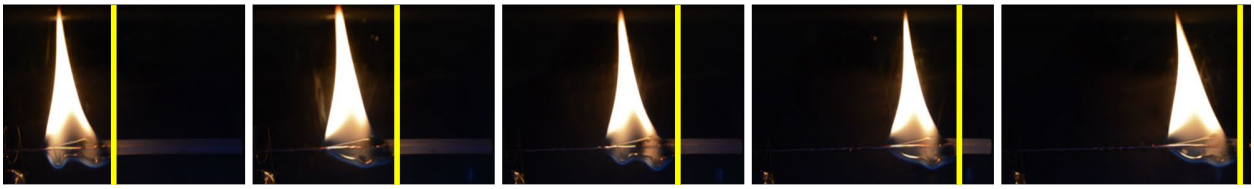

Figure 2.6 Example of tracking the flame front, as indicated by the yellow lines, across various video frames to measure flame spread rate.

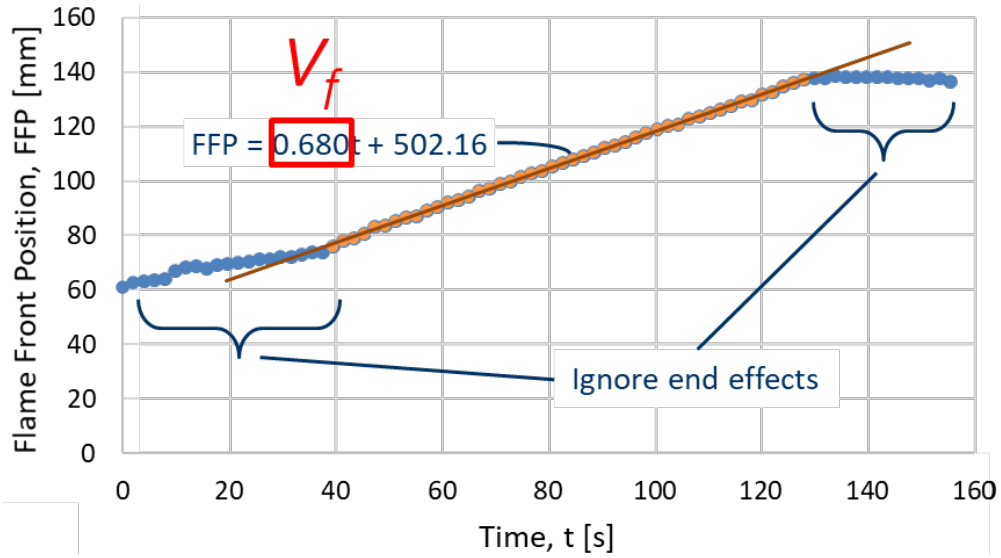


Figure 2.7 Example of flame spread rate experiment results showing flame front position versus time with the calculated slope of the line resulting in the flame spread rate ($V_f$).

## Dripping

The dripping was much simpler to measure than the flame spread rate. The mass of insulation material dripped was determined by weighing the drip plate placed beneath the wire sample before and after each experiment. The same was done for the wire sample itself, as it was desirable in some instances to compare the mass of insulation dripped versus burned. As for the insulation dripping frequency, the same videos used to determine the flame spread rate were analyzed again. The frequency of dripping was calculated by counting the number of drips that occurred during steady spread, noting the corresponding time frame, and averaging the number of drips during that time, resulting in a "drips per second" value.

# 2.5 Summary of Experimental Studies

In this work, there were four different experimental studies that were undertaken. The variables that were analyzed in each of these studies versus which were held constant are summarized in Table 2.3. The first study, as explored in Chapter 3, mainly focused on the wire characteristics and how those variables affected the burning behavior of the wires. The next study, as discussed in Chapter 4, was an intermediate study to determine whether or not the utilized ignition method had an impact on flame spread rate results. Next, the work shifted from concentrating mainly on the effects of wire characteristics and instead focused on environmental parameters that may affect wire flammability characteristics, as analyzed in Chapter 5. Finally, the study examined in Chapter 6 expanded upon those environmental parameters from the previous study to create an experimental atmosphere that would most similarly replicate the SEAs of interest in this work.

Table 2.3 Matrix summary of experimental studies.

| Study Number | Wire Characteristics | | | Environmental Parameters | | | |
|---|---|---|---|---|---|---|---|
| | Core Material | Core Diameter | Insulation Thickness | Flow Velocity | Ambient Pressure | Oxygen Concentration | Ignition Time |
| 1 | *Variable* | *Variable* | *Variable* | *Variable* | Constant | Constant | Constant |
| 2 | *Variable* | *Variable* | *Variable* | Constant | Constant | Constant | *Variable* |
| 3 | Constant | Constant | Constant | *Variable* | *Variable* | Constant | Constant |
| 4 | Constant | Constant | Constant | *Variable* | *Variable* | *Variable* | Constant |

# Chapter 3. Effect of Wire Type and Flow Velocity

## 3.1 Motivation and Prior Research on Effect of Wire Type and Flow Velocity

Many prior studies have examined the effect of forced on the flame spread over electrical wires. However, it is uncommon for forced flow to be the main environmental variable considered in these studies. More frequently, the effects of forced flow are analyzed in combination with the effects of other environmental parameters. Of the studies that have focused on examining the effects of horizontal forced flow velocity Kobayashi *et al.* [36] investigated the effects of opposed flow on thick wire samples, and Lu *et al.* [47] investigated the effect of concurrent flow on thin wire samples. In their studies, Kobayashi *et al.* found the flame spread rate to decrease with increasing opposed flow speeds, while Lu *et al*. found the flame spread rate to increase with increasing concurrent flow speeds. These results were found to hold true for all wire types tested across both studies. While these results provide some information on their own, it is thought that directly comparing the results of both opposed and concurrent experiments could be more beneficial in understanding the wire burning problem. Therefore, in the following work, the forced flow is described as the flow velocity, and the negative flow values correspond to opposed flow.

Regarding the effects of wire type on flame spread rate, some studies on wire combustion have varied the size of the metal core and the insulation thickness [26, 36, 48, 43] of simulated electrical wires to determine their effects. Investigations have also examined the effect of the metal core by exploring different core materials [48, 37] or by replacing the solid core with a thin-walled stainless-steel tube [36, 43] and even testing insulation samples without a core at all [43]. Accounting for the effect of the wire core can be especially tricky, as Huang *et al.* [29] observed that the wire core, depending on its material composition, can act as a heat sink during ignition and the transition to flame spread. While working with PE insulated wires, Kobayashi *et al.* [43] showed that, as the core conductance increased, opposed flame spread increased over a horizontal wire and decreased over a vertical one because of the core's simultaneous dual effect as a heat source and heat sink. The current work aims to add to this body of knowledge as well as to introduce the effects of the wire type on the dripping of molten insulation that is observed to occur in these experiments.

## 3.2 Experimental Design

As stated, the goal of this study was to add to prior research and examine how the burning, in terms of flame spread rate, of electrical wires is affected by the flow conditions and characteristics of the wire. Thus, the experiments for this analysis were conducted using the wire sample types pictured in Figure 3.1. These samples are wire types A, C, D, and E, as identified in Table 2.1. Recall that sample types A and C contain copper cores with diameters of 0.64 mm and 2.5 mm, respectively. Wires of sample type D contain 0.64 mm nichrome cores, and wires of sample type E contain stainless steel tube cores with outer diameters or 2.4 mm. All these sample types, have insulation outer-diameters of 4 mm, corresponding to insulation thicknesses of either 1.7 mm for

the thinner-cored samples, types A and D, and 0.75 mm for the thicker-cored samples, types C and E.

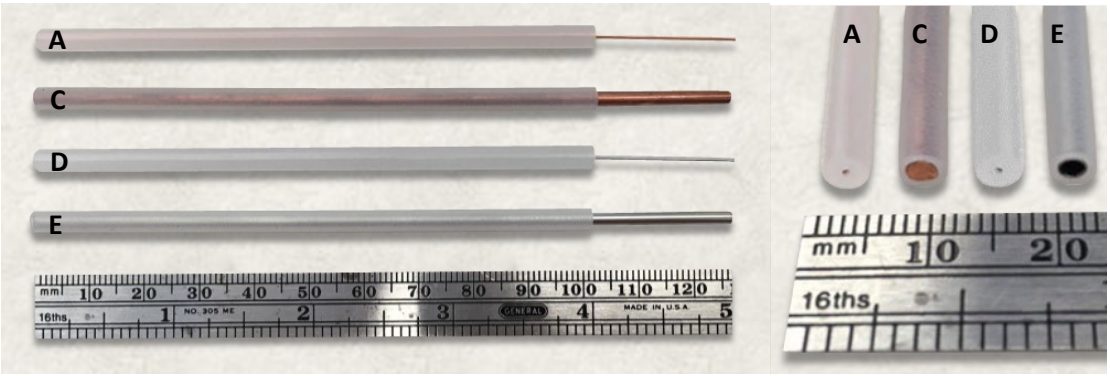


Figure 3.1 Wire sample types A, C, D, and E used in flow velocity and sample type study.

These wire sample types were particularly selected for comparison of flame spread rate behavior between wires with highly conductive cores versus their much less conductive counterparts. Additionally, comparisons were made between thick and thin wire types of the same or similar thermal conductivity. Therefore, the flame spread rate over the thin, copper type A samples could be compared to that over the thin, nichrome type D samples. Similarly, the flame spread rate over the thick, copper type C samples could be compared to that over the thick, stainless steel tube type E samples. Finally, the flame spread rate over the thin and thick copper wire samples, types A and C, respectively, could be compared as well as the flame spread rate over the thin and thick less conductive wire samples, types D and E, respectively.

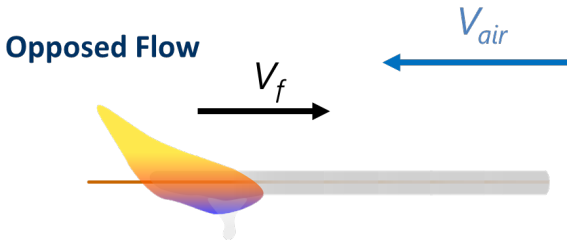


Figure 3.2 Depiction of horizontal opposed flow over a wire.

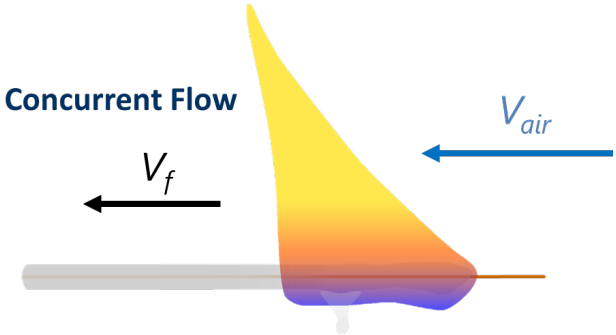


Figure 3.3 Depiction of horizontal concurrent flow over a wire.

To study the effects of flow speed on the flame spread rate over these different wire types, seven different flow rates were used throughout experimentation. These flows consisted of a no forced flow condition, three opposed flow conditions, and three concurrent flow conditions. The

arrangement for the opposed flow configuration is shown in Figure 3.2, and the arrangement for the concurrent flow configuration is shown in Figure 3.3. For both of these two different flow directions, speeds of 10, 20, and 30 cm/s were tested. As for the rest of the conditions in the burning environment, the ambient pressure was 101 kPa, and air was used as an oxidizer.

## 3.3 Flame Spread Rate Results

The experimental results for flame spread rates along the insulation surfaces of wire sample types A, C, D, and E for various forced airflow velocities are shown in Figure 3.4. The average flame spread rates and corresponding standard deviation values reported in Table 3.1. The overall results show that as the airflow velocity transitions from strongly opposed to strongly concurrent, the flame spread rate increases. The increase of flame spread rate with increased flow speed, specifically in the concurrent regime, as seen in this wire study, has also been observed in previous studies with flat fuel surfaces and was attributed to the increase of the heat transfer from the flame to the fuel surface due to the closer proximity of the flame to the surface [49].

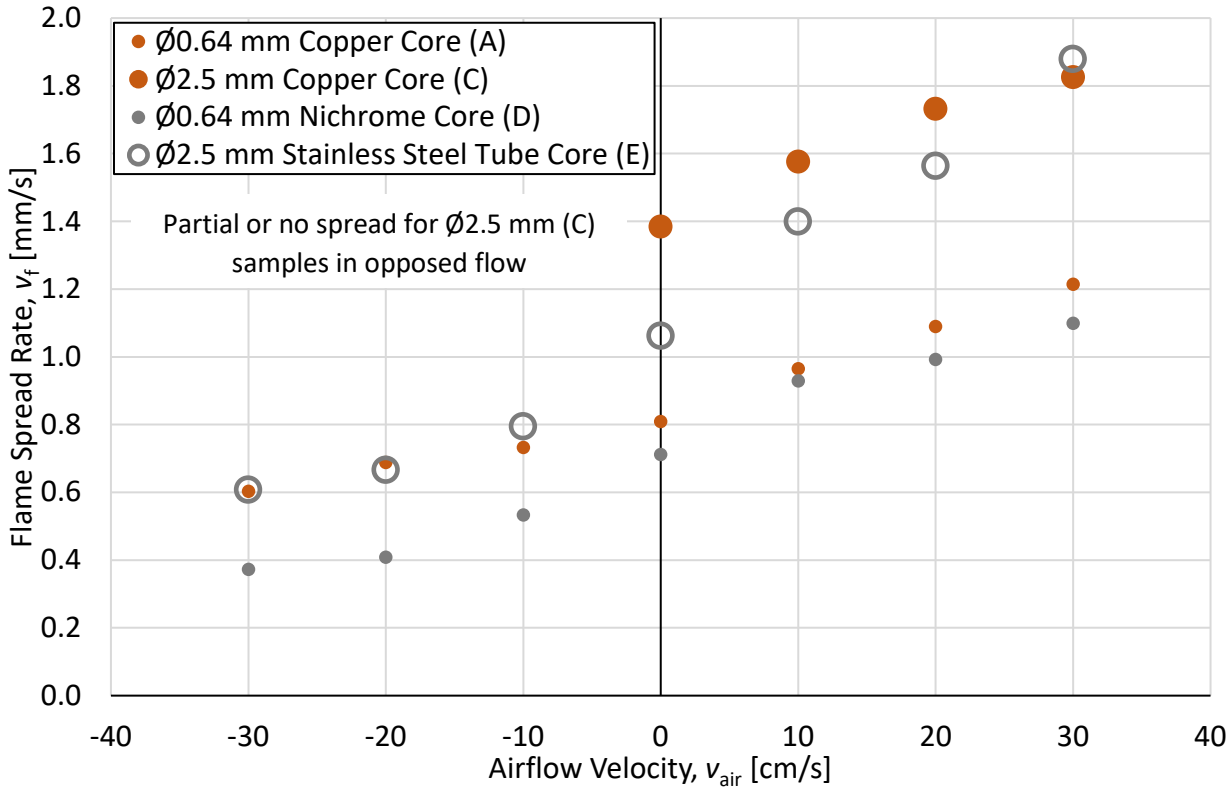


Figure 3.4 Flame spread rate for wire sample types A, C, D, and E under various flow velocity conditions.

Looking again at Figure 3.4, in the no forced flow and concurrent flow regimes, the samples with the thinner insulation thickness, sample types C and E, exhibited faster flame spread rates over the airflow speeds tested compared to the samples with thicker insulation thicknesses, sample types A and D. Because there is a significant range of conductance, defined as the product of thermal conductivity and cross-sectional area, for each of the core sizes, it can be surmised that the major factor causing this difference in flame spread rate is due to the insulation thickness rather

than core characteristics. Further observation of the concurrent flame spread regime shows that there is only a small difference in flame spread rate for cores of different materials with the same diameter, indicating that heat transfer in the sample core does only slightly affects concurrent flame spread, confirming that insulation thickness is the dominant factor affecting flame spread rate in this regime.

Table 3.1 Average flame spread rate and standard deviations for wire sample types A, C, D, and E under various flow velocity conditions.

| Sample Type Identifier | Average Flame Spread Rate [mm/s] for Various Flow Velocities | | | | | | |
|---|---|---|---|---|---|---|---|
| | -30 cm/s | -20 cm/s | -10 cm/s | 0 cm/s | 10 cm/s | 20 cm/s | 30 cm/s |
| A | 0.60 ± 0.01 | 0.69 ± 0.03 | 0.73 ± 0.01 | 0.81 ± 0.02 | 0.96 ± 0.02 | 1.09 ± 0.04 | 1.21 ± 0.03 |
| C | - | - | - | 1.38 ± 0.01 | 1.58 ± 0.08 | 1.73 ± 0.11 | 1.83 ± 0.03 |
| D | 0.37 ± 0.00 | 0.41 ± 0.02 | 0.53 ± 0.03 | 0.71 ± 0.00 | 0.93 ± 0.02 | 0.99 ± 0.02 | 1.10 ± 0.04 |
| E | 0.61 ± 0.00 | 0.67 ± 0.06 | 0.79 ± 0.05 | 1.06 ± 0.07 | 1.40 ±0.12 | 1.56 ± 0.08 | 1.88 ± 0.11 |

In contrast, in the no flow and opposed regimes, the insulation thickness did not appear to have a strong effect on heat transfer and a more complex effect of the core is observed. Instead, the small metal core samples, types A and D, and the stainless-steel tube samples, type E, had similar-valued, low flame spread rates. While for the large copper core type C sample, the flame initiated by the igniter only showed visibly unstable spread and did not achieve spread across the full length of the sample in 10 cm/s opposed flow and saw no flow at all as the opposed flow was increased. Because the samples with the similarly large-sized but less conductive cores, type E wires, showed full flame propagation at all opposed airflow conditions, these results indicate that the large copper core may have been acting as a heat sink and hindering flame spread for the type C samples.

For the smaller-cored type A and D samples, a different trend is seen. In this case, the type A copper core samples proved to facilitate faster flame spread for all the opposed airflows as compared to its type D nichrome counterpart. This elevated flame spread rate has the implication that the smaller copper core may be acting as a heat transfer medium, allowing heat from the flame to be transferred both ahead of and behind the flame. In the case of the large diameter copper core, the ability of the core to transfer heat away from the flame is so great that it acts only as a heat sink, preventing flame spread. For the small core diameter case, the core still removes heat from the flame and pyrolysis zone, and some heat is transferred to the surroundings through the bare end of the wire, thus resulting in a slower flame spread rate than in the concurrent regime. However, a significant fraction of that heat is also transferred along the wire ahead of the flame, preheating the unburned material and positively contributing to spread, such that the flame is able to travel faster over the type A wires than over the type D wires with the less conductive cores.

## 3.4 Simple Analysis of Flame Spread Rate

To further the understanding of these results, the flame spread over electric wire problem can be thought of in terms of basic heat transfer, as shown in Figure 3.5 which depicts the wire problem setup and a zoomed-in view of the insulation fuel surface. To take the most simplistic approach, the equation for concurrent flame spread rate over a solid fuel [49], as give in Equation 2, can be utilized.

$$V_{\mathrm{f}} = \frac{l_{\mathrm{h}}}{t_{\mathrm{ig}}} \tag{2}$$

Note that the definitions for the variables appearing in Equation 2 as well as the following equations are given in the List of Symbols. Here, the ignition length is defined in Equation 3 [49], with the surface heat flux given in Equation 4 [49], where the radiative and re-radiative heat fluxes are considered to cancel one another out.

$$t_{ig} = \frac{\pi \rho c_p k (T_{py} - T_\infty)^2}{4(\dot{q}''_{surf})^2} \quad (3$$

**Error! Bookmark not defined.Error! Bookmark not defined.**)

$$\dot{q}''_{surf} = \dot{q}''_{conv} + \dot{q}''_{rad} + \dot{q}''_{ext} - \dot{q}''_{rerad} \quad (4$$

**Error! Bookmark not defined.Error! Bookmark not defined.**)

Since there is no external radiation in the current problem, the surface heat flux is simplified down to just the convective heat flux from the flame, as given in Equation 5.

$$\dot{q}''_{surf} = \dot{q}''_{conv} = h(T_{flame} - T_{surf}) \quad (5$$

**Error! Bookmark not defined.Error! Bookmark not defined.**)

Finally, to more accurately apply this equation to a cylindrical fuel, the heat transfer coefficient can be calculated with the Nusselt number for axial flow over a cylinder, as given in Equation 6 [50].

$$Nu_L = \frac{1}{L}\int_0^L 0.295\sqrt{\frac{xV_{air}}{\nu_{air}}} + 0.6785\left(\frac{x}{r}\right)dx = \frac{1}{L}\left(0.1475\sqrt{\frac{LV_{air}}{\nu_{air}}}L + 1.357\left(\frac{L^2}{r}\right)\right) \quad (6$$

**Error! Bookmark not defined.Error! Bookmark not defined.**)

From these equations, the trend of increased concurrent flow speed producing higher flame spread rate can be deduced. Here, an increased concurrent flow speed results in a shorter flame height, which places the flame closer to the surface of the wire. This increased proximity allows for greater heat transfer from the flame to the fuel surface, resulting in an increased flame spread rate. The small effect of the wire core observed experimentally can also be deduced from these equations. As the thermal conductivity for the core increases, the heated length of the wire would also presumably increase, thus resulting in a faster flame spread rate as well.

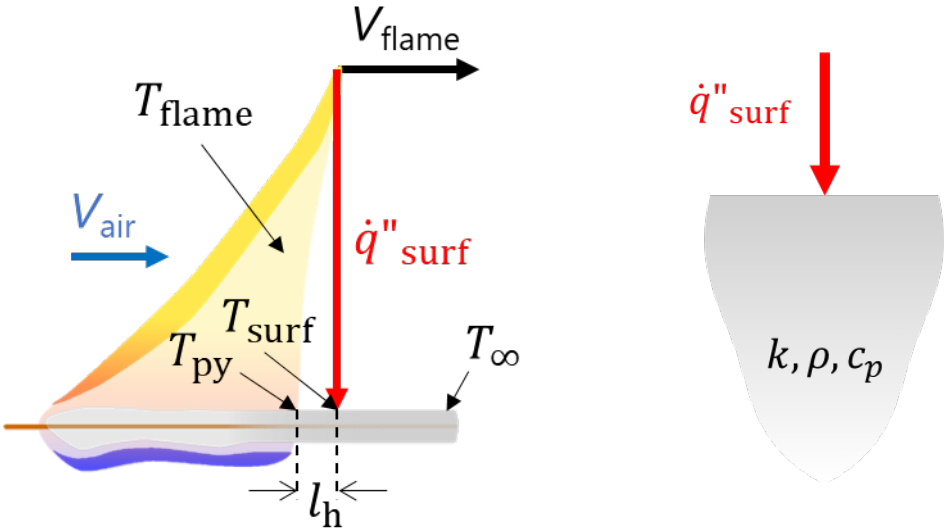


Figure 3.5 (left) Basic heat transfer setup for concurrent flame spread over electric wire problem and (right) zoomed-in view of the wire insulation fuel surface.

Things become slightly more complicated in the opposed flow configuration. This complexity comes from the fact that opposed flow flame spread is controlled by a small region in front of the

flame [49] and that the flame is now leaning over the bare end of the wire where the fuel has already been burned away. With this behavior, as the opposed flow speed increases, rather than an increase in flame spread rate, a decrease in flame spread rate is observed. This result come from the fact that the increased flow speed still results in a shorter flame height and increased heat transfer from the flame to the surface. This time, however, as stated, this surface is the bare wire core, which will end up conducting heat away from the flame and become lost to the environment. Thus, a reduction in flame spread rate results.

## 3.5 Dripping Results

Aside from the flame spread rate, the total mass loss by dripping was also recorded throughout experimentation. These results are presented in Figure 3.6, with the mass loss due to dripping values and corresponding standard deviations given in Table 3.2. As shown in this figure, the mass loss was approximately constant across all tested airflow velocities but did vary between the different wire sample types. The smaller-cored type A and D samples showed significantly more insulation mass loss due to dripping as compared to the larger-cored type C and E samples. This result can potentially be partially attributed to the fact that more insulation is present in the smaller diameter wire samples compared to the larger diameter wire samples, which can facilitate increased dripping.

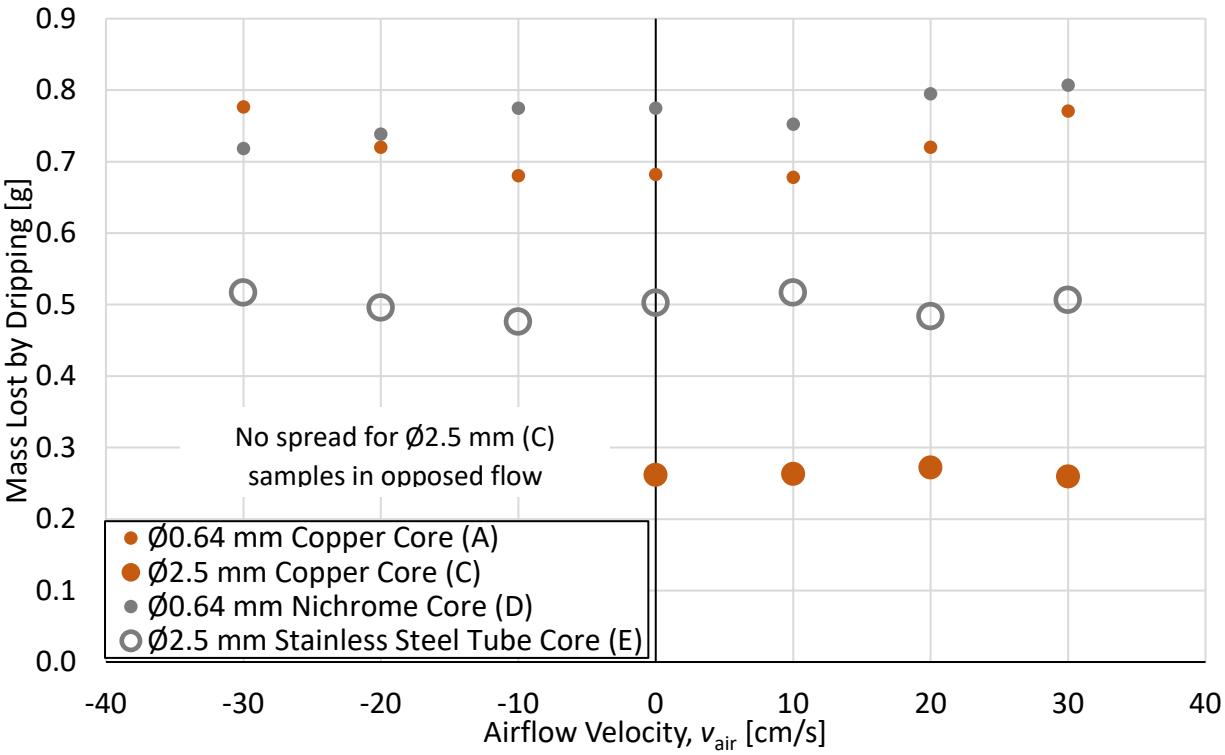


Figure 3.6 Mass loss due to dripping for wire sample types A, C, D, and E under various flow velocity conditions.

Examining the less dramatic amount dripping that was observed from the type C samples with large copper cores, this behavior can be compared to the moderate amount of dripping displayed by the type E samples with same diameter sizes yet less conductive cores. It may be that the

there, thus facilitating adhesion to the core rather than dripping. Because the type E samples contain much less conductive stainless-steel tube cores, this effect would not be seen.

Table 3.2 Average mass loss due to dripping and standard deviations for wire sample types A, C, D, and E under various flow velocity conditions.

| Sample Type Identifier | Average Mass Loss due to Dripping [g] for Various Flow Velocities | | | | | | |
|---|---|---|---|---|---|---|---|
| | -30 cm/s | -20 cm/s | -10 cm/s | 0 cm/s | 10 cm/s | 20 cm/s | 30 cm/s |
| A | 0.78 ± 0.01 | 0.75 ± 0.03 | 0.68 ± 0.03 | 0.68 ± 0.04 | 0.68 ± 0.02 | 0.72 ± 0.03 | 0.77 ± 0.01 |
| C | - | - | - | 0.26 ± 0.00 | 0.26 ± 0.01 | 0.27 ± 0.02 | 0.26 ± 0.03 |
| D | 0.72 ± 0.05 | 0.74 ± 0.03 | 0.77 ± 0.00 | 0.77 ± 0.01 | 0.75 ± 0.00 | 0.79 ± 0.01 | 0.81 ± 0.04 |
| E | 0.52 ± 0.05 | 0.50 ± 0.01 | 0.48 ± 0.01 | 0.50 ± 0.01 | 0.52 ± 0.01 | 0.48 ± 0.02 | 0.51 ± 0.06 |

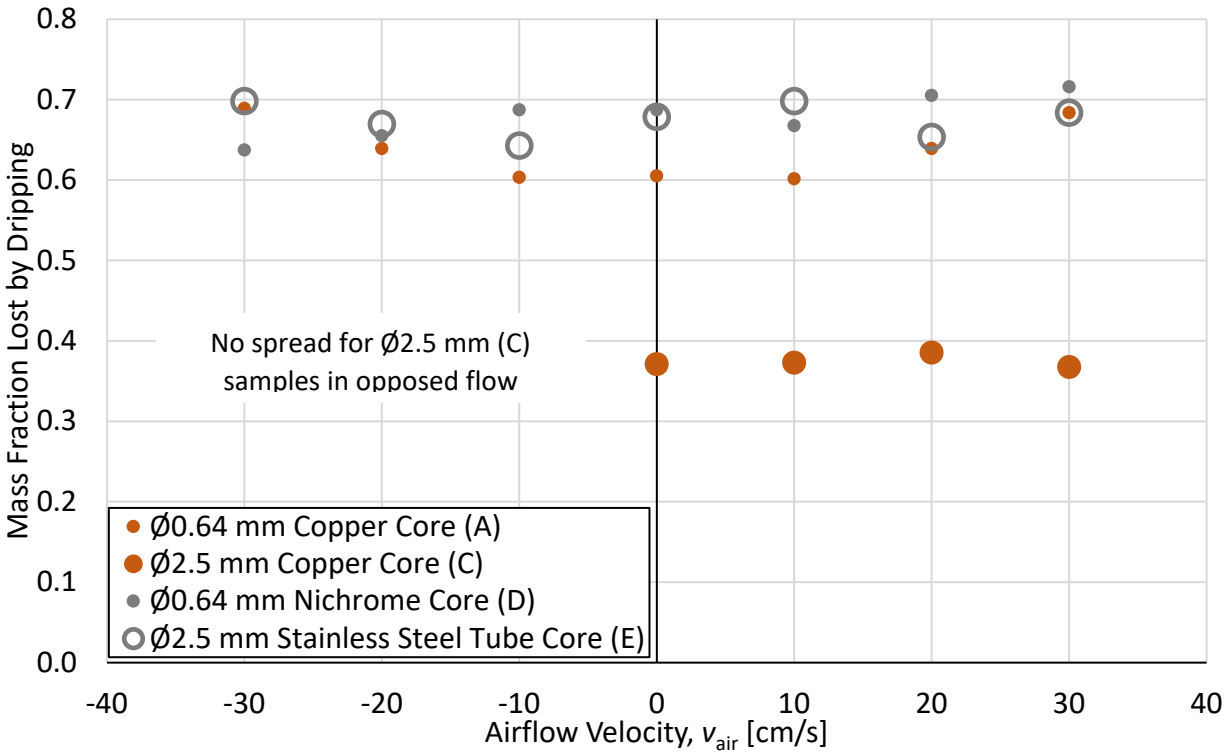


Figure 3.7 Fractional mass loss due to dripping for wire sample types A, C, D, and E under various flow velocity conditions.

To gain further insight into results for the mass loss of the simulated wires due to dripping, the previous data shown in Figure 3.4 was normalized by the mass of the samples and displayed in Figure 3.7. The fraction of mass lost by dripping shows a clearer picture of how the conductance of each wire is affecting the dripping while removing the factor of the amount of insulation present on each wire sample. Again, it is observed that the mass loss due to dripping is approximately constant across all tested airflow velocities. However, the mass loss by dripping results from the type E samples has now collapsed onto those from sample types A and D. This result shows that the conductance of the wire sample has the greatest influence on the fractional mass loss due to insulation dripping, again indicating that the type C samples with the large copper cores are able cool the pyrolysis zone, increasing the viscosity and surface tension of the molten LDPE insulation and thus limiting the ability of drips to form.

## 3.6 Conclusions on Effect of Wire Type and Flow Velocity

After burning type A, C, D, and E simulated electrical wires in various forced flow configurations, the flame spread rate was found to vary linearly with the airflow velocity. An increasing trend was observed for concurrent flame spread, and a decreasing trend was observed for opposed flame spread. The flame spread rate was also found to be lower for samples with the larger of the two insulation thicknesses. The mass loss due to dripping was found to remain approximately constant for all airflow velocities. However, the overall amount of dripping was found to be much less for samples with less insulation thickness. Normalizing the dripping results to fractional mass loss by dripping showed that the conductance of the wire also had a significant reduction effect on the dripping.

Overall, these results indicate that, for the wires tested here, in concurrent flame spread, the effect of the metal core is less important compared to the effect of the insulation thickness. For opposed flame spread, the effect of the core is more important than the effect of insulation thickness. Additionally, opposed flow was found to be more complex, with flame spread being small for conductive cores and entirely prevented in the case of large, highly conductive cores. Future work should address which mechanisms exactly control the observed behaviors.

# Chapter 4. Effect of Igniter Exposure Time

## 4.1 Motivation and Prior Research on the Effect of Igniter Exposure Time

As previous studies have shown, due to the effect that wire characteristics, environmental conditions, and geometric parameters may have on material flammability and the desire to understand their specific impacts on the flame spread over electric wire problem, it is reasonable to limit other variables that may influence experimental results. This reduction of variables allows for the material flammability results in any one environment to be more accurately attributed to the conditions being investigated rather than a secondary variable.

The main motivation for this analysis was inspired by the work of Huang *et al.* [29], who reported that reduced pressures can result in weaker flames with decreased heating efficiency, leading to the hindering of flame spread. Also reported in this study was that wires with conductive cores can act as heat sinks during ignition, taking energy away from the flames and not allowing them to spread [29]. These results imply that longer lengths of igniter exposure time are required to achieve ignition and flame spread across simulated electrical wire samples, especially highly conductive ones, in environments which are not well suited to burning, such as low-pressure environments.

Because reduced ambient pressure is one of the environmental conditions of interest in this study, it is important to isolate the effects of this environment on flame spread rate. However, because the study by Huang *et al.* indicates that increased igniter exposure time may be required to ignite highly conductive wire samples at these lower pressures, it must be determined whether or not this change in ignition time affects flame spread rate. So far, prior studies have not explored the potential effect differing lengths of igniter exposure time may have on flame spread rate results. Thus, the goal of this analysis was to investigate whether utilizing different lengths of igniter exposure times to ignite various types of simulated electrical wire samples subject to differing pressure environments influenced flame spread rate.

## 4.2 Experimental Design

The main experiments for this analysis were conducted using the samples pictured in Figure 4.1. These samples are wire types A, B, and C, as identified in Table 2.1, containing copper cores with diameters of 0.64 mm, 1.8 mm, and 2.5 mm, respectively. Recall that samples A and C both have insulation outer-diameters of 4 mm, corresponding to insulation thicknesses of 1.7 mm and 0.75 mm, respectively. Also recall that sample type B has an insulation outer-diameter of 3 mm, corresponding to an insulation thickness of 0.60 mm.

As stated, the main dependent variable of interest throughout testing was the flame spread rate along the wire as a function of the sample type, the ambient pressure, and, most importantly, the length of time the igniter was on. As such, experiments were performed at pressures of both 60 and 100 kPa subject to opposed flows of ~20 cm/s with air used as the oxidizer. Additionally, three different ignition methods, corresponding to different lengths of time, were utilized.

The first ignition method allowed the igniter to be on for the shortest amount of time. For this method, the igniter was turned off as soon as a flame appeared on the wire sample, as shown in

Figure 4.2. It should be noted that for the purposes of this analysis, the appearance of a flame refers to the development of a diffusion flame rather than a premixed, blue flame. The second ignition method allowed the igniter to be on until a flame appeared and spread far enough so that its tail was past the final coil of the igniter, as shown in Figure 4.3. Finally, Figure 4.4 shows the third ignition method which allowed the igniter to be on until the flame naturally extinguished after full spread. Experiments with each combination of wire type, pressure, and ignition method were repeated a minimum of three times.

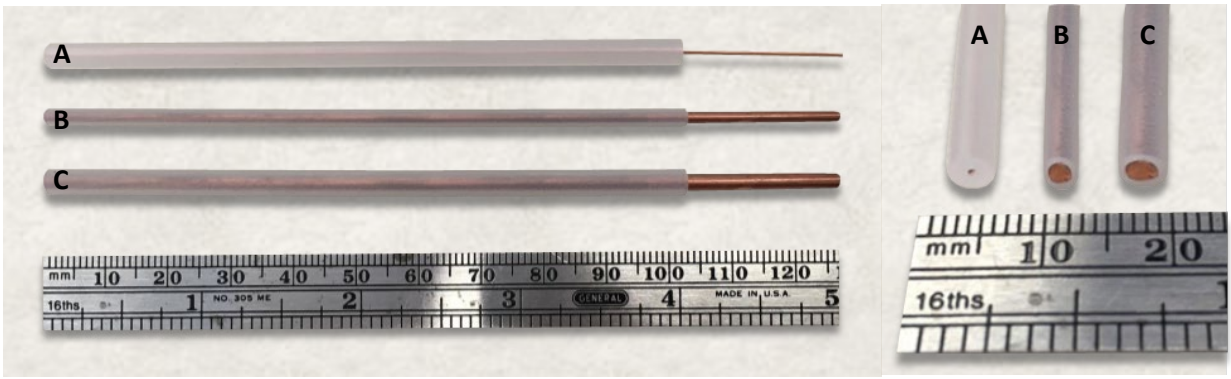


Figure 4.1 Wire sample types A, B, and C used in ignition study.

These same experiments were also carried out for wire sample types D and E, as identified in Table 2.1, with these samples being composed of thin nichrome or stainless-steel tubing cores, respectively. However, these experiments were performed more for confirmation of the predicted flame spread behavior, as these materials are not highly conductive, and were not the main interest of this analysis. Therefore, the results and discussion focus on the flame spread rates measured for the three copper sample types and the comparison between their behavior.

Figure 4.2 Ignition Method I – igniter turned off once a diffusion flame appears on the sample.

Figure 4.3 Ignition Method II – igniter turned off when the flame spreads past igniter coils.

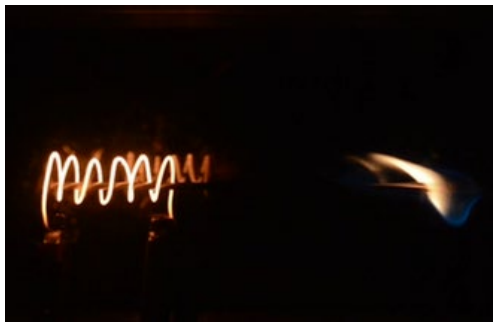

Figure 4.4 Ignition Method III – igniter remains on until the flame spreads along entire wire length.

## 4.3 Flame Spread Rate Results

The experimental results for opposed flame spread rate along the insulation surfaces of the copper wire samples for the different ignition methods and pressures are shown in Figure 4.5. These results along with their standard deviations as wells as the results from the experiments performed with wire types D and E are summarized in Table 4.1 for the 100 kPa environment and Table 4.2 for the 60 kPa environment.

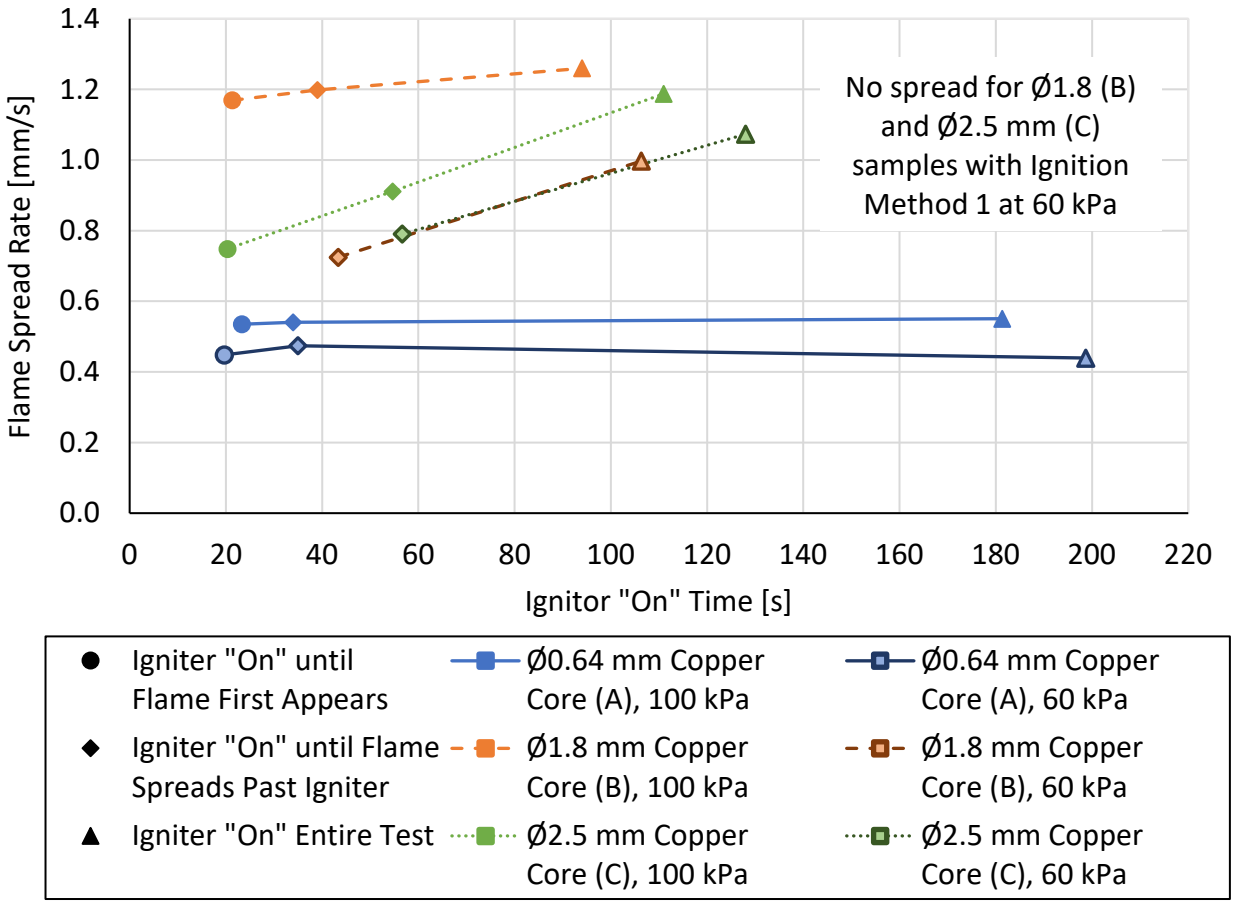


Figure 4.5 Flame spread rate results for wire sample types A, B, and C subject to opposed airflow of ~20 cm/s at pressures of 60 and 100 kPa with varied igniter exposure times.

Looking at Figure 4.5, it was observed that for the wire samples containing thicker copper cores, types B and C, longer lengths of exposure to the igniter produced faster flame spread rates. This result proved to hold true for the experiments performed both at 60 and 100 kPa. For the type B wire samples, the flame spread rate increased from 1.17 to 1.26 mm/s in the 100 kPa environment as the ignition time increased and from 0.72 to 1.00 mm/s in the 60 kPa environment as the ignition time increased. For the type C wire samples, the flame spread rate increased from 0.75 to 1.19 mm/s in the 100 kPa environment as the ignition time increased and from 0.79 to 1.07 mm/s in the 60 kPa environment as the ignition time increased. These results indicate that the high conductivity of these samples allowed for a significant amount of heat to transfer to the wires from the igniter. Subsequently, the heat absorbed by the wires was able to act as a heat source to the flame and increase its spread rate as more heat was added to the wires with increased ignition times.

Table 4.1 Averages ± standard deviations for igniter exposure times and flame spread rates for various simulated electrical wire sample types subject to opposed airflow of ~20 cm/s subject to pressure of 100 kPa.

| Sample Type Identifier | Avg. Igniter Exposure Time [s] | | | Average Flame Spread Rate [mm/s] | | |
|---|---|---|---|---|---|---|
| | Method 1 | Method 2 | Method 3 | Method 1 | Method 2 | Method 3 |
| A | 23 ± 3 | 34 ± 2 | 181 ± 2 | 0.54 ± 0.01 | 0.54 ± 0.01 | 0.55 ± 0.00 |
| B | 21 ± 3 | 39 ± 3 | 94 ± 8 | 1.17 ± 0.04 | 1.20 ± 0.16 | 1.26 ± 0.09 |
| C | 20 ± 5 | 55 ± 5 | 111 ± 5 | 0.75 ± 0.09 | 0.91 ± 0.05 | 1.19 ± 0.06 |
| D | 14 ± 1 | 30 ± 1 | 117 ± 1 | 0.84 ± 0.02 | 0.84 ± 0.01 | 0.85 ± 0.01 |
| E | 19 ± 1 | 29 ± 1 | 170 ± 5 | 0.62 ± 0.03 | 0.61 ± 0.03 | 0.56 ± 0.01 |

Table 4.2 Averages ± standard deviations for igniter exposure times and flame spread rates for various simulated electrical wire sample types subject to opposed airflow of ~20 cm/s subject to pressure of 60 kPa.

| Sample Type Identifier | Avg. Igniter Exposure Time [s] | | | Average Flame Spread Rate [mm/s] | | |
|---|---|---|---|---|---|---|
| | Method 1 | Method 2 | Method 3 | Method 1 | Method 2 | Method 3 |
| A | 20 ± 1 | 35 ± 1 | 199 ± 6 | 0.45 ± 0.13 | 0.47 ± 0.01 | 0.44 ± 0.02 |
| B | 17 ± 3 | 43 ± 2 | 106 ± 11 | - | 0.73 ± 0.10 | 1.00 ± 0.07 |
| C | 18 ± 4 | 57 ± 4 | 128 ± 7 | - | 0.79 ± 0.10 | 1.07 ± 0.07 |
| D | 15 ± 2 | 29 ± 1 | 206 ± 25 | 0.50 ± 0.15 | 0.46 ± 0.03 | 0.48 ± 0.02 |
| E | 18 ± 2 | 35 ± 1 | 239 ± 1 | 0.36 ± 0.11 | 0.35 ± 0.01 | 0.34 ± 0.01 |

Figure 4.5 also shows that in both the 60 and 100 kPa environments, the flame spread rate across wire sample type A was virtually unaffected by the length of igniter exposure time. Despite having extensive ranges of time where the igniter was on, between 23 and 181 s, the flame spread rate across all ignition methods for this wire type was consistently around 0.54 mm/s in the 100 kPa environment and around 0.45 mm/s in the 60 kPa environment with some small variation. With the same being true for the less conductive D and E wire sample types, this result suggests that these samples were not absorbing excess heat from the igniter that could act as a heat source toward the flame to increase its spread rate across the wire insulation surface.

These results displaying how all the different wire types were affected by varying lengths of igniter exposure time are important because, as found by Huang *et al.* [29] and confirmed in Figure 4.5, the wire samples generally take longer to ignite at lower pressures. Thus, if the ignition

time to be used across all experiments were to be based on the ignition time required by the most difficult to ignite wire sample type in the harshest environment, using that same igniter time in more combustion friendly environments with easier to ignite samples could bias the results by inputting excess heat into the wires and affecting the flame spread rate.

## 4.4 Conclusions on Effect of Igniter Exposure Time

The discussed results clearly show that an effect is observed for certain, highly conductive wire types, where increased igniter exposure time results in faster flame spread rates. Despite knowing that the igniter exposure time can affect the flame spread rate of certain wire sample types, it would still be extremely difficult to disentangle the effect of excess heat inputted into the sample from the igniter versus the effect of environmental conditions on the flammability of these wires. As such, additional research and analyses are needed to further quantify the effect of igniter exposure time on flame spread rate along electrical wires and to develop an ignition method that allows for consistent results for these highly conductive wire types across all environments of interest. Unfortunately, these endeavors were considered to be beyond the scope of this work.

Moving forward, it is still desirable to only consider how heat from the flame itself, rather than excess heat inputted into the wire by the igniter, and the environmental conditions affect the flame spread rate. In this work, the igniter should be used just as a tool to initiate the experiments rather than affect their results. Therefore, to simplify the problem in subsequent experiments with variations in ambient pressure as well as oxygen concentration, only type A wire samples were utilized. Although sample types D and E also showed not to be affected by igniter exposure time, due to time constraints as well as a desire to more closely mimic actual electrical wires, these sample types were also not used moving forward.

# Chapter 5. Effect of Pressure

## 5.1 Motivation and Prior Research on the Effect of Pressure

As has been discussed above, several previous studies have investigated the effect of many parameters on wire burning, including various wire characteristics, environmental conditions, and geometries. However, there are only a limited number of studies which have examined the effect of ambient pressure, specifically sub-atmospheric, on wire flame spread [12, 23, 24, 51, 52]. This research is important because it has previously been found that low pressure environments can approximately mimic results found in microgravity environments [10, 11, 12]. Among the studies that have examined the effect of pressure on wire flammability, Nakamura *et al.* [23] found flame spread rate to increase with decreasing pressure for wires with nichrome cores. However, in the same study, iron wires were also examined, and it was found that the flame spread rate along these wires remained constant with varying pressure, showing that flame spread behavior at different pressures can vary for different core materials.

Zhao *et al.* [51] performed experiments with wires containing copper cores and found that the flame spread rate decreased with decreasing pressure. Hu *et al.* [52] studied the flame spread of both copper and nichrome wires, and it was again confirmed that flame spread over nichrome wires increases with decreasing pressure. The results for flame spread over the copper wires were more interesting, however, as it was found that there was an initial decrease in flame spread rate with pressure, and further decreasing the pressure resulted in an increase in flame spread rate. Additionally, the effect was found to be less prominent as the core diameter increased, with a solely decreasing flame spread rate as pressure decreased being observed for a copper core with a diameter of 0.80 mm, as opposed to wire diameters of 0.30 or 0.50 mm in the same study.

Additionally, it is important to look at the combined effect of low-velocity forced flows and ambient pressure on flame spread because spacecrafts designed for human crews typically have low flows of 6 – 20 cm/s generated by their HVAC systems [8]. At the present, only one study has examined the combined effect of sub-atmospheric pressures and low opposed flows [24], and none have looked at the combined effect of sub-atmospheric pressures with concurrent flows. In the opposed flow and sub-atmospheric study, flame spread rate along nichrome wires was found to decrease at higher opposed flows and increase with decreasing pressure. For iron wires, the flame spread at first decreased but then remained constant for increasing opposed flows. The flame spread along these iron wires was also found to increase with decreasing pressure. While these results are informative, this work did not include any analysis of wires with high-conductivity cores, which are more similar to actual electrical wires.

Considering this study [24] and previous studies which did examined copper wires in sub-atmospheric pressures but in the absence of forced flow [51, 52], there are still some gaps in the knowledge regarding the effect of low pressure on flame spread along electrical wires. Moreover, it is thought that additional research concerning the described variables will bring more clarity to the available findings. Therefore, one of the goals of this analysis was to investigate the combined effect of sub-atmospheric ambient pressure and low forced flows on both opposed and concurrent flame spread over wires with high conductivity cores, such as copper. The insulation dripping off these wires was also analyzed under these conditions, since it is possible that the dripping affects the rate of flame spread and burning of insulated wires. Furthermore, since dripping does not

occur in the absence of gravity, these results are particularly relevant for comparison with similar experiments to be conducted in the ISS [6, 7].

## 5.2 Experimental Design

The experiments for this analysis were conducted using type A wire samples, as pictured in Figure 5.1 and identified in Table 2.1. Recall that sample type A wires consist of copper cores with diameters of 0.64 mm and insulation sheaths with outer diameters of 4 mm, corresponding to insulation thicknesses of 1.7 mm and average insulation masses of 1.13 g. To study the combined effect of sub-atmospheric ambient pressure and low forced flow velocities on horizontal flame spread, four different pressure conditions and four different flow conditions were investigated. The pressure was varied from 40 to 100 kPa, with an average standard deviation of 0.2 kPa, in intervals of 20 kPa. At each of these pressures, the flow velocities were set to speeds of either 10 or 20 cm/s ± 0.5 cm/s parallel to the wire, and experiments were performed in both the opposed and concurrent configurations. Recall the setup of these configures by referring to Figure 3.2 and Figure 3.3, respectively. Experiments with each combination of pressure, flow speed, and flow direction were repeated a minimum of six times using air as the oxidizer.

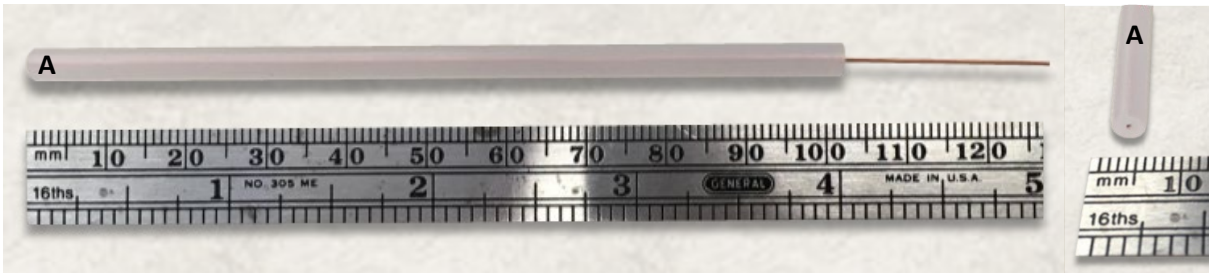


Figure 5.1 Wire sample type A used in combined forced flow and sub-atmospheric ambient pressure study.

## 5.3 Flame Spread Rate Results

Figure 5.2 shows the experimental results for the combined effect of reduced ambient pressure and low forced flow velocities on the flame spread rate along type A wire samples, with the opposed flow results being previously reported by Gagnon *et al.* [53]. The corresponding flame spread rate data and standard deviations are given in Table 5.1. This data shows a decrease in flame spread rate as the opposed flow speed was increased, agreeing with Nakamura *et al.* [24], which found flame spread rate to either decrease or remain constant, depending on wire core material, as the opposed flow speed was increased. However, regarding potential error in this analysis, it should be noted that the average uncertainty in the opposed flame spread rate data was calculated to be 0.06 mm/s (assuming an accuracy within 5 mm when tracking the positions of the flame front), which is comparable to the average 0.06 mm/s difference in the flame spread rate observed between the two tested opposed flow speeds, so more testing may be needed to confirm this effect.

Looking at the tests performed in concurrent flow, conditions show a similar effect on flame spread rate when changing the flow speed. However, because the flame is travelling in the same direction as the forced flow in this configuration, a small increase in flame spread rate now results

as the flow speed is increased. For this configuration, the uncertainty was calculated to be 0.08 mm/s, which is again on the order of magnitude of the average 0.05 mm/s difference between the two tested concurrent flow speeds, so more testing may be needed to verify this effect.

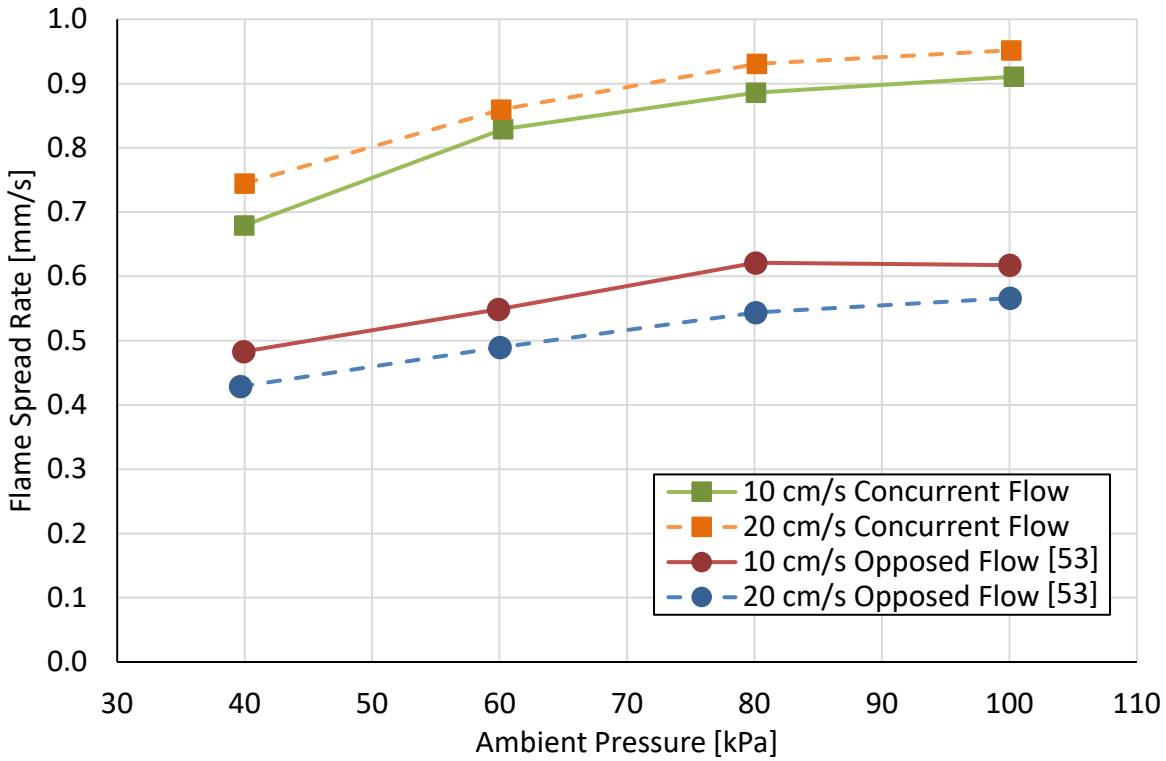


Figure 5.2 Effect of reduced ambient pressure and air flow speed on opposed and concurrent flame spread rate over type A LDPE-insulated copper wires.

Table 5.1 Average flame spread rate and standard deviations for wire sample type A under various pressure and flow velocity conditions.

| Forced Flow Velocity [cm/s] | Average Flame Spread Rate [mm/s] for Various Pressures | | | |
|---|---|---|---|---|
| | 40 kPa | 60 kPa | 80 kPa | 100 kPa |
| 20 cm/s, opposed | 0.43 ± 0.01 | 0.49 ± 0.02 | 0.54 ± 0.02 | 0.57 ± 0.03 |
| 10 cm/s, opposed | 0.48 ± 0.03 | 0.55 ± 0.02 | 0.62 ± 0.04 | 0.62 ± 0.04 |
| 10 cm/s, concurrent | 0.68 ± 0.03 | 0.83 ± 0.01 | 0.89 ± 0.02 | 0.91 ± 0.01 |
| 20 cm/s, concurrent | 0.74 ± 0.01 | 0.86 ± 0.01 | 0.93 ± 0.03 | 0.95 ± 0.02 |

While there is only a small effect present from changing the flow speed, there is a much larger effect from changing the flow direction, with an average difference of 0.26 mm/s between the flame spread rates exhibited by wires in 10 cm/s opposed versus concurrent flow, and a 0.37 mm/s difference on average between the flame spread rates exhibited by wires in 20 cm/s opposed versus concurrent flow. This result indicates that flow velocity has a significant impact on flame spread rate behavior, as was also observed previously when looking at the effect of flow velocity on various wire types, as shown in Figure 3.4.

Looking at the effect of pressure in Figure 5.2, the flame spread rate along the wire insulation was found to decrease as the pressure decreased across all flow conditions, which is consistent

with some previous findings [51]. As well, the aforementioned calculated flame spread rate uncertainties of 0.06 mm/s in the opposed configuration and 0.08 mm/s in the concurrent configuration are significantly less than the total variation in flame spread rate of 0.2 mm/s in opposed flow and 0.3 mm/s in concurrent flow across the range of tested ambient pressures, which confirms that reducing the pressure has a significant effect on the flame spread rate along these wires.

Interestingly, this trend showing reduced ambient pressure causing slower flame spread is in opposition to the trend of increasing flame spread rate with reduced ambient pressure observed by Nakamura *et al.* [24]. Because other studies looking at low-conductivity nichrome wires also saw this increase in flame spread rate with decreasing pressure [23, 52], it is thought that whether or not the flame spread increases or decreases with reduced pressure is dependent on the conductivity of the wire core and the relative thicknesses of the insulation and core. This idea is further confirmed by the agreement between the results of the work presented here and the study by Zhao *et al.* [51], which also showed the flame spread rate over copper wires to decrease with decreasing pressure. However, there is only partial agreement with the results of Hu *et al.* [52], which showed the flame spread rate along thin LDPE-insulated copper wires to first decrease then increase with decreasing pressure. It is still uncertain why the discrepancy between these results exists, as the wire size and absence of forced flow were the same as in the study by Zhao *et al.*, which did show full agreement with the present results.

## 5.4 Changes in Flame Appearance

It is thought that the joint effect of reduced ambient pressure and forced flow velocity on flame spread rate along electric wires is most likely due to a combination of their effect on the rate of heat transfer from the flame to the insulation and thermal contact with the wire core. However, because of the uncertainties discussed in the flame spread rate results, the exact effects of reduced pressure and flow velocity on flame spread behavior remain slightly ambiguous. Therefore, Figure 5.3 and Figure 5.4 [53] were developed to bring further understanding to the problem through visual means. Figure 5.3 shows the appearance of flames in concurrent flow as pressure varies, and Figure 5.4, as previously reported by Gagnon *et al.* [53], shows the appearance of flames in opposed flow as pressure varies. In these figures, it can be seen that the flame shape and strength both change with changes in ambient pressures and opposed or concurrent flow speeds.

These figures confirm that, as the flow speed increases in either the opposed or concurrent direction, the flame leans further towards the wire in the direction of flow. Therefore, while the flow speed effect on flame spread rate still needs to be confirmed through testing in both the opposed and concurrent flow regimes, the basis for this observation is most likely due to this leaning effect, as previously discussed in Chapter 3. To reiterate the ideas discussed there, increasing the flow speed decreases the flame height by pushing the flame closer to the wire. This increase in proximity to the wire increases the heat transfer from the flame to the wire. In the concurrent flow case, the increased heat transfer is to the fuel's surface, thus resulting in an increase in flame spread rate. In the opposed flow case, the increased heat transfer is to the bare end of the wire, where the heat can be conducted away and lost to the environment. The reason for such a small dependence on flow speed observed in these experiments may be due to the effect of buoyancy induced flows, which are on the order of 0.3 m/s [9] and larger than the low 0.1 to 0.2 m/s flows of the experiments. These buoyancy-induced flows, especially because they are of a higher magnitude than the forced flows, contribute to reducing the tilting of the flame.

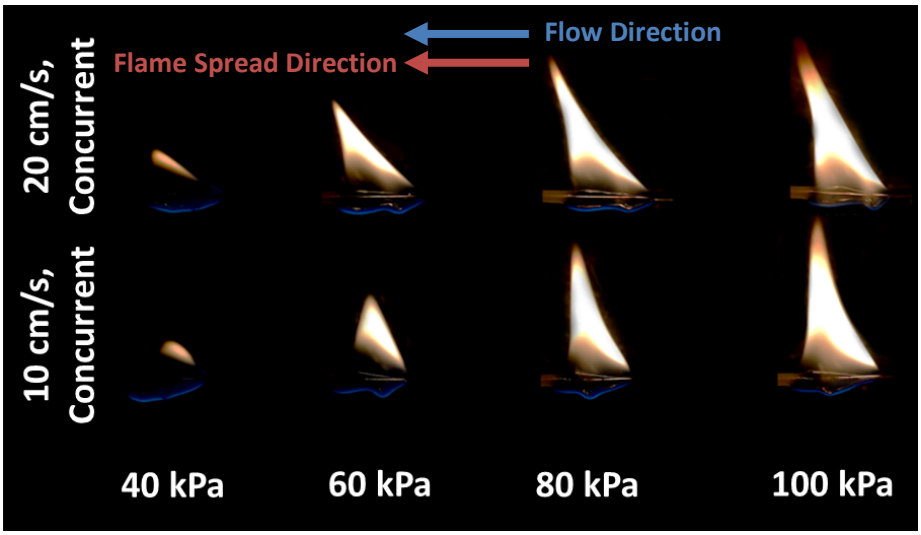


Figure 5.3 Effects of reduced ambient pressure (columns) and concurrent flow speeds (rows) on flame appearance of type A LDPE-insulated copper wires.

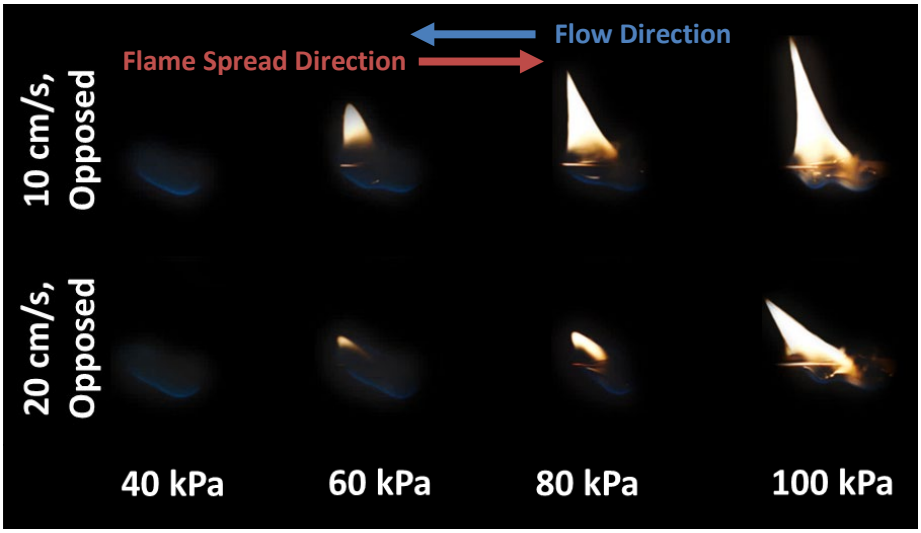


Figure 5.4 Effects of reduced ambient pressure (columns) and opposed flow speeds (rows) on flame appearance of type A LDPE-insulated copper wires [53].

Additionally, it can also be observed from these figures that the flame became less luminous and weaker at lower pressures, which agrees with previous studies [12, 23], and corresponds to the decrease in mass of insulation burned as these lower pressures, as will be discussed in the following section. Because the heat release rate decreases for weaker flames, the heat that is transferred from the flame into the wire insulation and core also deceases and thus, as discussed in a previous study [52], may be an explanation for the reduction in flame spread rate observed for high conductivity wires.

## 5.5 Dripping Results

### Analysis of Insulation Mass Loss due to Dripping versus Burning

Figure 5.5 shows the combined effect of reduced ambient pressure and flow velocity on the total mass burned or dripped of LDPE insulation from type A wire samples during flame spread, with the opposed flow results being previously reported by Gagnon *et al.* [53]. The corresponding values for mass loss due to dripping or burning as well as corresponding standard deviations are reported in Table 5.2 and Table 5.3, respectively. While there is no significant dependence on flow velocity, the trends in relation to pressure show that the total mass dripped per flame spread test decreased as the pressure increased, and correspondingly, the total mass burned per flame spread test showed the opposite result. The uncertainty of this data is quite low at only 0.001 g due to the precision of the utilized mass balance. Therefore, because the difference in total mass dripped across the range of pressures is on average 0.1 g, it was determined that pressure has a notable effect on the mass of molten insulation dripping from the wire during flame spread.

These results agree with those from previous studies [12], which found that LDPE insulation is burnt less in low-pressure environments, potentially due to the decrease in flame temperature caused by the reduction of the absolute amount of oxygen in the air. It may also be possible that a small part of the effect can be attributed to the wire core acting as a heat sink to an already weakened flame. As discussed in another previous study [24], when heat is transferred to the wire core from the flame, a fraction is conducted ahead of the flame into the pre-heat zone helping flame spread and burning, while a fraction is also conducted away along the bare end of the wire and subsequently lost to the ambient surroundings, hindering flame spread and burning.

If it is assumed that the relative fraction of heat transfer in each direction is constant across the tested conditions, increased heat transfer from the flame to the wire would mean more heat losses to the environment, but also a larger molten section of the preheat zone. A larger molten section of the preheat zone would provide more conducive conditions for dripping, explaining the increase in total mass dripped. Thus, the phenomena of decreased flame spread rate and increased total mass dripped with increased opposed flow velocity may be linked if they are indeed both caused by an increase in flame to metal core heat transfer.

### Analysis of Molten Insulation Dripping Frequency

Figure 5.6 shows the combined effect of reduced ambient pressure and air flow velocity on the dripping frequency of molten LDPE insulation from type A wire samples during flame spread, with the opposed flow results being previously reported by Gagnon *et al.* [53]. The corresponding drip frequency values as well as corresponding standard deviations are reported in Table 5.4. The trend displayed in this figure in relation to pressure shows that the frequency of dripping decreased as pressure decreased. The average uncertainty for each test condition, assuming a discrepancy of 2 drips either above or below the actual counted value, was calculated to be 0.03 drips/s, which is considerably smaller than the total variation of 0.2 drips/s observed on average for each flow condition across the range of ambient pressures tested. Therefore, the relationship between decreasing pressure and dripping frequency seems significant.

Interestingly, previous studies found that the insulation drip frequency increased with decreasing pressure [51, 12], which is in direct opposition to the present results. This discrepancy may be the result of the different wires used in the different studies. In these prior studies, thinner wires with core diameters of 0.50 mm were used, versus 0.64 mm in the current study, with thin

insulation thicknesses of 0.5 mm [51] and 0.15 mm [12], versus 1.7 mm thickness in the current study. This geometry difference corresponds to substantially more insulation mass per unit length of the wires in the current study. Furthermore, some experiments were only performed using nichrome wires [12], which have a significantly lower thermal conductivity than copper. Thus, it may not be possible to directly compare the different results, and more research is needed to determine how the wire properties, both core material and diameter as well as insulation thickness, impact the dripping behavior.

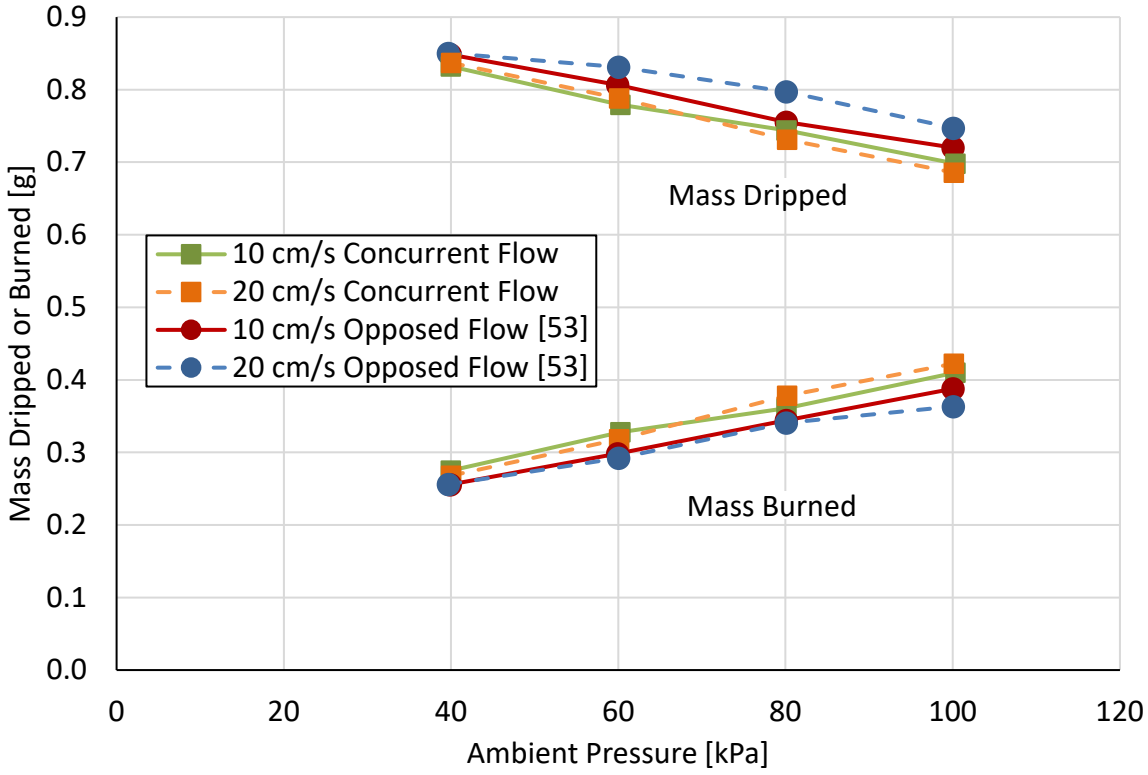


Figure 5.5 Effect of reduced ambient pressure and flow velocity on insulation mass loss due to dripping or burning of type A LDPE-insulated wires.

Table 5.2 Average insulation mass loss due to dripping and standard deviations for wire sample type A (initial mass of ~1.13 g) under various pressure and flow velocity conditions.

| Forced Flow Velocity [cm/s] | Average Mass Loss due to Dripping [g] for Various Pressures | | | |
|---|---|---|---|---|
| | 40 kPa | 60 kPa | 80 kPa | 100 kPa |
| 20 cm/s, opposed | 0.85 ± 0.01 | 0.83 ± 0.02 | 0.80 ± 0.01 | 0.75 ± 0.02 |
| 10 cm/s, opposed | 0.85 ± 0.01 | 0.81 ± 0.01 | 0.76 ± 0.02 | 0.72 ± 0.01 |
| 10 cm/s, concurrent | 0.83 ± 0.01 | 0.78 ± 0.02 | 0.74 ± 0.01 | 0.70 ± 0.04 |
| 20 cm/s, concurrent | 0.84 ± 0.02 | 0.79 ± 0.01 | 0.73 ± 0.02 | 0.69 ± 0.04 |

Now looking at the effect of flow velocity on dripping frequency, these results show some dependence on flow speed, but there is a much more significant jump in dripping frequency when the flow direction changed from opposed to concurrent flow. Comparing the total mass of insulation dripped results from Figure 5.5 with the frequency of insulation dripping from Figure 5.6, it is observed that higher flow velocities produced more frequent dripping with the

same total mass dripped as their lower flow velocity counterparts. Combined, these results imply that the size of the drips decreased with flow velocity. This result could again be due to the leaning effect of the flame. Bringing together some of the ideas brought forth in Chapter 3, the increased heat transfer from the leaning flame to the wire in concurrent flow may result in a warmer pyrolysis zone, thus decreasing the viscosity and surface tension of the molten LDPE insulation and aiding the ability of drips to form, hence the increase in dripping frequency and the smaller drop size. In opposed flow with the flame leaning away from the pyrolysis zone, the opposite effect occurs, increasing the viscosity and surface tension of the molten LDPE insulation, thus limiting the ability of drips to form.

Table 5.3 Average insulation mass loss due to burning and standard deviations for wire sample type A (initial mass of ~1.13 g) under various pressure and flow velocity conditions.

| Forced Flow Velocity [cm/s] | Average Mass Loss due to Burning [g] for Various Pressures | | | |
|---|---|---|---|---|
| | 40 kPa | 60 kPa | 80 kPa | 100 kPa |
| 20 cm/s, opposed | 0.26 ± 0.00 | 0.29 ± 0.02 | 0.34 ± 0.02 | 0.36 ± 0.02 |
| 10 cm/s, opposed | 0.26 ± 0.00 | 0.30 ± 0.02 | 0.34 ± 0.02 | 0.39 ± 0.01 |
| 10 cm/s, concurrent | 0.28 ± 0.01 | 0.33 ± 0.01 | 0.36 ± 0.2 | 0.41 ± 0.03 |
| 20 cm/s, concurrent | 0.27 ± 0.01 | 0.32 ± 0.01 | 0.38 ± 0.02 | 0.42 ± 0.03 |

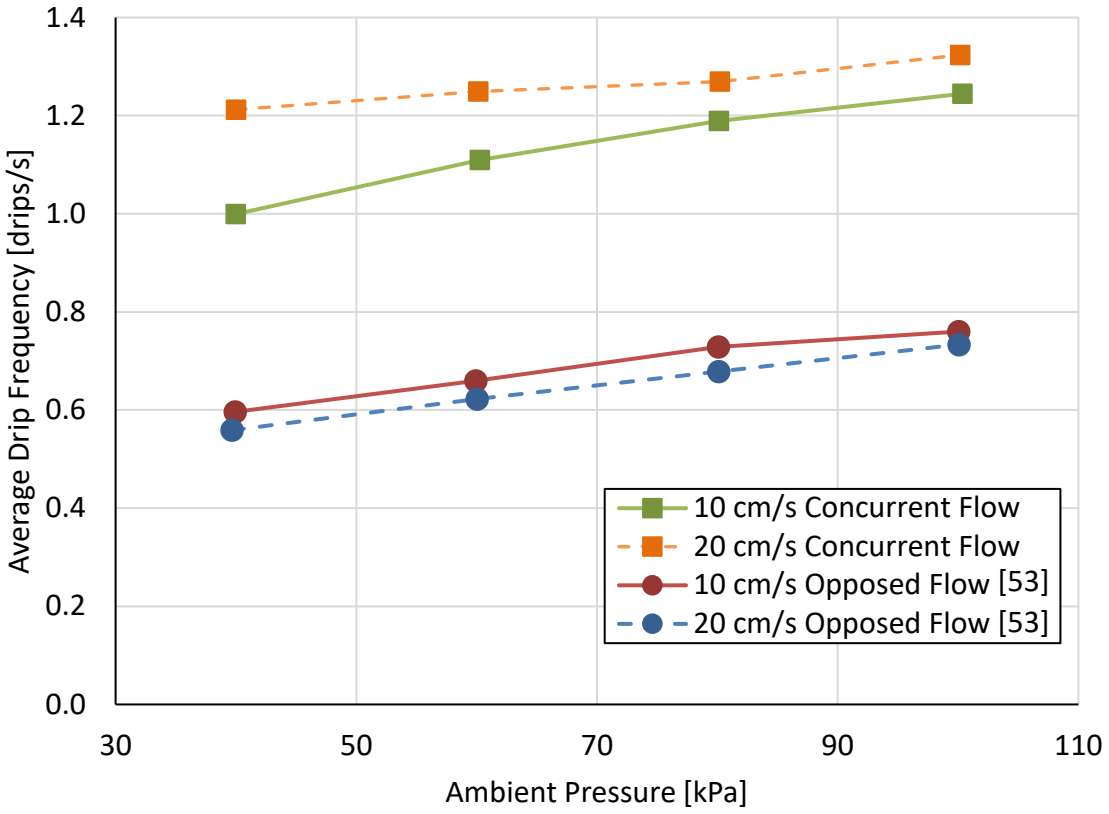


Figure 5.6 Effect of reduced ambient pressure and flow velocity on insulation dripping frequency of type A LDPE-insulated wires.

Table 5.4 Average molten insulation dripping frequency and standard deviations for wire sample type A under various pressure and flow velocity conditions.

| Forced Flow Velocity [cm/s] | Average Drip Frequency [drips/s] for Various Pressures | | | |
|---|---|---|---|---|
| | 40 kPa | 60 kPa | 80 kPa | 100 kPa |
| 20 cm/s, opposed | 0.56 ± 0.03 | 0.62 ± 0.01 | 0.68 ± 0.02 | 0.73 ± 0.05 |
| 10 cm/s, opposed | 0.60 ± 0.05 | 0.66 ± 0.02 | 0.73 ± 0.03 | 0.75 ± 0.04 |
| 10 cm/s, concurrent | 1.00 ± 0.05 | 1.11 ± 0.04 | 1.19 ± 0.05 | 1.24 ± 0.11 |
| 20 cm/s, concurrent | 1.21 ± 0.05 | 1.25 ± 0.06 | 1.27 ± 0.02 | 1.32 ± 0.09 |

## 5.6 Conclusions on Effect of Pressure

The combined effect of reducing the ambient pressure and exposure to various low forced flows on horizontal flame spread and dripping of type A wire samples was examined through experiments to increase understanding of the fire hazard electrical wires pose in spacecraft environments, and to provide data for comparison with future microgravity experiments. Results showed that the flame spread rate as well as the molten insulation dripping frequency decrease both with decreasing pressure and flow velocity. Contrarily, it was found that the total mass dripped increased with decreasing pressure and was not significantly affected by flow velocity. It is thought that these results may be due to variations in heat transfer to the insulation from the flame as well as from the core to the insulation. Comparison with results from other studies with wires of different core material or dimensions show that the effect of the environmental parameters on the flame spread and mass burning of insulated wires depends strongly on the core conductivity as well as core and insulation diameters. Consequently, data obtained from specific wire tests should not be extended to other wires without justification.

# Chapter 6. Effect of Oxygen Concentration

## 6.1 Motivation and Prior Research on the Effect of Oxygen Concentration

There have only been a limited number of prior investigations that have examined the effect of oxygen concentration on horizontal flame spread over electrical wires. Miyamoto *et al.* [28] examined horizontal flame spread over thick simulated electrical wires, both with and without external radiation, and found the flame spread rate to increase with increasing oxygen concentration. In addition, a couple studies by Fang *et al.* [54, 55] looked at the combined effect of reduced pressure and increased oxygen concentration on flame spread rate. In both these studies, effects of these varying conditions were investigated for various thin wire types. In one case, it was found that increased oxygen concentration caused the flame spread rate to increase but, interestingly, that increased pressure caused it to slightly decrease [54]. While these results mostly align with the other study by Fang *et al.* [55], some of the results from this other study also showed the flame spread rate to increase with pressure depending on the conductivity of the wire core and the oxygen concentration.

With such a limited number of studies in the field, it is highly desirable to further investigate the effect of oxygen concentration on the flame spread rate over horizontally oriented simulated electrical wires. Additionally, due to the lack of prior studies, there have been no investigations into the combined effects of oxygen concentration and pressure in environments with varying flow direction. One of the goals of this study is to examine the effect of all three of these environmental conditions on the flame spread rate of horizontal wires, as all of these conditions are important to the space exploration atmospheres of interest to this work.

## 6.2 Experimental Design

The experiments for this analysis were again conducted using type A wire samples, as pictured in Figure 6.1 and identified in Table 2.1. Recall that type A wire samples consist of copper cores with diameters of 0.64 mm and insulation sheaths with outer diameters of 4 mm, corresponding to insulation thicknesses of 1.7 mm. To study the combined effect of elevated oxygen concentration, sub-atmospheric ambient pressure, and low forced flow velocities, four different oxygen concentrations, pressure conditions, and flow velocities were investigated. The oxygen concentration was varied from 18% to 27% ± 0.2% in intervals of 3%, and the pressure was again varied from 40 to 100 kPa ± 0.2 kPa in intervals of 20 kPa.

At each combination of oxygen concentration and pressure, it was intended to perform experiments at each of four flow velocity conditions, which included flow speeds of either 10 or 20 cm/s ± 0.5 cm/s parallel to the wire in both the opposed and concurrent configurations. Recall the setup of these configurations by referring to Figure 3.2 and Figure 3.3, respectively. Unfortunately, due to lab closures as a result of the COVID-19 pandemic, the full set of experimental data was unable to be collected with many of the experiments at elevated oxygen concentrations going unperformed. This missing data is summarized in Table 6.1 and indicated by "N/A" in Table 6.2 through Table 6.5. For this same reason, a dripping analysis was not

completed for these experiments. Each combination of oxygen concentration, pressure, and flow velocity that were tested were repeated a minimum of three times.

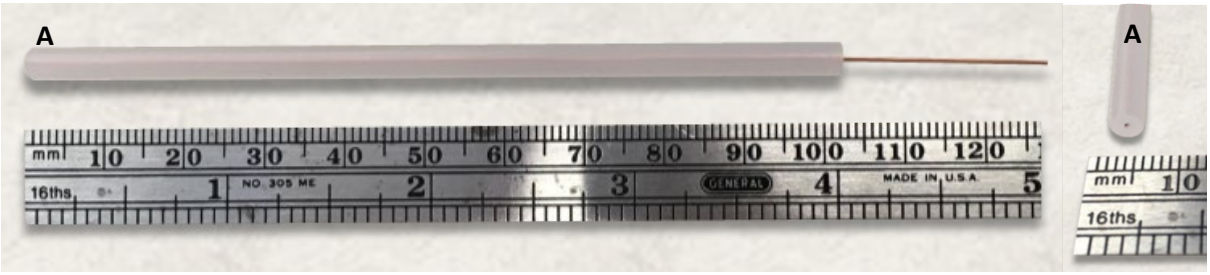


Figure 6.1 Wire sample type A used in combined forced flow, sub-atmospheric ambient pressure, and elevated oxygen concentration study.

Table 6.1 Summary of experimental matrix for this study with hollow shapes indicating unperformed experiments due to lab closures caused by the COVID-19 pandemic.

| Pressure | Oxygen Concentration | | | | | | | |
|---|---|---|---|---|---|---|---|---|
| | 18% | | 21% | | 24% | | 27% | |
| 40 kPa | ● | ▲ | ● | ▲ | ● | △ | ● | △ |
| | ■ | ⬟ | ■ | ⬟ | ■ | ⬟ | ■ | ⬟ |
| 60 kPa | ● | ▲ | ● | ▲ | ● | △ | ● | △ |
| | ■ | ⬟ | ■ | ⬟ | ■ | ⬠ | ■ | ⬠ |
| 80 kPa | ● | ▲ | ● | ▲ | ● | △ | ○ | △ |
| | ■ | ⬟ | ■ | ⬟ | ■ | ⬠ | □ | ⬠ |
| 100 kPa | ● | ▲ | ● | ▲ | ● | △ | ○ | △ |
| | ■ | ⬟ | ■ | ⬟ | ■ | ⬠ | □ | ⬠ |

| Flow Velocity Legend |
|---|
| 10 cm/s, opposed<br>Complete: ●, incomplete: ○ |
| 20 cm/s, opposed<br>Complete: ▲, incomplete: △ |
| 10 cm/s, concurrent<br>Complete: ■, incomplete: □ |
| 20 cm/s, concurrent<br>Complete: ⬟, incomplete: ⬠ |

## 6.3 Flame Spread Rate Results

The results for the data that was able to be collected prior to the lab closure is shown in Figure 6.2 and Figure 6.3 for opposed flame spread and concurrent flame spread, respectively. Table 6.2 and Table 6.3 contain the measured values for the opposed flame spread rates shown in Figure 6.2 as well as their corresponding standard deviations, for 10 cm/s and 20 cm/s flow speed, respectively. Table 6.4 and Table 6.5 contain the measured values for the concurrent flame spread rates shown in Figure 6.3 as well as their corresponding standard deviations for 10 cm/s and 20 cm/s flow speed, respectively.

From both of these plots, it was observed that the flame spread rate increases with oxygen concentration, which agrees with both the previous findings of Miyamoto *et al.* [28] and Fang *et al.* [54, 55] and is most likely due to the increase in flame temperature caused by the elevated oxygen concentration. Such an increase in temperature in turn increases the heat transfer from the flame to both the wire core and insulation. The increase in heat transfer from the flame to the insulation allows it to pyrolyze and burn more easily, while the increase in heat transfer from the flame to the core allows more heat to be conducted ahead of the wire and preheat the insulation before it is burned, as discussed in previous chapters. Adding to previous results from the literature, Figure 6.2 and Figure 6.3 also show that this trend of increasing flame spread rate with

increasing oxygen concentration holds true across all measured pressures and flow speeds for both opposed and concurrent flow.

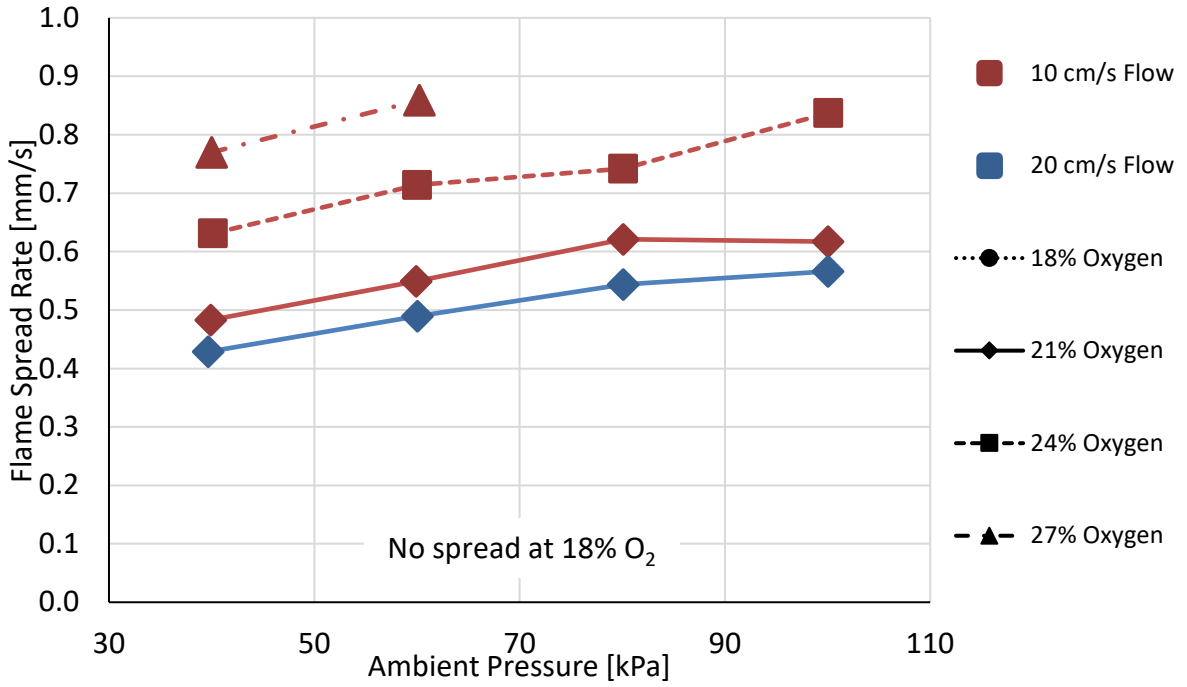


Figure 6.2 Dependence of flame spread rate over type A wire samples on pressure for different oxygen concentrations and opposed flow speeds.

Table 6.2 Dependence of flame spread rate over type A wire samples on pressure for different oxygen concentrations in 10 cm/s opposed flow.

| Oxygen Concentration | Average Flame Spread Rate [mm/s] for Various Pressures | | | |
|---|---|---|---|---|
| | 40 kPa | 60 kPa | 80 kPa | 100 kPa |
| 18% | - | - | - | - |
| 21% | 0.48 ± 0.03 | 0.55 ± 0.03 | 0.62 ± 0.08 | 0.62 ± 0.04 |
| 24% | 0.53 ± 0.02 | 0.71 ± 0.06 | 0.74 ± 0.07 | 0.84 ± 0.09 |
| 27% | 0.77 ± 0.04 | 0.86 ± 0.00 | N/A | N/A |

Table 6.3 Dependence of flame spread rate over type A wire samples on pressure for different oxygen concentrations in 20 cm/s opposed flow.

| Oxygen Concentration | Average Flame Spread Rate [mm/s] for Various Pressures | | | |
|---|---|---|---|---|
| | 40 kPa | 60 kPa | 80 kPa | 100 kPa |
| 18% | - | - | - | - |
| 21% | 0.43 ± 0.02 | 0.49 ± 0.03 | 0.54 ± 0.04 | 0.56 ± 0.06 |
| 24% | N/A | N/A | N/A | N/A |
| 27% | N/A | N/A | N/A | N/A |

Comparing the results from Fang *et al.* [54, 55] to previous studies which did not vary oxygen concentration [23, 24, 52], it can be observed that the trend for flame spread rate over low-conductivity nichrome wires to decrease with increasing pressure holds true across multiple

oxygen concentrations. However, further experiments performed by Fang *et al.* [55] with thin copper wires showed an increase in flame spread rate as pressure increased at an oxygen concentration of 30% and a mostly constant flame spread as pressure increased at an oxygen concentration of 21%. The results reported both in Figure 6.2 and Figure 6.3 and in Chapter 5 show increasing flame spread rate along high-conductivity copper wires with increasing pressure at 21% oxygen concentration, displaying disagreement with the results from Fang *et al.* [55]. The results from Fang *et al.* [55] also indicate that increasing the oxygen concentration results in a more dramatic increase of flame spread rate as the pressure increases. Unfortunately, this effect was unable to be confirmed with the current results due incomplete experiments at the higher end of the range of oxygen concentrations that were tested.

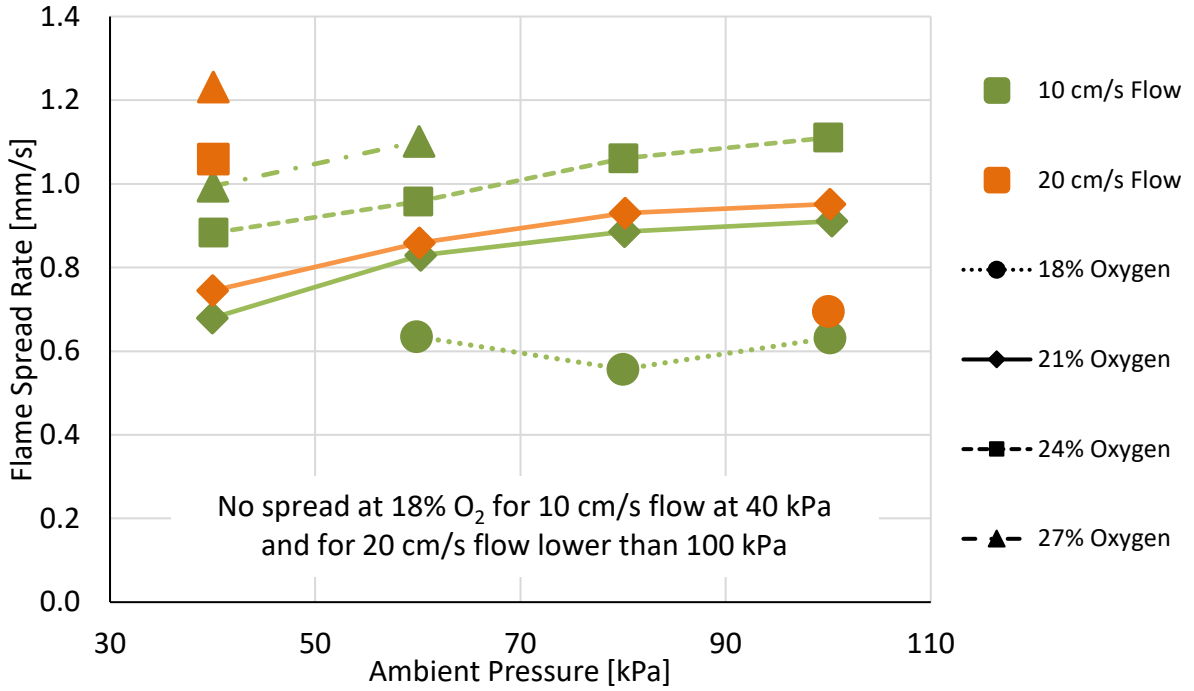


Figure 6.3 Dependence of flame spread rate over type A wire samples on pressure for different oxygen concentrations and concurrent flow speeds.

Table 6.4 Dependence of flame spread rate over type A wire samples on pressure for different oxygen concentrations in 10 cm/s concurrent flow.

| Oxygen Concentration | Average Flame Spread Rate [mm/s] for Various Pressures | | | |
|---|---|---|---|---|
| | 40 kPa | 60 kPa | 80 kPa | 100 kPa |
| 18% | - | 0.64 ± 0.11 | 0.56 ± 0.02 | 0.63 ± 0.00 |
| 21% | 0.68 ± 0.07 | 0.83 ± 0.02 | 0.89 ± 0.05 | 0.92 ± 0.03 |
| 24% | 0.88 ± 0.10 | 0.96 ± 0.09 | 1.06 ± 0.07 | 1.11 ± 0.04 |
| 27% | 1.00 ± 0.05 | 1.10 ± 0.08 | N/A | N/A |

Another observation that can be made from the presented results is that the limiting oxygen concentration, at least for burning the type A wires that were used in these experiments, appears to be somewhere between 18 and 21% for most pressures and flow velocities that were tested. For all opposed flow cases, no spread was seen across all pressures at 18% oxygen concentration, while full spread was observed for these same conditions at 21% oxygen concentration. For most

concurrent flow conditions, the same no spread behavior was observed. However, there was some spread observed under these concurrent conditions at higher pressures. While this spread was overall unsteady, it does indicate that the limiting oxygen concentration for these conditions is most likely around 18%

Table 6.5 Dependence of flame spread rate over type A wire samples on pressure for different oxygen concentrations in 20 cm/s concurrent flow.

| Oxygen Concentration | Average Flame Spread Rate [mm/s] for Various Pressures | | | |
|---|---|---|---|---|
| | 40 kPa | 60 kPa | 80 kPa | 100 kPa |
| 18% | - | - | - | 0.70 ± 0.00 |
| 21% | 0.75 ± 0.03 | 0.86 ± 0.02 | 0.93 ± 0.05 | 0.95 ± 0.04 |
| 24% | 1.06 ± 0.11 | N/A | N/A | N/A |
| 27% | 1.23 ± 0.12 | N/A | N/A | N/A |

Finally, while currently unconclusive due to lack of data, one interesting observation from these results is that, for the range of oxygen concentrations and pressures investigated, the oxygen concentration seems to have a greater effect on the flame spread rate than the pressure. This idea is indicated by, in some cases, the flame spreading at a faster rate for the elevated oxygen concentrations at even the lowest tested pressure than for sea-level pressure at 21% oxygen concentration. For example, at 40 kPa and 27% oxygen concentration in 10 cm/s opposed flow, the flame spread rate was 0.77 mm/s compared to 0.62 mm/s at 100 kPa and 21% oxygen concentration in the same flow condition. Such results were observed to a greater extent in concurrent flow. These results are precedented by Thomsen *et al.* [56], who found similar increases in flammability when burning PMMA cylinders in normoxic conditions.

## 6.4 Conclusions on Effect of Oxygen Concentration

Overall, results showed that flame spread rate along horizontal simulated electrical wires tends to increase with increasing oxygen concentration, agreeing with prior results [28, 54, 55]. It was also found that this increase in flame spread rate for increasing oxygen concentration occurred for all tested forced flow velocities and pressures. The limiting oxygen concentration for burning type A wire samples was identified to be between the range of 18 to 21% oxygen concentration but is most likely around 18%. Other trends identified by prior studies from the literature, such as the more drastic increase in flame spread rate along high-conductivity wires as pressure increases for higher oxygen concentrations [55], were unable to be confirmed due to an incomplete dataset for the current work. Similarly, the possible observation of elevated oxygen concentrations allowing for increased flame spread rates even at lower pressures compared to atmospheric sea-level conditions was also unable to be confirmed for this reason. Therefore, further research is required to more accurately record and understand the exact effects of oxygen concentration on flame spread rate over electrical wires.

# Chapter 7. Artificial Neural Network Model

## 7.1 Motivation for Developing Artificial Neural Network Model

As discussed previously, one of the main burning mechanisms this work uses to assess the flammability of wire insulation materials is flame spread rate. Recall that flame spread rate was chosen to characterize wire flammability because after a material is ignited, the rate of heat released by the fire is dependent on its rate of spread. There have been many previous studies which have analyzed analytical solutions to the flame spread rate along electrical wire problem. Among these studies, two of the most commonly cited models [28, 36, 37, 42, 47, 57], shown in Equations 7 and 8 (see List of Symbols for variable definitions), are derived simply from the fundamentals of flame spread [49, 58].

$$v_{\mathrm{f}} = \frac{\dot{q}''_{\mathrm{f}} l_{\mathrm{f}} + \dot{q}''_{\mathrm{c}} l_{\mathrm{c}} + \dot{q}''_{\mathrm{m}} l_{\mathrm{m}} - \dot{q}''_{\mathrm{s,r}} l_{\mathrm{h}}}{\rho_{\mathrm{i}} c_{\mathrm{i}} \delta_{\mathrm{i}} (T_{\mathrm{py}} - T_{\infty})} \tag{7}$$

$$v_{\mathrm{f}} = \frac{\dot{Q}_{\mathrm{f}\to\mathrm{i}} + \dot{Q}_{\mathrm{c}\to\mathrm{i}}}{(A_{\mathrm{i}} \rho_{\mathrm{i}} c_{\mathrm{p,i}} + A_{\mathrm{c}} \rho_{\mathrm{c}} c_{\mathrm{p,c}})(T_{\mathrm{py}} - T_{\infty})} \tag{8}$$

While these flame spread models bring great insight to the problem, unfortunately, they have shown varying success in their prediction capabilities, especially when variables of interest to this work, including forced flow, pressure, oxygen concentration, gravitational strength, and wire inclination deviate from the standard.

Other flame spread rate equations have also been explored [54, 59, 51] and still others have attempted to expand on the problem to account for parameters such as wire inclination [41, 40] and electrical current [40, 31]. However, there has yet to be found an all-encompassing equation for the flame spread rate along electrical wire problem. While the current work does not attempt to find such an equation, it does, for the first time in this field, bring together and unify the current existing database of results for flame spread rate along electrical wires from the available literature. This comprehensive database includes flame spread rate data from the works of Fang *et al.* [54, 55], Fujita *et at.* [20], Gagnon *et al.* [53], Hu *et al.* [41, 52], Kikuchi *et al.* [18], Kobayashi *et al.* [36, 57], Konno *et al.* [26, 37, 38], Lim *et al.* [32], Lu *et al.* [39, 47], Ma *et al.* [42], Miyamoto *et al.* [28], Nagachi *et al.* [35], Nakamura *et al.* [12, 23, 24], Takahashi *et al.* [33], Wang *et al.* [59, 31], and Zhao *et al.* [40, 51] as well as the data reported in the previous chapters of this work.

Altogether, the comprehensive database used for analysis in this study consisted of approximately 1200 data points, with approximately one third (400) coming from internal experiments reported in previous chapters and two thirds (800) coming from external sources. This information is provided in more detail in Table 7.1 and Table 7.2. This data was used in conjunction with an artificial neural network (ANN), developed by Gagnon *et al.* [60], to predict flame spread rate over various types of electrical wires under a wide range of conditions to further the understanding of the wire burning problem.

An artificial neural network was selected as the modelling method for this problem for several reasons. For context, this work regarding the effects of different SEA conditions on the burning behavior of electrical wires was originally intended to be highly experimental with the potential for some modeling work to accompany the experimental results at some point in the future. However, with the COVID-19 pandemic causing many changes, including interruptions to further

experimental work due to lab closures, a pivot toward modelling work was required earlier than anticipated.

While it was outside the scope of this work to evaluate all potential models that could be used for this problem, both an artificial neural network and a genetic algorithm (GA) were considered as options. Using a type of machine learning to model the wire burning problem was highly desirable because it was something that had never been done in this field before. In the end, the ANN was selected over the GA because it was believed that it would provide the most success for this problem. While the GA has many benefits, considering how many variables are of interest in the wire burning problem, there were concerns that the rigid equation form produced by the GA could be somewhat limiting. As well, ANNs are considered to be highly adaptable and tend to produce more accurate results.

Table 7.1 Summary of references used to create flame spread rate over electrical wire database (cont. in Table 7.2).

| 1st Author, Year, Ref # | Core Material | Insulation Material | Core Diameter [mm] | Insulation Thickness [mm] | Axial Flow Velocity [m/s] |
|---|---|---|---|---|---|
| Fang, 2020, [54] | NiCr | ETFE, PE | 0.50 | 0.15 | 0.0 |
| Fang, 2019, [55] | Cu, NiCr | PE | 0.50 | 0.15 | 0.0 |
| Fujita, 2002, [20] | NiCr | PE | 0.50 | varied | varied |
| Gagnon, 2020, [53] | Cu | LDPE | 0.64 | 1.7 | varied |
| Gagnon (current work) | varied | LDPE | varied | varied | varied |
| Hu, 2015, [41] | Cu | PE | varied | varied | 0.0 |
| Hu, 2019, [52] | Cu, NiCr | PE | varied | varied | 0.0 |
| Kikuchi, 1998, [18] | Cu | ETFE | 0.32 | 0.25 | 0.0 |
| Kobayashi, 2018, [36] | Cu, steel | HDPE, LDPE | varied | varied | varied |
| Kobayashi, 2020, [57] | Cu, steel | LDPE | 2.5 | 0.75 | 0.0 |
| Konno, 2019, [37] | Cu, NiCr | LDPE | 0.50 | 0.15 | -0.15 |
| Konno, 2020, [26] | Cu | LDPE | varied | varied | -0.10 |
| Konno, 2020, [38] | varied | LDPE | 0.50 | 0.15 | -0.04 |
| Lim, 2017, [32] | NiCr | PE | 0.50 | 0.15 | 0.0 |
| Lu, 2019, [47] | Cu | PE | varied | varied | varied |
| Lu, 2019, [39] | Cu | PE | 0.50 | 0.15 | varied |
| Ma, 2020, [42] | Cu, NiCr | PE | varied | varied | varied |
| Miyamoto, 2016, [28] | Cu, steel | HDPE, LDPE | varied | varied | -0.04 |
| Nagachi, 2019, [35] | Cu, NiCr | PE | 0.50 | 0.30 | varied |
| Nakamura, 2008, [12] | NiCr | PE | 0.50 | 0.15 | 0.0 |
| Nakamura, 2008, [24] | Fe, NiCr | PE | 0.50 | 0.15 | varied |
| Nakamura, 2009, [23] | Fe, NiCr | PE | 0.50 | 0.15 | 0.0 |
| Takahashi, 2013, [33] | NiCr | LDPE | 0.50 | 0.15 | varied |
| Wang, 2020, [59] | Cu | PE | varied | varied | 0.0 |
| Wang, 2020, [31] | Cu, NiCr | PE | 0.80 | 0.15 | 0.0 |
| Zhao, 2017, [51] | Cu | PE | 0.48 | 0.50 | 0.0 |
| Zhao, 2020, [40] | Cu | PE | 0.50 | 0.15 | 0.0 |

Table 7.2 Summary of references used to create flame spread rate over electrical wire database (cont. from Table 7.1).

| 1st Author, Year, Ref # | Gravitational Strength [g's] | Oxygen Concentration [%] | Ambient Pressure [kPa] | Wire Orientation | Data-points |
|---|---|---|---|---|---|
| Fang, 2020, [54] | 1 | varied | varied | horizontal | 30 |
| Fang, 2019, [55] | 1 | varied | varied | horizontal | 47 |
| Fujita, 2002, [20] | $10^{-5}$ | varied | 101 | - | 31 |
| Gagnon, 2020, [53] | 1 | 21 | varied | horizontal | 46 |
| Gagnon (current work) | 1 | varied | varied | horizontal | 319 |
| Hu, 2015, [41] | 1 | 21 | varied | varied | 80 |
| Hu, 2019, [52] | 1 | 21 | varied | horizontal | 40 |
| Kikuchi, 1998, [18] | varied | varied | 101 | horizontal | 9 |
| Kobayashi, 2018, [36] | 1 | varied | 101 | varied | 123 |
| Kobayashi, 2020, [57] | 1 | 21 | varied | horizontal | 20 |
| Konno, 2019, [37] | 1 | varied | 101 | vertical | 25 |
| Konno, 2020, [26] | 0.03 | varied | 101 | vertical | 10 |
| Konno, 2020, [38] | 1 | varied | 101 | vertical | 30 |
| Lim, 2017, [32] | 1 | 21 | 101 | varied | 17 |
| Lu, 2019, [47] | 1 | 21 | 101 | horizontal | 36 |
| Lu, 2019, [39] | 1 | 21 | 101 | varied | 48 |
| Ma, 2020, [42] | 1 | 21 | 101 | horizontal | 82 |
| Miyamoto, 2016, [28] | 1 | varied | 101 | vertical | 20 |
| Nagachi, 2019, [35] | 0.01 | varied | 101 | - | 30 |
| Nakamura, 2008, [12] | 1 | 21 | varied | horizontal | 6 |
| Nakamura, 2008, [24] | 1 | 21 | varied | horizontal | 34 |
| Nakamura, 2009, [23] | 1 | 21 | varied | horizontal | 16 |
| Takahashi, 2013, [33] | 0.01 | 17 | 101 | - | 4 |
| Wang, 2020, [59] | 1 | 21 | varied | horizontal | 12 |
| Wang, 2020, [31] | 1 | 21 | varied | horizontal | 15 |
| Zhao, 2017, [51] | 1 | 21 | varied | horizontal | 11 |
| Zhao, 2020, [40] | 1 | 21 | 101 | varied | 11 |

## 7.2 Artificial Neural Network Overview

The basics of an ANN can be thought of in terms of a single node or neuron, as shown in Figure 7.1. This node takes various inputs ($x_{i,j,k}$), multiplies them by weights ($w_{i,j,k}$), linearly combines those products along with a bias value ($b_{i,j}$), and inputs the result ($z_{i,j}$) into a non-linear activation function ($\sigma$), to determine the node output ($a_{i,j}$). Scaling up to a full-sized network, such as the example in Figure 7.2, this calculation is carried out for all nodes in the ANN. These nodes are typically arranged in layers, as shown in the figure, where the first layer takes in the relevant parameters to the problem; the middle layers are hidden, dense layers where the majority of the calculations take place; and the final layer produces the relevant output(s) for the problem. Using this arrangement of nodes, the outputs from every node in one layer become the inputs for each node in the next, as shown in Equation 9.

$$a_{i,j} = \begin{cases} x_{i+1,1,k} \\ \vdots \\ x_{i+1,j,k} \end{cases} \tag{9}$$

Once the calculations have been iterated through the entire ANN, one epoch is considered to have passed. This process is then repeated for multiple epochs with the weights and biases being adjusted each time to refine the ANN output, leading to more accurate predictions. Further explanation of the fundamentals of how an ANN works is given by Kröse and Smagt [61], the details of which are not covered here.

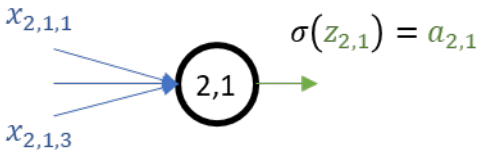


$$z_{2,1} = w_{2,1,1}x_{2,1,1} + w_{2,1,2}x_{2,1,2} + +w_{2,1,3}x_{2,1,3} + b_{2,1}$$

Figure 7.1 ANN single neuron schematic.

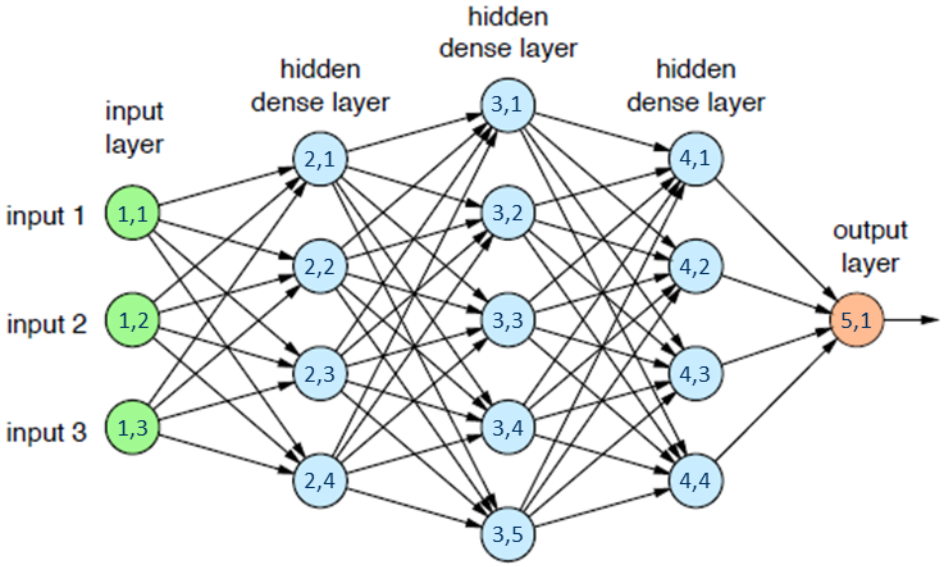


Figure 7.2 Example of more complex artificial neural network.

As can be imagined, the calculations for the ANN can get quite complex as the network gets more and more intricate. For example, take again the moderately complex network shown in Figure 7.2. A subsection of the series of equations required to calculate the output for this network is shown in Figure 7.3. Due to the shear number of nested equations required to calculate the output, ANN models do not result in an equation form that can be used to calculate the dependent variables of interest. Instead, as described, the independent variables are fed directly into the network itself, and the ANN is what produces the output of interest. Therefore, an equation such as the ones presented in Equations 7 and 8 and will not be determined through this method. However, because the results provided by the ANN are not held to the rigid structure of a particular equation, the results have the potential to be more accurate than models created by other methods.

$$\text{Output} = a_5 = \sigma(z_5)$$

$$\text{Output} = \sigma(w_{51}a_{41} + w_{52}a_{42} + w_{53}a_{43} + w_{54}a_{44} + b_5)$$

$$a_{41} = \sigma(w_{411}a_{31} + w_{412}a_{32} + w_{413}a_{33} + w_{414}a_{34} + w_{415}a_{35} + b_{41})$$

$$a_{31} = \sigma(w_{311}a_{21} + w_{312}a_{22} + w_{313}a_{23} + w_{314}a_{24} + b_{31})$$

$$a_{21} = \sigma(w_{211}a_{11} + w_{212}a_{12} + w_{213}a_{13} + b_{21})$$

$$a_{11} = \sigma(w_{11}\text{input}_1 + b_{11})$$

Figure 7.3 Subsection of the series of equations required to calculate the output for the example network given in Figure 7.2.

## 7.3 Structure

The structure of the ANN developed by Gagnon *et al.* [60] is shown in Figure 7.4 and was created with the open-source python package, Keras [62]. This ANN has four layers: an input layer, two hidden layers, and an output layer. The input layer consists of 15 nodes, corresponding to the 12 selected input parameters, as summarized in Table 7.3, two of which were vectors with multiple components, with each assigned its own node. Figure 7.4 is depicted as having 12 input nodes for simplicity. These input parameters were selected based on the variables considered to be important to the flame spread over electrical wire problem, particularly as it relates to SEAs. These variables consisted of wire characteristics, including the material properties of the core and insulation as well as their diameters and thicknesses, respectively, geometric parameters, including the direction of forced flow relative to flame spread and the orientation of the wire, and ambient conditions while burning, including oxygen concentration, ambient pressure, forced flow speed, and gravitational strength. How each of these variables were converted to input parameters is also shown in Table 7.3. Similarly, the output layer consists of only one node, corresponding to the single output parameter of interest, the flame spread rate.

Based on the number of input parameters, it was determined that two dense hidden layers with 12 nodes each should be used (again, Figure 7.4 is depicted with 9 for simplicity) in this ANN. Initially, the ANN was designed with three dense hidden layers, with the first and third dense layers each containing slightly more nodes than input layer and the second dense layer containing the most nodes. This structure was selected to mirror networks such as those depicted in Figure 7.2. However, after further review, it was decided to reduce the size and number of the hidden layers to be more appropriately sized and to ensure that the ANN would not be overly trained, a process that is described in the following section, and begin to memorize the data [63, 64, 65].

Finally, the chosen activation function was a hyperbolic tangent. Prior to the hyperbolic tangent function, a rectified linear unit activation function was used. However, the ANN was not able to converge while utilizing this activation function. After further analysis of this function, it was determined that the rectified linear unit activation function is not appropriate when negative input data is present. Therefore, the hyperbolic tangent function was selected because it adequately dealt with positive and negative input parameters, which are present in both the velocity and gravitational strength input vectors.

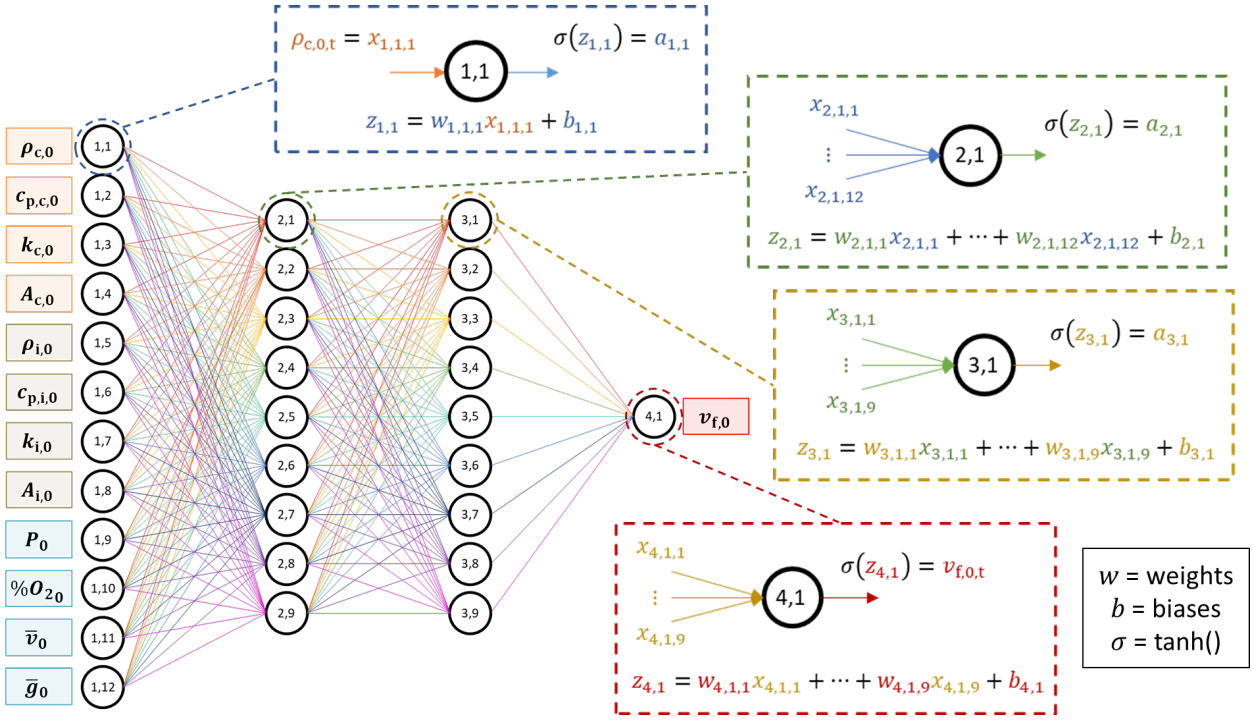


Figure 7.4 Visual representation of ANN used to predict flame spread rate across electrical wires [60].

Table 7.3 List of input parameters used in the ANN.

| Wire Burning Problem Variables | Input Parameter Name | Input Parameter Symbol |
|---|---|---|
| Core material | Wire core density<br>Wire core thermal conductivity<br>Wire core specific heat | $\rho_c$<br>$k_c$<br>$c_{p,c}$ |
| Core diameter | Wire core cross-sectional area | $A_c$ |
| Insulation material | Wire insulation density<br>Wire insulation thermal conductivity<br>Wire insulation specific heat | $\rho_i$<br>$k_i$<br>$c_{p,i}$ |
| Insulation thickness | Wire insulation cross-sectional area | $A_i$ |
| Oxygen concentration | Oxygen concentration | $\%O_2$ |
| Ambient pressure | Pressure | $P$ |
| Flow Speed<br>Flow Direction | Flow velocity vector | $\vec{v} = (v_x, v_y, v_z)$ |
| Gravitational Strength<br>Wire Orientation | Gravitational strength vector | $\vec{g} = (g_x, g_y)$ |

# 7.4 Training to Predict Flame Spread Rate

## Input Data

To take the developed ANN and use it to predict flame spread rate across various wire types in a multitude of environmental conditions and geometric configurations, it was taken through a training process using the data from the comprehensive data base summarized in Table 7.1 and Table 7.2. Experiments from all sources in the database were analogous to the ones presented in previous chapters of this work and were conducted with simulated electrical wires consisting of metal cores and plastic insulation sheaths. The represented core materials within this comprehensive database include copper, nichrome, iron, and stainless-steel tubing with diameters ranging from 0.30 to 5.5 mm, and the represented plastic insulation materials include and HDPE, LDPE, and ethylene tetrafluoroethylene (ETFE) with thicknesses ranging from 0.075 to 2.3 mm.

During testing, wires were also exposed to different ambient conditions, including varying flows, pressure, oxygen concentration, wire orientation, and gravitational strength. Flow velocities ranged from 3.5 m/s opposed to the flame spread direction to 6.8 m/s concurrent to the flame spread direction. Ambient pressures ranged from 10 kPa to 1000 kPa. Ambient oxygen concentrations ranged from 14% to 50%. Wire orientation/inclination ranged from horizontal to vertical. And finally, gravitational strengths ranged from $10^{-5}$g to 1g. These ranges of environmental parameters as well as wire sizes and compositions are summarized in Table 7.4.

Table 7.4 Wire material properties and sizes and environmental parameters spanned by the flame spread rate over electrical wire database.

| Parameter | Minimum Value | Maximum Value |
|---|---|---|
| $\rho_c$ | 7800 kg/m$^3$ (NiCr) | 8880 kg/m$^3$ (Cu) |
| $k_c$ | 17.4 W/m·K (steel) | 398 W/m·K (Cu) |
| $c_{p,c}$ | 390 J/kg·K (Cu) | 500 J/kg·K (steel) |
| $d_c$ | 0.30 mm | 5.5 mm |
| ↳ $A_c$ | ↳ 0.071 mm$^2$ | ↳ 24 mm$^2$ |
| $\rho_i$ | 923 kg/m$^3$ (LDPE) | 1700 kg/m$^3$ (ETFE) |
| $k_i$ | 0.238 W/m·K (ETFE) | 0.338 W/m·K (HDPE) |
| $c_{p,i}$ | 1800 J/kg·K (ETFE) | 2075 J/kg·K (HDPE) |
| $\tau$ | 0.075 mm | 2.3 mm |
| ↳ $A_i$ | ↳ 0.14 mm$^2$ | ↳ 40.6 mm$^2$ |
| $\%O_2$ | 14% | 50% |
| $P$ | 10 kPa | 1000 kPa |
| $\vec{v}$ | -3.5 m/s | 6.8 m/s |
| $\vec{g}$ | $10^{-5}$g | 1g |

It should be noted that some references from which data was gathered for use in the comprehensive flame spread rate along electrical wire database included other experimental parameters, such as dilution gas [18], external radiation [26, 28], or electric fields [31, 32, 33]. While those parameters are highly important to the wire flame spread rate problem, there were either too few data points or too much variation in experimental design for the current analysis. Therefore, any experimental data with parameters in addition to the ones listed in Table 7.3 were excluded.

## Training Process

The way in which this amalgamated dataset was used in conjunction with the ANN is shown in Figure 7.5, which depicts the full procedure of data preparation, then training, and finally validation of that training. The data preparation stage includes all the boxes in Figure 7.5 which are touching the black arrows, each of which is called out the subsequent process description. This stage involves transforming all the input data, as listed in Table 7.3, from the comprehensive database ("Input Parameters") as well as the corresponding experimentally gathered flame spread rate data ("Output Parameter") into normalized values ("Normalized Inputs"). This calculation is carried out by taking each data point of a specific parameter and dividing it by the corresponding median of that parameter ("Median Values of Inputs"). The result of this normalization allows the input data to the network to both be dimensionless and closer to unity, putting each parameter on the same order of magnitude.

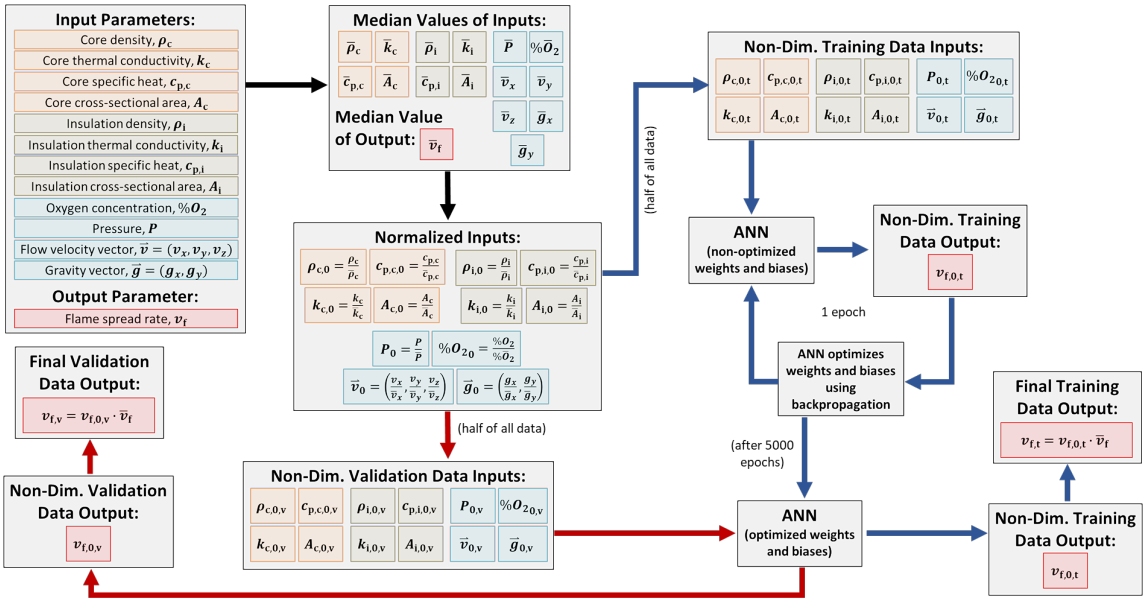


Figure 7.5 ANN flow chart showing stages for data preparation, training, and validation processes.

Next, the training stage occurs, which includes all the boxes in Figure 7.5 which are touching the blue arrows. First, the normalized input data ("Normalized Inputs") is split into two halves, where one half of the non-dimensional data is taken for use in training the process ("Non-Dim. Training Data Inputs"), while the remaining half is reserved for validation of the training ("Non-Dim. Training Data Inputs"). The calculations described in the previous section are then iterated through the entire network ("ANN (non-optimized weights and biases)") to obtain the network's first flame spread rate prediction ("Non-Dimensional Training Data Output"). To achieve more accurate flame spread rate predictions, the weight and bias values were refined ("ANN optimizes weights and biases using backpropagation") using the Root Mean Square Propagation (RMSprop) function, a popular gradient descent optimization algorithm which is reliable and fast in deep learning networks [66] within the Keras package. This process was continued over approximately 5,000 epochs, which allowed the resulting trained network to make satisfyingly accurate flame spread rate predictions ("ANN (optimized weights and biases)"). Finally, the non-dimensional output from the fully trained network ("Non-Dimensional Training Data Output")

was re-dimensionalized ("Final Training Data Output"), and the ANN's flame spread rate predictions could be compared to the experimentally obtained values.

## Training Results

Figure 7.6 provides the results from the ANN's training, with the ANN's predictions on the *y*-axis, the original experimental values on the *x*-axis, and the 45° line indicating a perfect flame spread rate prediction by the ANN. With an average error of 12%, the results show very strong agreement between the ANN's predictions and the experimentally measured values. However, it is expected to see good agreement between the predicted ANN flame spread rate and the experimental values, as this is the same data that was used to train the ANN. The true indication of the ANN's performance is revealed by the validation results, which is the focus of the next section.

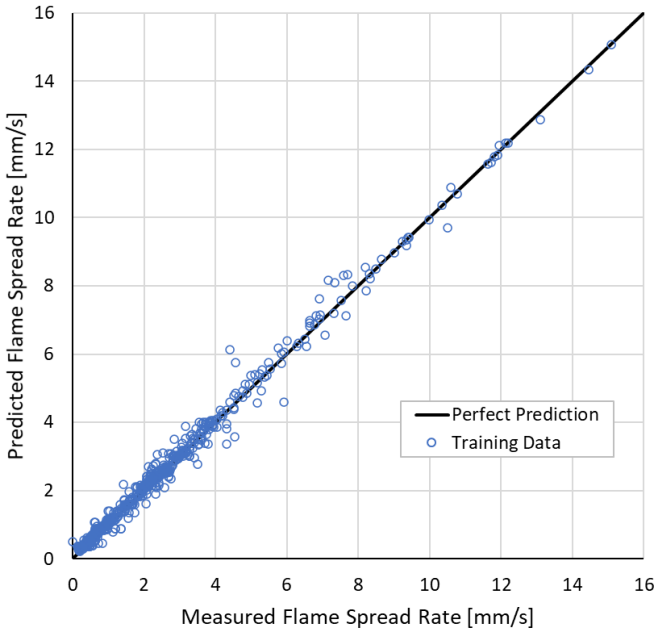


Figure 7.6 ANN training results comparing ANN predicted flame spread rate vs experimentally measured flame spread rate.

# 7.5 Validation of the Model

The validation stage includes all the boxes in Figure 7.5 that are touching the red arrows. Previously, the normalized input data ("Normalized Inputs") was split into two halves, where one half of the non-dimensional data was taken for use in training the process ("Non-Dim. Training Data Inputs"), and the remaining half was reserved for validation of the training ("Non-Dim. Training Data Inputs"). For validation, that reserved half of the normalized data is then input into the fully trained network ("ANN (optimized weights and biases)"), and calculations are iterated through the network for only one epoch to obtain the predicted, non-dimensional output flame spread rate ("Non-Dim. Validation Data Output"). In this stage, there is no need to run the network for more than one epoch because the weights and biases of the network have already been optimized in the training process and do not need to be refined any further. Finally, this non-

dimensional output data was re-dimensionalized ("Final Validation Data Output"), and the ANN's flame spread rate predictions could be compared to the experimentally obtained values. This comparison between predicted and experimental values is highly important for this stage because the point of the validation process is to test the ANN's capabilities with data it has never encountered before. Therefore, its performance can show whether or not the ANN is actually able to make predictions and has not just memorized the patterns found in the training data.

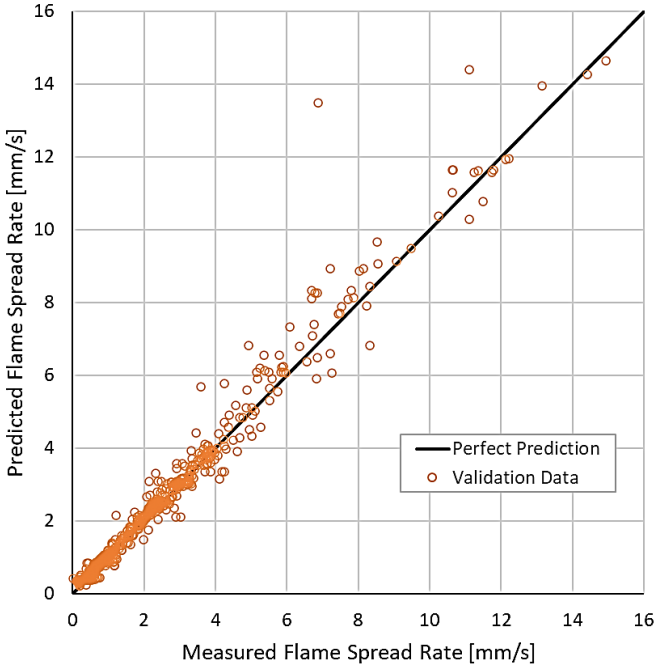


Figure 7.7 ANN validation results comparing ANN predicted flame spread rate vs experimentally measured flame spread rate.

Figure 7.7 provides the results of the ANN's validation. Again, strong agreement is observed between the ANN's predictions and the experimentally measured values, with an average error of 16% for data the ANN had never encountered before, effectively validating the training of the ANN. The strong agreement between the ANN predictions also gives the indication that the selected input parameters of core and insulation densities, thermal conductivities, specific heats, and cross-sectional areas, oxygen concentration, pressure, flow velocity, and gravitational strength are all highly important to the wire flame spread problem. Furthermore, such results prove that a comprehensive model of the available flame spread rate over electrical wire data in the field is possible to obtain. However, these results also show that there is great room for improvement in the ANN predictions.

## 7.6 Analysis of Outliers and Potential Improvements

By combining datasets from a multitude of sources at a scale that has never been done before and training an artificial neural network to predict flame spread rates across various types of electrical wires under many different ambient conditions, for the first time ever, results showed that it is possible to unify this wire flame spread problem. With an average error of 12% from the ANN's training results and 16% from the ANN's validation results, great potential is shown by the ANN to provide a comprehensive model of this problem.

However, while most of the predictions given by the ANN's validation results show good agreement with the measured values, there are two data points in Figure 7.7 which stand out from the rest. These two points show much higher predictions for flame spread rate given by the ANN than were measured experimentally. It is currently unknown exactly why these two data points in particular show such poor agreement between the measured and predicted values. Because these data points fall on the higher side of flame spread rate values, the first thought may be to assume that perhaps these data points represent experimental conditions that were unlike any the ANN had encountered before, and thus resulted in poor predictions. However, each of the input parameters for these data points fall well within the ranges previously cited for this dataset in Table 7.4.

While it is possible that experimental errors could have been made for these particular data points, this disagreement between the measured values and the ANN predicted values of flame spread rate in conjunction with the average 16% error rate is more likely indicating that there may be other input parameters necessary for the ANN to produce more accurate results.

One such input parameter may be more specific values for insulation material and thermal properties. While many of the data sources utilized some form of PE for the insulation, the precise type, HDPE or LDPE, was not always indicated, and specifications of the material properties were not always provided. As well, even when the type of PE was indicated and material properties were provided, there was a significant range in cited properties, such that different types of PE had nearly overlapping values. For example, densities cited for LDPE ranged from 920 to 940 $kg/m^3$, and densities cited for HDPE ranged from 944 to 959 $kg/m^3$.

Due to such variation and without cited values from each source, averages of the material and thermal properties for each insulation type were utilized as input parameters. As well, through necessity, whenever the insulation material was listed as PE with no material properties provided, it was assumed that it was of the low-density variety, as that is the more popular material of choice in the field. Since LDPE and HDPE have such different behavior during flame spread along their surfaces, particularly regarding melting and dripping, it is probable that with more precision in these parameters, the ANN's predictions could improve.

Looking at Equations 7 and 8, another obvious and easily measured potential additional input parameter can be identified: the temperature difference between the pyrolysis temperature of the insulation and the ambient temperature. Unfortunately, this is another situation of poorly cited information, with few sources providing data on ambient temperature during experiments or pyrolysis temperature for their specific insulation material. It is hoped that these issues can be resolved in future iterations of the ANN. However, creating a fully optimized model at this time was outside the scope of this work.

# Chapter 8. Model Flame Spread Predictions

## 8.1 Motivation for using Artificial Neural Network Predictions

While there is definitely room for improvement in the ANN model, that is not to say that nothing further can be learned from it in its current state. As stated in the previous chapter, one goal of using the artificial neural network was to be able to unify the current existing database of flame spread rate data along electrical wires from the available literature. Bringing together these works is desirable because it can help demonstrate whether or not different aspects of the wire burning problem can be thought of as a whole. For example, although analyzed side-by-side in this work, opposed and concurrent flow are normally considered to display different behavior from one another and are thus not usually directly compared. The same could be said for experiments including horizontal, vertical, and microgravity wires subject to flame spread, which are of particular interest to this study.

Another advantage provided by the artificial neural network is the ability to make predictions based on already existing data for experiments that have not yet been carried out. Using such predictions can help increase the resolution of the data from discrete points to a continuous dataset, as the ANN can provide results for many more conditions than are reasonable to analyze experimentally. The ANN predictions can also, to an extent, fill in the gaps of unobtained data, such as when a no forced flow condition was unable to be tested or in the case of the analysis described previously which varied oxygen concentration but was unable to be fully carried out due to disruptions to the experiments.

Additionally, making comparisons between predictions such as these and the experimentally obtained data could help in gaining more insight into the wire burning problem and increase understanding of differences in flame spread behavior. For example, the ANN could be used to compare microgravity and 1g gravity environments, even when extensive microgravity data is not available. However, caution does need to be exercised when analyzing the ANN predictions, as machine learning techniques, such as the ANN, mainly identify correlations between different variables, rather than causal relationships. Therefore, it should not be assumed that the ANN predictions are definitive results, but rather a starting place for further research while waiting for more experimental data, such as the wire burning data that will be returned from the ISS [6, 7], to verify the results.

## 8.2 Elaboration on Validation Results

Figure 8.1 shows the ANN validation results again, this time with data sets categorized based on reference origin. Analyzing such results confirms that there are no biases toward results from any particular source and that the ANN is able to capture the effects of all the different parameters that were varied across the range of experiments that were included in the network's training. Figure 8.2 and Figure 8.3 shed further light on the wire burning problem by separating the ANN's validation results into categories based on wire orientation. These results provide definitive proof that the wire flame spread problem that is so often investigated separately based on wire orientation and the strength of gravity can actually be viewed as one unified problem. The same is true for

opposed and concurrent flame spread, which are also both represented in the ANN results as well. The implications from this application of ANN are important because they demonstrate that this wire burning problem may be able to be analyzed more simplistically than the way it has been traditionally studied. These results also extend the concept proposed by Fernandez-Pello and Mao [67] for concurrent flame spread to other flame spread configurations as well. That concept being that the wire burning problem can be analyzed in a unified manner.

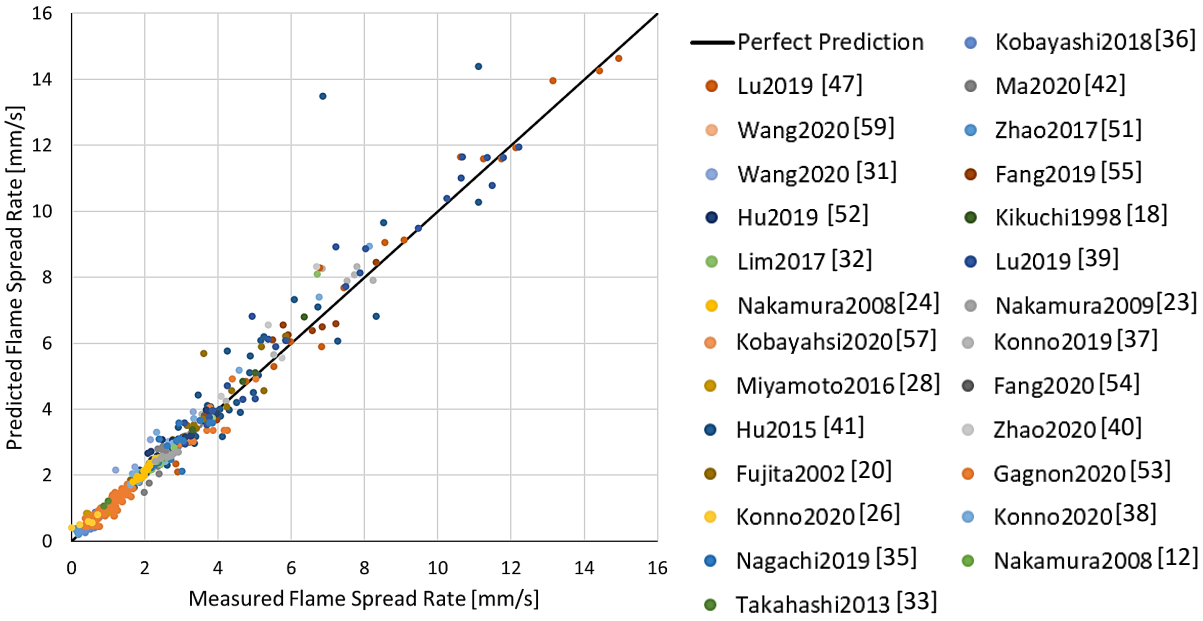


Figure 8.1 ANN validation results comparing ANN predicted flame spread rate versus experimentally measured flame spread rate with datasets distinguished by reference origin.

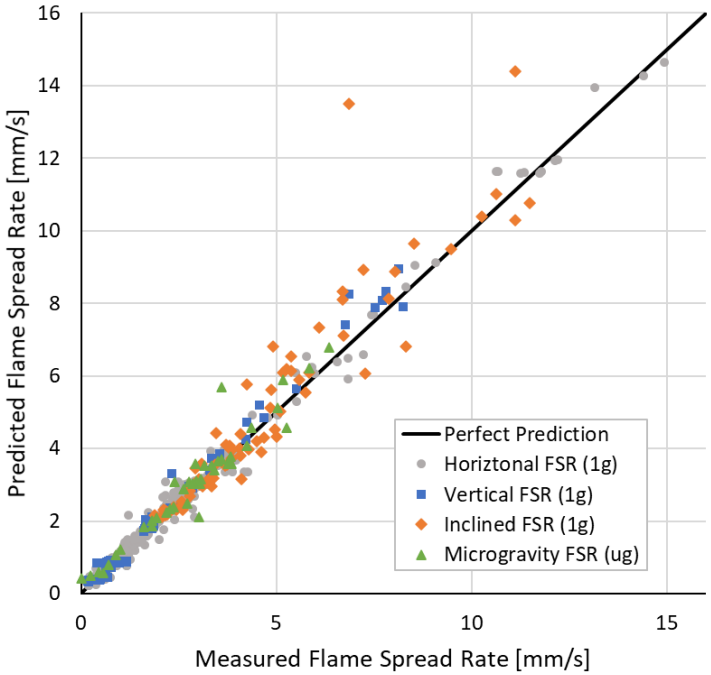


Figure 8.2 ANN validation results comparing ANN predicted flame spread rate versus experimentally measured flame spread rate with datasets distinguished by wire orientation.

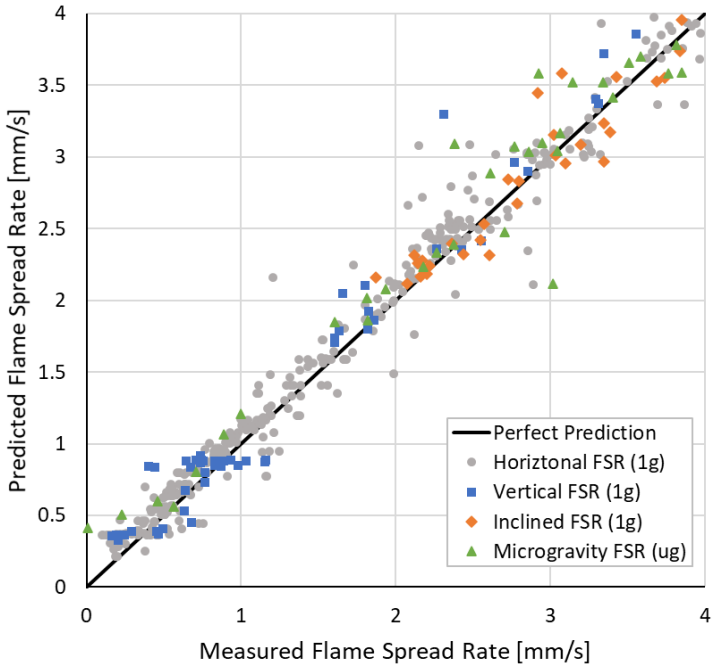


Figure 8.3 ANN validation results comparing ANN predicted flame spread rate versus experimentally measured flame spread rate focusing on the majority of results which fall between 0 and 4 mm/s with datasets distinguished by wire orientation.

## 8.3 Dependence on Wire Type

With these validations results, there can be some confidence that the ANN is able to make accurate flame spread rate predictions for different wire types under various environmental conditions to an extent. Therefore, as long as it is recalled that the ANN mainly results in correlations rather than causal relationships, it is possible to use the ANN to look at predicted parametric trends of flame spread rate and its dependence on environmental parameters of interest for various wire compositions, which can be used for preliminary analyses.

Figure 8.4 shows one such parametric trend: flame spread rate dependence on both insulation cross-sectional area and wire core thermal conductivity. It should be noted that to create this surface, a no forced flow condition, 100 kPa ambient pressure, and 21% oxygen concentration were used. Because the wire core conductivity was singled out as the only varying core property, the core diameter was fixed at 0.64 mm, the same diameter as the type A wire samples used throughout this work. For the same reason, the wire core density and specific heat were averaged for copper, iron, steel, and nichrome, which were the wire core materials used in the present and referenced studies. Therefore, a density of 8192 kg/m$^3$ and specific heat of 427 J/kg·K were used.

This parametric surface captures the dependence of flame spread rate on wire composition by looking at the variations due to both insulation cross-sectional area and wire core thermal conductivity. It is observed that as the wire insulation becomes thicker, the flame spread rate decreases. For low core thermal conductivities, the flame spread rate increased from about 0.5 to 2.1 mm/s, and for high core thermal conductivities, the flame spread rate increased from about 0.5 to just over 3.0 mm/s. These significant increases in flame spread rate are well over the 16% error rate found through the ANN validation process, lending some confidence to these predictions. Additionally, this trend of reduced flame spread rate observed alongside increasing wire insulation

thickness was also observed experimentally in Chapter 3, providing further confidence in these ANN predictions. Again, this trend of reduced flame spread rate with increasing insulation thickness is thought to most likely be due to the increased mass of insulation material required for the flame to heat and burn through.

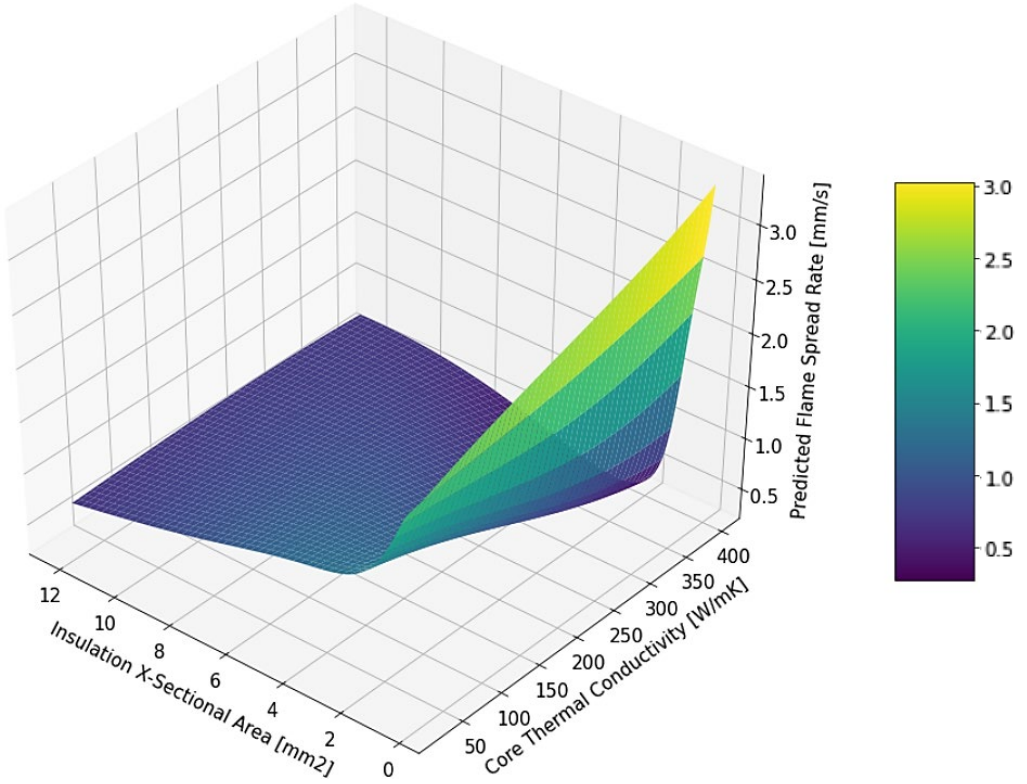


Figure 8.4 Parametric surface showing ANN horizontal flame spread rate predictions for varying insulation cross-sectional area and core thermal conductivities with no forced flow, 100 kPa ambient pressure, 21% oxygen concentration, and core diameter of 0.64 mm; other wire core properties averaged for copper, iron, steel, and nichrome ($\rho_c$ = 8192 kg/m$^3$, $c_{p,c}$ = 427 J/kg·K).

Figure 8.4 also shows that as the thermal conductivity of the core increases, the flame spread rate shows a significant increase, which was also observed in Chapter 3 for the no forced flow condition. It is thought that this effect is due to similar mechanisms which were postured about in pervious chapters. To reiterate, the wire core can act both as heat source and a heat sink. While the heat sink effect may be more dominant with the weakened flames observed in lower pressures, the heat source effect, being the wire core conducting heat ahead of the flame to preheat the unburned insulation, appears to be more dominant at the standard pressure of 100 kPa used to create this parametric surface. However, this effect seems to become less significant as the insulation thickness increases, which may be due to less effective preheating by the flame of such thick insulation.

## 8.4 Predicting Flame Spread Rate for Elevated Oxygen Concentrations

As discussed in Chapter 6, due to unfortunate circumstances, the set of experimental data regarding the effect of oxygen concentration on the flame spread rate over electrical wires was not able to be fully captured. While initial conclusions could be drawn from the incomplete work, there was still a desire to obtain a more complete picture of how variations in ambient oxygen concentration can affect flame spread rate. Thus, after the development of an ANN which can predict flame spread rate over electrical wires in a multitude of environmental conditions based on correlations between the different variables it picked up during training, the gaps within the previously gathered experimental data were examined through predictions made by the ANN.

The figures presented in this section are all predictions made by the ANN for the dependence of flame spread rate over type A wire samples, as identified in Table 2.1, on both oxygen concentration and ambient pressure. Recall that type A samples correspond to wires with copper core diameters of 0.64 mm and LDPE insulation thicknesses of 1.7 mm. Additionally, the ranges of oxygen concentration and pressure used to make these predictions mimic the ranges of experimental conditions from the study presented in Chapter 6.

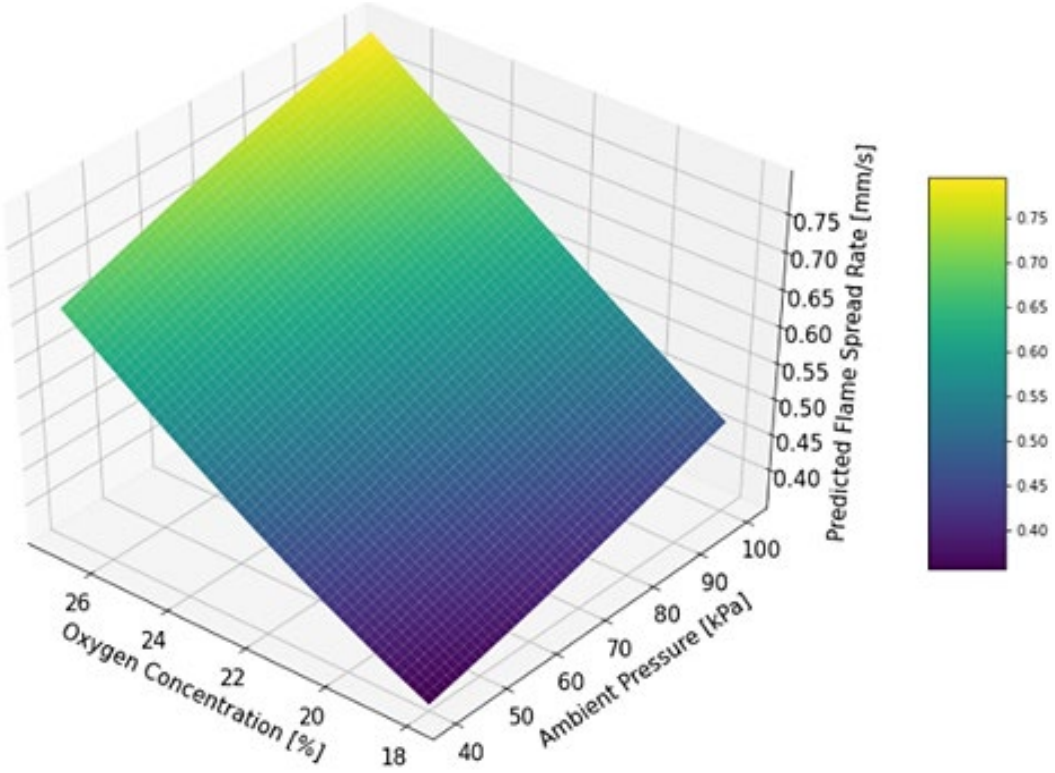


Figure 8.5 ANN-predicted parametric surface showing dependence of flame spread rate over type A wire samples on oxygen concentration and ambient pressure in 10 cm/s opposed flow.

Figure 8.5 and Figure 8.6 show parametric surfaces depicting the variation of flame spread rate as it changes with oxygen concentration and ambient pressure conditions with the wire samples being subject to 10 and 20 cm/s opposed flows, respectively. Figure 8.8 and Figure 8.9 show these same results but for wire samples being subject to 10 and 20 cm/s concurrent flows, respectively. Figure 8.7, for which the data is summarized in Table 8.1 and Table 8.2, shows discrete opposed

flame spread results from both Figure 8.5 and Figure 8.6 analogous to how the experimental results were presented in Chapter 6. Similarly Figure 8.10, for which the data for which is summarized in Table 8.3 and Table 8.4, gives the same discrete treatment to the concurrent flame spread results presented in Figure 8.8 and Figure 8.9.

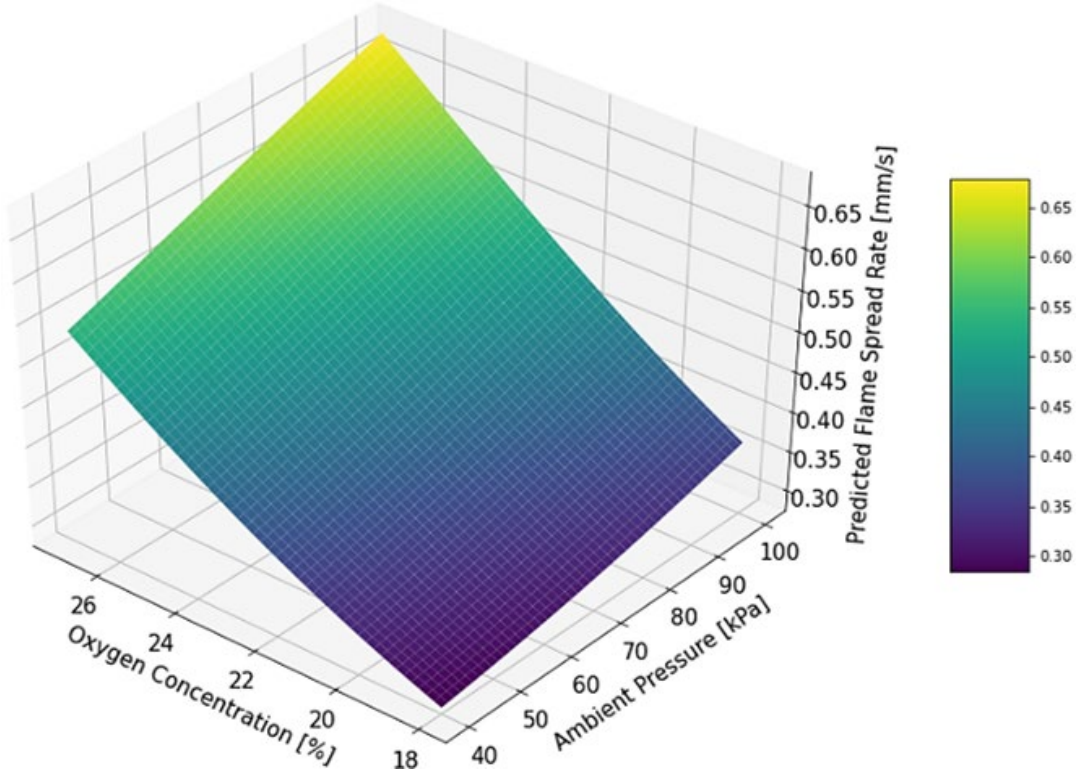


Figure 8.6 ANN-predicted parametric surface showing dependence of flame spread rate over type A wire samples on oxygen concentration and ambient pressure in 20 cm/s opposed flow.

All of these figures clearly display the expected trend for flame spread rate to increase both with increasing oxygen concentration and increasing pressure. Looking at more of the nuances of these graphs, it can be seen that Figure 8.5 and Figure 8.6 show that, for the range of conditions analyzed, opposed flame spread rate has a greater dependence on oxygen concentration than it does on the ambient pressure. Figure 8.8 and Figure 8.9 show the same trend for the concurrent flame spread rate as well. Such a result was unable to be confirmed previously by looking at the incomplete experimental data alone.

Another result that began to take shape but was not conclusive from the experimental data was the implication of this high dependence of flame spread rate on oxygen concentration. As shown in all the figures in this section, but which can be more clearly seen in Figure 8.7 for opposed spread and Figure 8.10 for concurrent spread, the flame spread rates for the elevated oxygen concentrations at even the lowest tested pressure of 40 kPa are faster than the flame spread rates occurring at 21% oxygen concentration and sea-level pressure. For example, the worst-case scenario is seen in 20 cm/s concurrent flow, where the flame spread rate occurring at 40 kPa in 27% oxygen concentration is predicted to be 1.09 mm/s comparted to 0.95 mm/s at 100 kPa in 21% oxygen concentration. On average, the flame spread rate at 40 kPa in 27% oxygen concentration was 0.11 mm/s faster than the flame spread rate at 100 kPa in 21% oxygen concentration across all flow conditions.

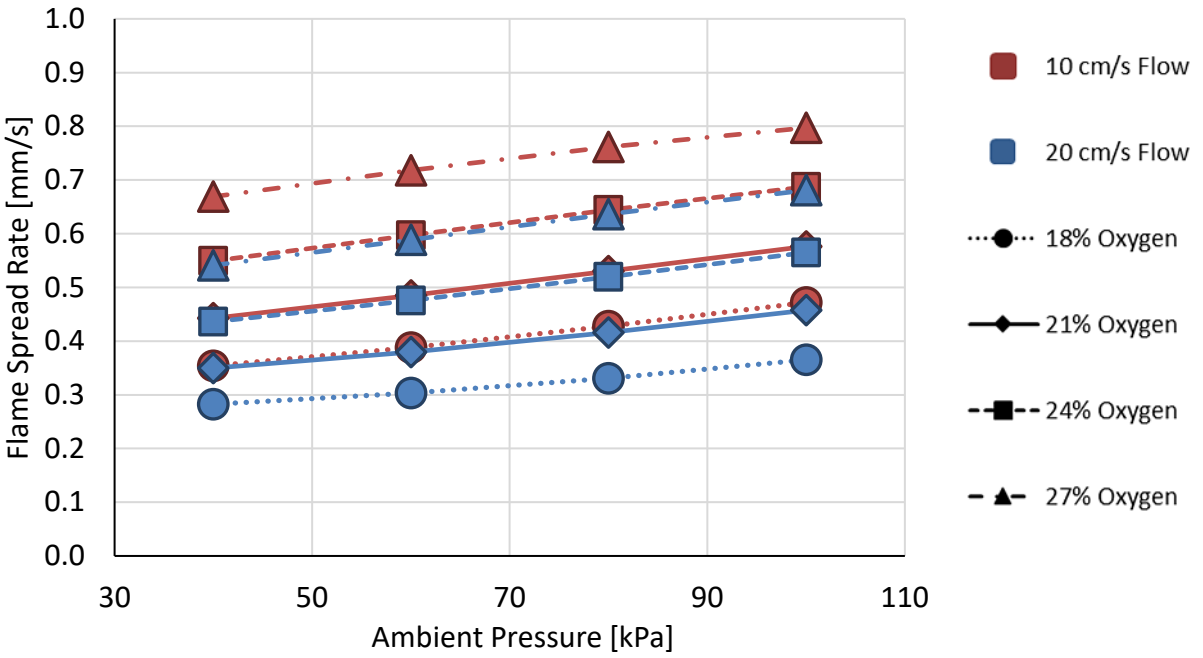


Figure 8.7 ANN predictions showing dependence of flame spread rate over type A wire samples on pressure for different oxygen concentration and opposed flow speeds.

Table 8.1 ANN-predicted dependence of flame spread rate over type A wire samples on pressure for different oxygen concentrations in 10 cm/s opposed flow.

| Oxygen Concentration | ANN-Predicted Flame Spread Rate [mm/s] for Various Pressures | | | |
|---|---|---|---|---|
| | 40 kPa | 60 kPa | 80 kPa | 100 kPa |
| 18% | 0.35 | 0.39 | 0.43 | 0.47 |
| 21% | 0.44 | 0.48 | 0.53 | 0.58 |
| 24% | 0.55 | 0.60 | 0.64 | 0.69 |
| 27% | 0.67 | 0.72 | 0.76 | 0.80 |

Table 8.2 ANN-predicted dependence of flame spread rate over type A wire samples on pressure for different oxygen concentrations in 20 cm/s opposed flow.

| Oxygen Concentration | ANN-Predicted Flame Spread Rate [mm/s] for Various Pressures | | | |
|---|---|---|---|---|
| | 40 kPa | 60 kPa | 80 kPa | 100 kPa |
| 18% | 0.28 | 0.30 | 0.33 | 0.37 |
| 21% | 0.35 | 0.38 | 0.42 | 0.46 |
| 24% | 0.44 | 0.48 | 0.52 | 0.56 |
| 27% | 0.54 | 0.59 | 0.64 | 0.68 |

These results are particularly relevant for the SEAs of interests, which, recall, are planned to operate under reduced pressure and elevated oxygen concentration conditions. Comparing the predictions for flame spread rate over simulated electrical wires in these environments show that the elevated oxygen concentration, despite the decrease in pressure, presents an elevated flammability risk. However, as shown in Figure 8.7, these results can be minimized if the forced flow is carefully implemented and balanced with only a slightly elevated oxygen concentration. The opposed flow results in this plot show the only predicted conditions for which the flame spread

rates at an elevated oxygen concentration but lower than sea-level pressure are actually slower than the flame spread rate in the standard atmospheric conditions. In 10 cm/s opposed flow at 40 kPa with 24% oxygen concentration, the flame spread rate was actually predicted to be 0.55 mm/s compared to 0.58 mm/s at 100 kPa with 21% oxygen concentration, and in 20 cm/s opposed flow at 40 kPa with 24% oxygen concentration, the flame spread rate was predicted to be 0.44 mm/s compared to 0.46 mm/s at 100 kPa with 21% oxygen concentration.

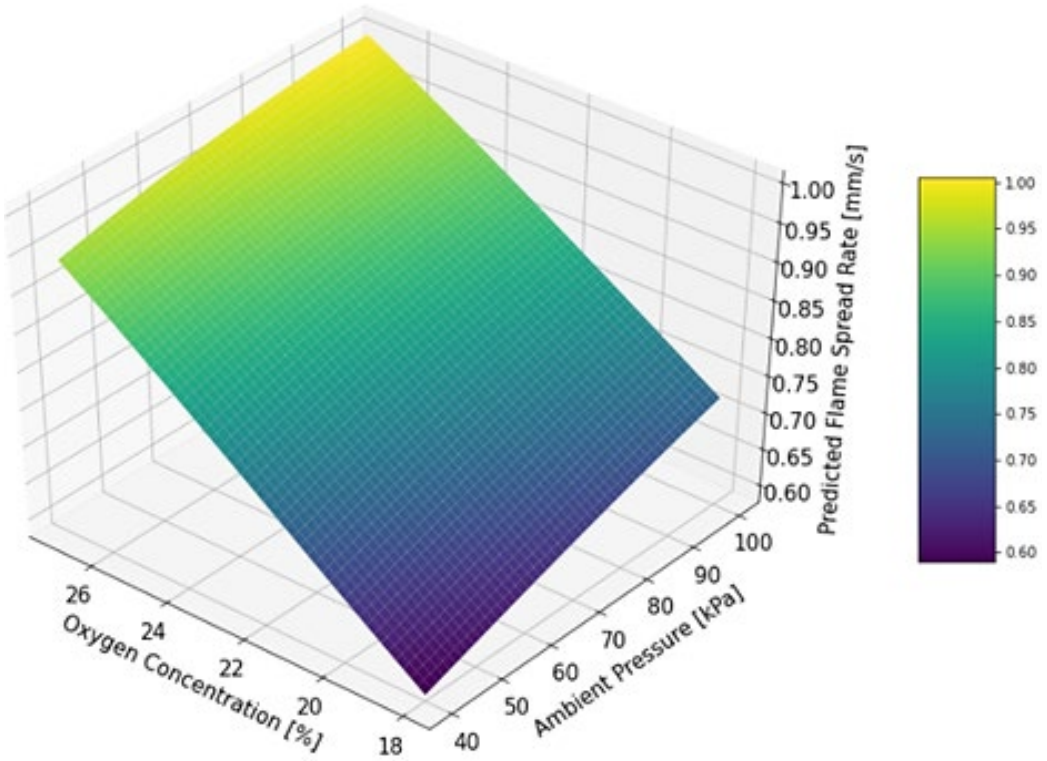


Figure 8.8 ANN-predicted parametric surface showing dependence of flame spread rate over type A wire samples on oxygen concentration and ambient pressure in 10 cm/s concurrent flow.

While these results for dependence of flame spread rate on oxygen concentration are highly interesting, they must be taken with a grain of salt. It must be remembered that the ANN predictions are not perfect. For the opposed case, for each examined oxygen concentration, there was a 19-34% change in flame spread rate across the range of pressures and flow conditions used, which is well above the 16% error rate of the ANN predictions from the validation process. However, for the concurrent case, for each examined oxygen concentration, there is only a 4.6-16% change in flame spread rate across the range of pressures and flow conditions used, which doesn't lend as much confidence to these predictions.

Additionally, the experimental results given in Figure 6.2 and Figure 6.3 both show that under 18% oxygen concentrations conditions, there was no flame spread rate observed for wires subject to opposed flows and limited flame spread rate observed for wires subject to concurrent flows, respectively. Comparing these results to the ones presented in this section indicate that the database from which the ANN was trained did not include enough data on blow-off limit conditions. Thus, the ANN has a clear weakness in its predictions where it is not able to accurately predict that flame spread would not actually occur in certain conditions, such as low enough

oxygen concentration. Therefore, it remains important to check the ANN's predictions against actual experimental results.

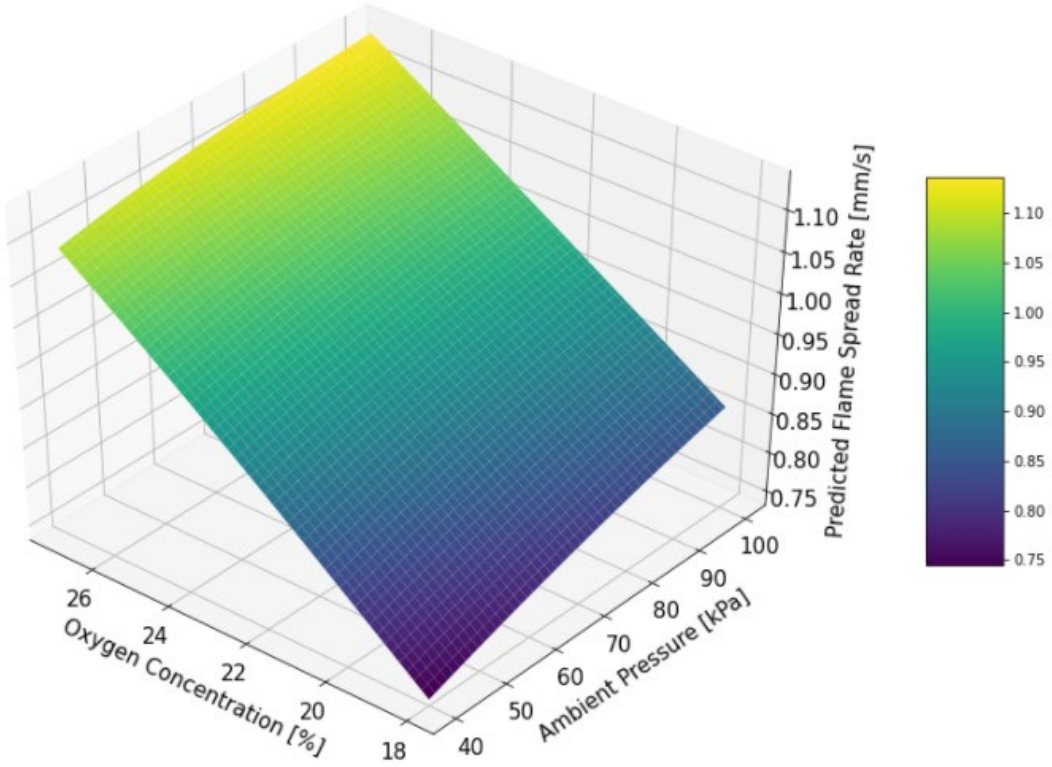


Figure 8.9 ANN-predicted parametric surface showing dependence of flame spread rate over type A wire samples on oxygen concentration and ambient pressure in 20 cm/s concurrent flow.

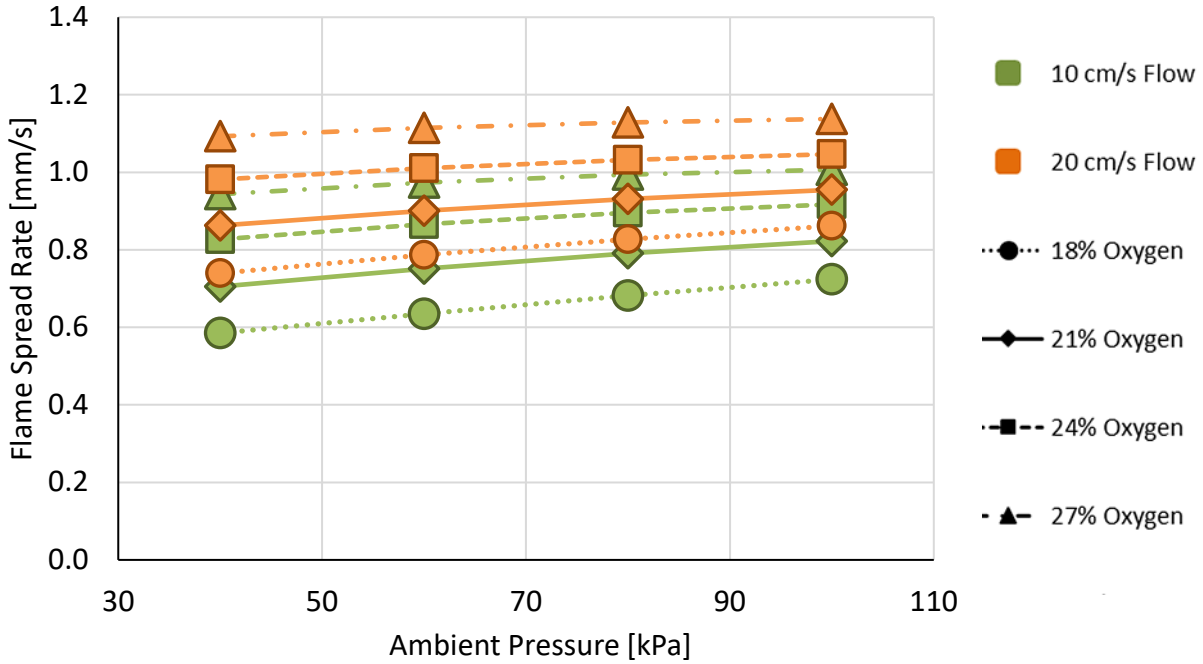


Figure 8.10 ANN predictions showing dependence of flame spread rate over type A wire samples on pressure for different oxygen concentration and concurrent flow speeds.

Table 8.3 ANN-predicted dependence of flame spread rate over type A wire samples on pressure for different oxygen concentrations in 10 cm/s concurrent flow.

| Oxygen Concentration | ANN-Predicted Flame Spread Rate [mm/s] for Various Pressures | | | |
|---|---|---|---|---|
| | 40 kPa | 60 kPa | 80 kPa | 100 kPa |
| 18% | 0.59 | 0.63 | 0.68 | 0.72 |
| 21% | 0.71 | 0.75 | 0.79 | 0.82 |
| 24% | 0.83 | 0.87 | 0.90 | 0.92 |
| 27% | 0.94 | 0.97 | 0.99 | 1.01 |

Table 8.4 ANN-predicted dependence of flame spread rate over type A wire samples on pressure for different oxygen concentrations in 20 cm/s concurrent flow.

| Oxygen Concentration | ANN-Predicted Flame Spread Rate [mm/s] for Various Pressures | | | |
|---|---|---|---|---|
| | 40 kPa | 60 kPa | 80 kPa | 100 kPa |
| 18% | 0.74 | 0.79 | 0.83 | 0.86 |
| 21% | 0.86 | 0.90 | 0.93 | 0.95 |
| 24% | 0.98 | 1.01 | 1.03 | 1.05 |
| 27% | 1.09 | 1.11 | 1.13 | 1.14 |

## 8.5 Predicting Flame Spread Rate for Reduced Pressures and Varying Flow Velocities

Looking at the analysis performed in Chapter 5, the ANN can help to expand upon these results regarding flame spread rate dependence on pressure and flow velocity. Figure 8.11 shows the ANN's predicted flame spread rate dependence on both ambient pressure and axial flow velocity. It should be noted that this surface was developed for type A wire samples, as identified in Table 2.1, with copper core diameters of 0.64 mm and LDPE insulation thicknesses of 1.7 mm, in 21% oxygen concentration.

From these predictions, the flame spread rate is observed to increase from 0.59 mm/s to 0.72 mm/s for highly opposed flows across the range of pressures analyzed and from 1.1 mm/s to 1.3 mm/s for highly concurrent flows across the range of pressures analyzed. These increases correspond to a 22% change in flame spread rate for the highly opposed case and an 18% change in flame spread rate for the highly concurrent case, which are both above the 16% error rate found for the ANN predictions through the validation process, lending some confidence to these predictions. Additionally, the trends observed in this surface reinforce the experimental results displayed in Figure 5.2. Just as was shown in that figure, here it can once again be observed that flame spread rate does indeed tend to increase both with increasing pressure and increasing flow velocity.

From this parametric surface, it can also be observed that, for the ranges of pressures and flow velocities analyzed, the flow velocity seems to have a greater impact on the flame spread rate than the pressure. This trend was also observed experimentally for this flow velocity range, as the forced concurrent flow is able to significantly increase the flame spread rate, while the forced opposed flow hinders it greatly. One interesting observation here is that there appears to be a smooth transition from opposed flame spread to concurrent flame spread. This trend was also

observed experimentally both in Figure 3.4 and Figure 5.2, and reinforces the idea that opposed and concurrent flame spread can be directly compared to one another.

Another trend that this surface confirms is that the dependence on flow velocity remains approximately constant for all the pressures within the observed range. In other words, the change in flame spread rate for different flow velocities as the pressure increases remains about the same. Although, there does appear to be a slight increase in this change in flame spread rate at higher pressures, meaning that the flame spread rate might increase at a slightly faster rate for increased flow velocity at these higher pressures.

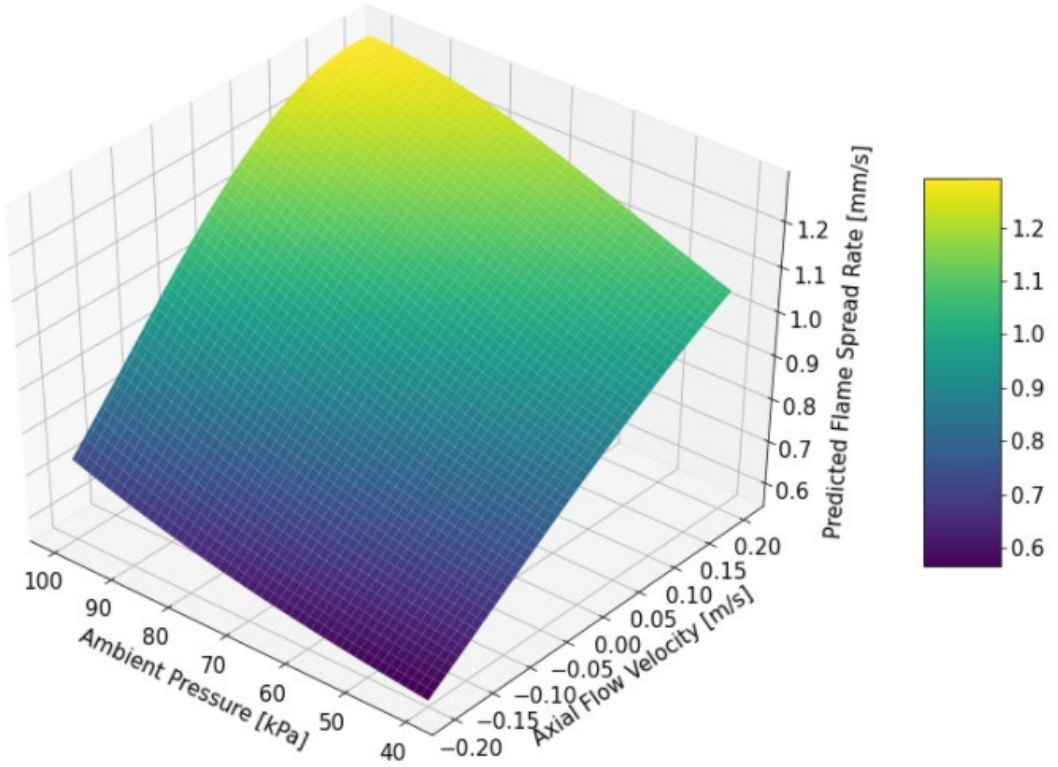


Figure 8.11 Parametric trends showing ANN horizontal flame spread rate predictions over type A wire samples for varying ambient pressures and axial flow velocities at 21% oxygen concentration.

# 8.6 Dependence on Gravitational Strength

Looking again to extend the analysis of Chapter 5, the ANN was also used to examine the dependence of flame spread rate on reduced ambient pressure and varying concurrent or opposed flow speeds for the type A wire samples in both a 1g environment and an estimated 0g environment. Recall, however, that the predictions made by the ANN are based off correlations rather than causal relationships, so the following analysis is just an initial look at potential flame spread rate results that must be verified through further experimental analysis. Continuing with this in mind, Figure 8.12 shows the concurrent flame spread rate results for these environments with varying gravitational strength, and Figure 8.14 shows the corresponding opposed flame spread rate results. Figure 8.13 takes the two concurrent spread surfaces in Figure 8.12 and subtracts the 0g flame spread rate results from the 1g flame spread rate results, so the difference

between the two can be seen more clearly. Figure 8.15 applies the same subtraction to the opposed flow surfaces given in Figure 8.14.

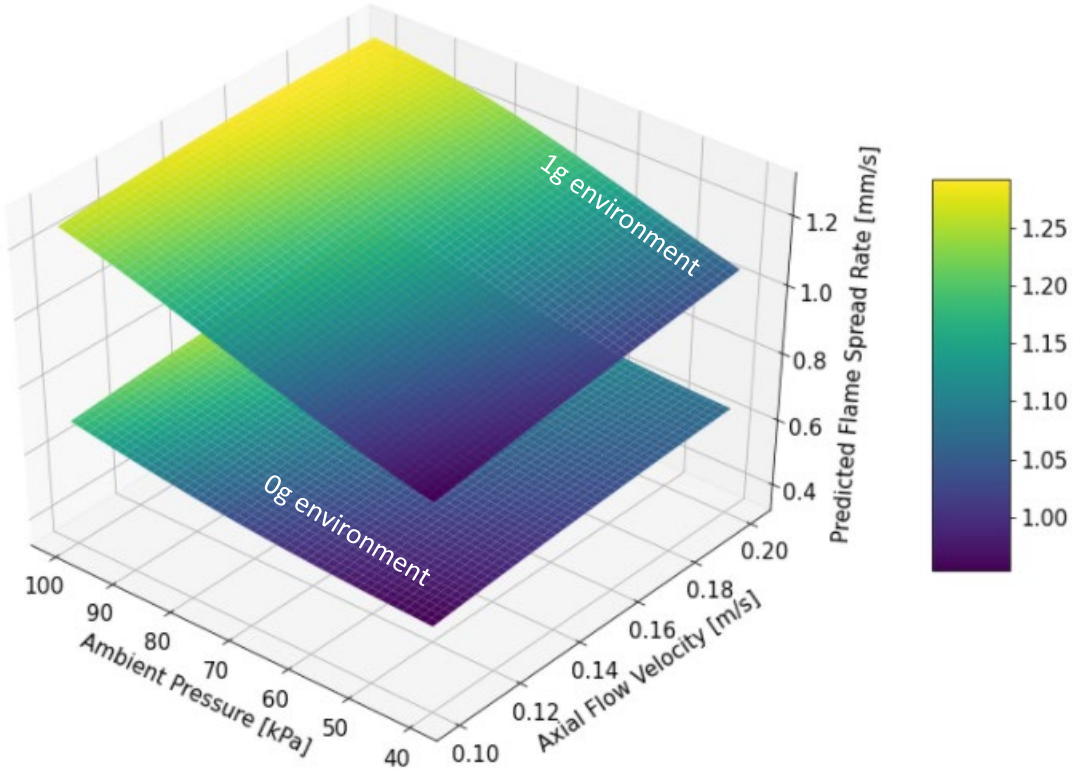


Figure 8.12 Parametric surfaces showing ANN flame spread rate predictions over type A wire samples for varying ambient pressure and concurrent flow speeds in 21% oxygen concentration and 1g (top surface) or 0g (bottom surface) environments.

Looking at the top surface in Figure 8.12, which reflects the 1g environment predictions, the flame spread rate is found to change by 32% for 10 cm/s flow and 22% for 20 cm/s flow across the range of pressures examined. Considering that these trends fall outside the 16% error range determined from the ANN validation process, some confidence can be had in these predictions. The trends also reinforce the concurrent flame spread rate results observed in Figure 5.2. As was found from the experimental work from the current study, the ANN accurately predicts that concurrent flame spread rate increases both with increasing pressure and increasing flow speed, with a much stronger dependence on the pressure and only a slight dependence on the flow speed for the ranges of those parameters viewed in the plot.

Looking at the bottom surface, which represents the estimated 0g gravity environment, the flame spread rate is again observed to decrease both with decreasing pressure and decreasing concurrent flow speed. This result is consistent with the finding of Nagachi *et al.* [35], who also found the flame spread rate over copper wires to decrease with reduced concurrent flow speed in a microgravity environment. Unfortunately, limited to no data is available for the effects of varying pressure on flame spread rate in microgravity. So, while the ANN predictions for the estimated microgravity environment are consistent with the 1g results presented in this work, and the flame spread rate under these conditions was predicted to change by 19% for 10 cm/s flow and 21% for 20 cm/s flow across the range or pressures examined, which is still above the 16% error

rate associated with the ANN predictions, these results must be analyzed with caution until they can be verified experimentally.

Despite these limitations of the ANN, it is still interesting to compare the two surfaces present in Figure 8.12 to get an initial idea of the differences between flame spread over electrical wires in a 1g vs estimated 0g environment. From this figure, it is observed that the ANN predicts the concurrent flame spread rate to be slower in a 0g environment. Recall it was discussed that the dripping effect observed in 1g environments does not occur in 0g environments and that this would cause discrepancies between experimental results in the two conditions. Because much of the material is dripping away in the 1g environment, the flame can spread faster compared to a 0g environment due to the reduced presence of material to burn through. This result was observed in Figure 8.4 as well, which showed that the flame spread rate increased as the insulation thickness decreased. This same effect is most likely contributing to a faster flame spread rate in the 1g environment as compared to a 0g environment with no dripping.

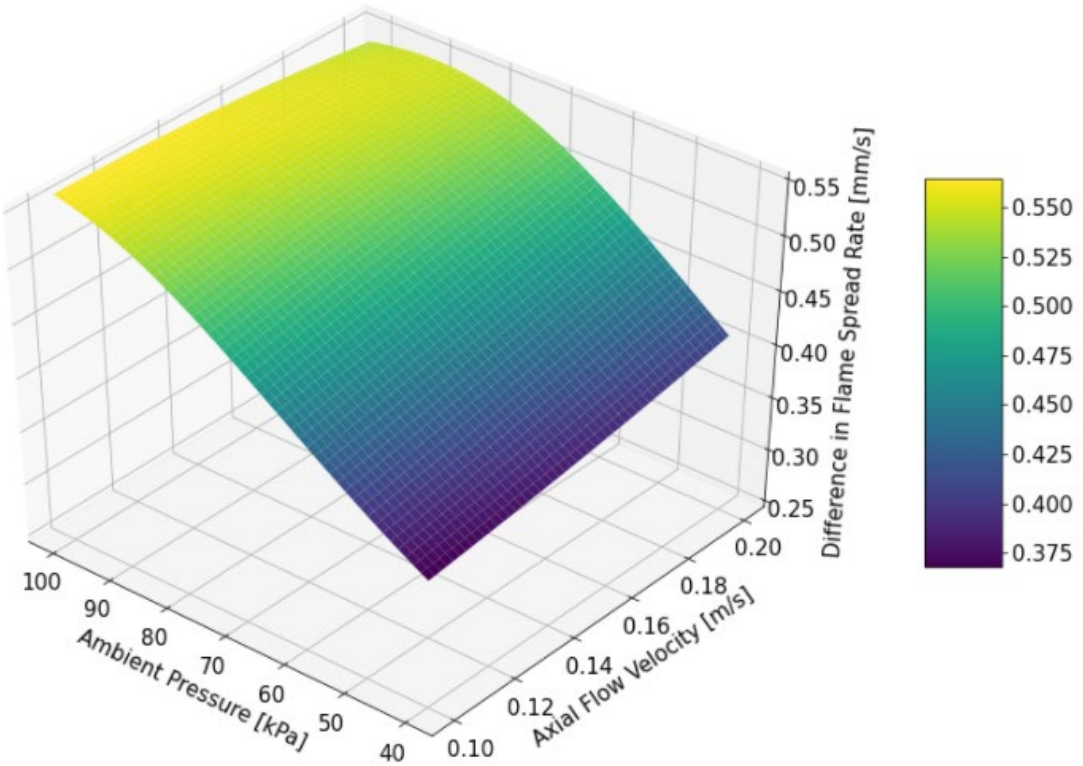


Figure 8.13 Parametric surfaces showing ANN predictions for differences in flame spread rate over type A wire samples for varying ambient pressure and concurrent flow speeds in 21% oxygen concentration and 1g (top surface) or 0g (bottom surface) environments.

Figure 8.13 shows a more detailed depiction of the discrepancies between the 1g and 0g predictions made by the ANN, with the *z*-axis in this figure representing the difference in concurrent flame spread rates between the 1g and 0g environments. In this figure, much larger differences between flame spread rates in 1g versus 0g environments are observed as the pressure increases. This result was anticipated, as it has been mentioned several times throughout this work that previous studies have found low pressure environments, even under 1g gravity conditions, can approximately mimic microgravity environments [10, 11, 12] due to the reduction of buoyancy-induced flows, which are not present at all in microgravity. Therefore, it would be expected for

the 0g and 1g flame spread rate results to be more similar to one another at lower pressures and to diverge at higher pressures. It is also possible that another contributor to this larger difference in flame spread rates at higher pressures may be an increased rate of insulation material removal due to the faster dripping frequency observed at higher pressures in 1g conditions, thus allowing the flame to spread faster.

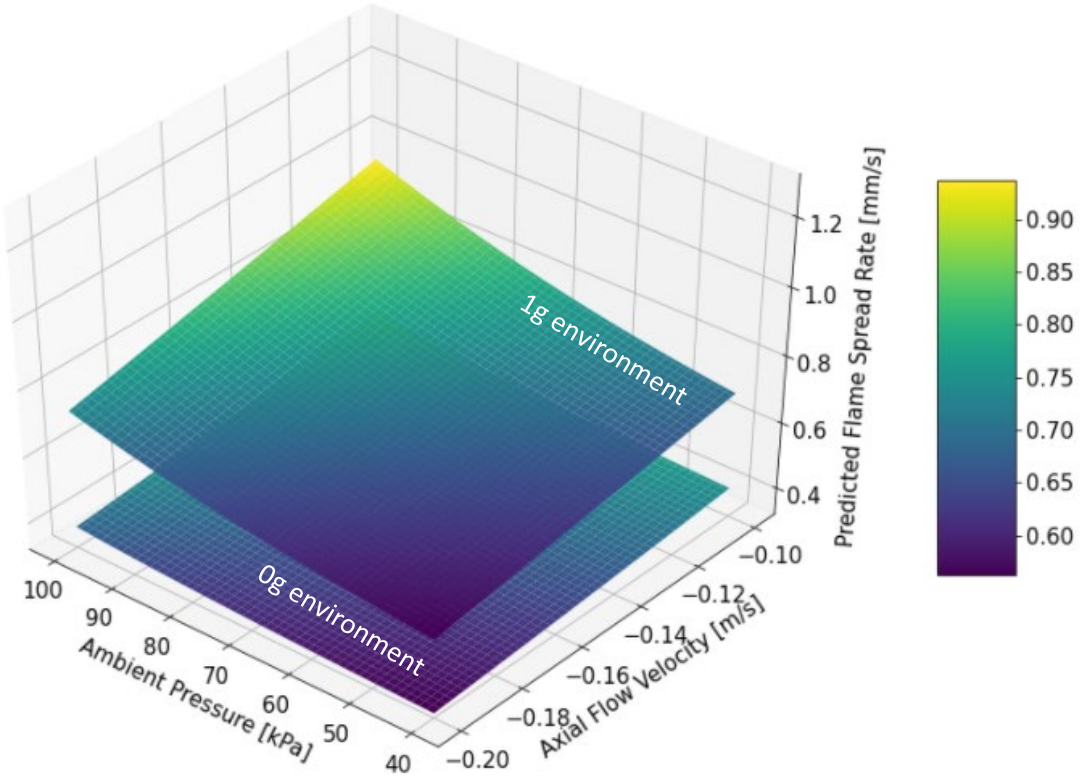


Figure 8.14 Parametric surfaces showing ANN predictions for differences in flame spread rate over type A wire samples for varying ambient pressure and opposed flow speeds in 21% oxygen concentration and 1g (top surface) or 0g (bottom surface) environments.

Figure 8.14 and Figure 8.15 show comparable results to those depicted in Figure 8.12 and Figure 8.13, respectively, but for opposed flame spread rate instead. Similarly, the trends observed in Figure 8.14 are analogous to those shown in Figure 8.12, with ANN predictions for opposed flame spread rate being slower in a 0g environment versus a 1g environment. As with the concurrent spread results, the opposed flow predictions provided by the ANN should be considered preliminary. It is encouraging that the change in flame spread rate across the range of pressures used varies between 20% and 38%, for most opposed flow speeds and strengths of gravity examined, which is above the 16% error rate found for the ANN predictions in the validation process. However, there was only a 7.9% change in the flame spread rate across the range of pressures used in these predictions for the 20 cm/s opposed flow in the case of the estimated 0g environtment. Because some of these results fall within the noise of the error of the ANN predictions, less confidence can be had in their accuracy. Therefore, it is important to remember that these results must still be verified experimentally in the future.

Keeping this in mind and moving forward with the analysis of the current results, it is again hypothesized that the slower flame spread observed in the estimated 0g environment is due to the dripping effect observed in 1g, where removing insulation material through dripping is allowing

the flame to burn through the remaining insulation material at a faster rate. Looking at Figure 8.15, the results for differences in flame spread rates subject to a 1g versus 0g environment in the opposed flow configuration, while not as prominent, are similar to those in the concurrent flow configuration. Again, it is observed that the flame spread rates occuring at higher pressures show greater discrepencies between the 1g and 0g behavior than for lower pressures. As was with the case for concurrent flow, it is hypothesized that this is due to the reduced buoyancy induced flows at lower pressures, which cause the 1g environment to more similar to a 0g environment.

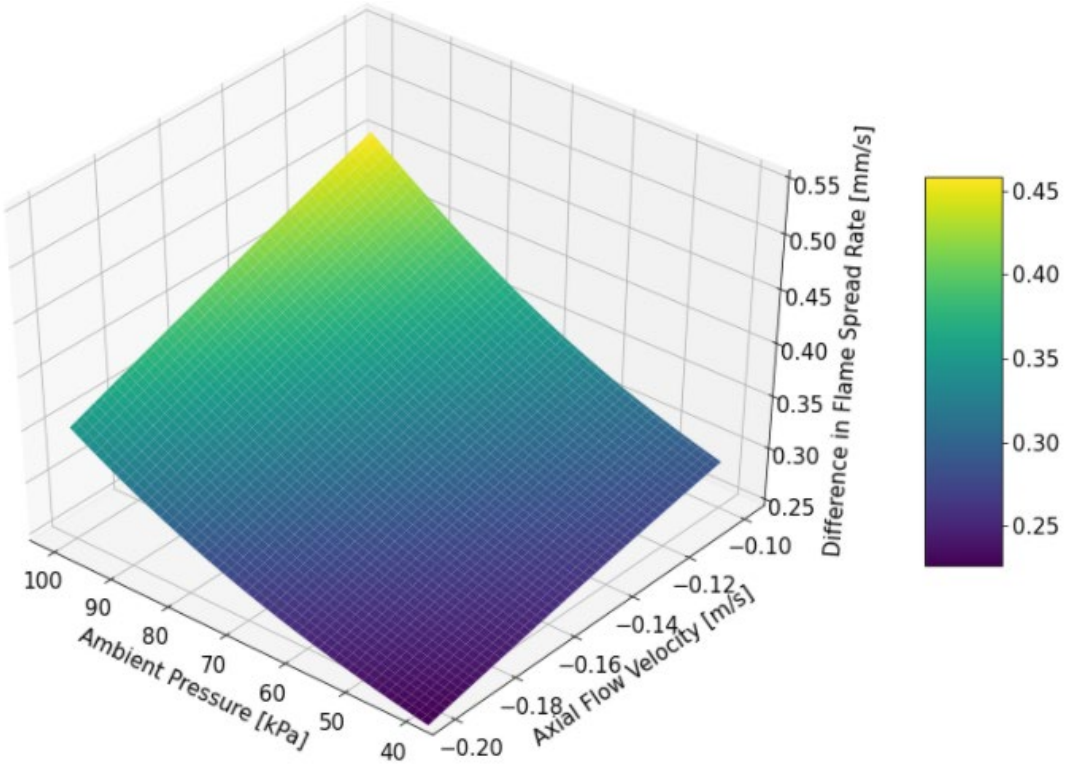


Figure 8.15 Parametric surfaces showing ANN predictions for differences in flame spread rate over type A wire samples for varying ambient pressure and opposed flow speeds in 21% oxygen concentration and 1g (top surface) or 0g (bottom surface) environments.

# 8.7 Future Work

The initial results from the ANN have shown to be very promising, and it is believed that the ANN could be used for much more in-depth analyses in the future. With some improvements, including more accurate input data, specifically insulation material properties, as well as more extensive input data, specifically more conditions that result in the blow-off limit of the flame being reached, the ANN can become a much stronger tool. Additionally, only a very few number of flame spread rate parametric surfaces were examined here. Analysis of all the other possible flame spread rate parametric surfaces could bring much further insight to the flame spread rate along electrical wire problem and potentially reveal results or nuances that have previously gone undiscovered. Furthermore, a sensitivity analysis examining each of the parameters affecting the flame spread rate along electrical wire insulation problem could also be performed using the predictions of the ANN. Such an analysis could be an immensely useful tool for shedding further

light onto which parameters in the problem are the most important and influential when it comes to flame spread rate and assessing fire safety. Finally, the ANN could be expanded to include further parameters. As mentioned previously, some variables such as electric fields or currents and external radiation were excluded from this analysis. However, adapting the comprehensive database and the ANN to account for these variables could make the ANN predictions even more comprehensive and relevant to the current applications as well as additional ones.

## 8.8 Conclusions on Artificial Neural Network Predictions

ANN predictions showed that, with careful consideration for relevant input parameters, it is possible to unify the wire burning problem and accurately predict flame spread rate for varying wire types and ambient conditions. Using these ANN predictions, parametric trends were developed depicting the dependence of flame spread rate along electrical wires for various ambient conditions and wire compositions. Keeping in mind the limitations of the ANN and the tendency for machine learning models such as these to only identify correlations rather than causal relationships, these predicted parametric trends were used as part of preliminary analysis of further flame spread rate results.

Many of the ANN predictions showed trends that reinforced what was observed in the experimental results, such as the increase of flame spread rate with ambient pressure and flow velocity. The effect of a high conductivity wire core acting as a heat source and preheating unburned insulation was also observed again, but this time with a range of wire compositions and granularity that was not practical experimentally. Further analysis of parametric surfaces developed from the predictions of the ANN showed many nuances in the flame spread rate's dependence on various parameters. For example, by examining the effects of oxygen concentration and pressure, their interactions with one another to allow for faster flame spread rates at elevated oxygen concentrations even with drastically reduced pressures could be seen.

The ANN was also used to show predictions for flame spread rate results under conditions that have not yet been widely tested by developing parametric surfaces predicting flame spread rate in 1g versus 0g environments. These surfaces were then compared and showed that dripping observed in 1g results in faster flame spread in these conditions. It was also observed that, as expected, there are larger discrepancies between flame spread rates subject to 0g versus 1g conditions at higher pressures, due to increased strength of buoyancy induced flows, which are not present in microgravity.

While the initial results from the ANN are exceedingly promising, it must be remembered that there are also still improvements that can be made to the ANN to increase the accuracy of its predictions. With further training using a wider variety and more accurate input data as well as greater insight into influential parameters, predictions may become even better with future iterations of the ANN.

# Chapter 9. Concluding Remarks

The problem of flame spread along electrical wire insulation is highly complex and can encompass many variables, including wire core and insulation material and their thermal properties, ambient oxygen concentration, pressure, flow velocity, wire orientation, and gravitational strength. With the current global-scale transition from fossil fuel energy technologies towards increasing use of electrically driven energy technologies and a resulting potential for electricity-produced energy consumption to double over the coming decades, it is highly important to further the understanding of electrical wire flammability. Additionally, there was a specific focus on flame spread rate behavior in space exploration atmospheres in this work because NASA's next generation of spacecrafts are designed to operate under elevated oxygen concentration and reduced ambient pressure conditions, creating a desire to be able to predict material flammability behavior under these conditions through testing performed on Earth.

By experimenting with many different simulated electrical wire samples under a multitude of environmental conditions, further insight was brought to the flame spread over electrical wire problem. First, by studying the effect of wire type and flow velocity on the flame spread rate and dripping of molten insulation in these conditions, it was found that, for the wires studied, flame spread rate varies linearly with the airflow velocity and is lower for samples with greater insulation thicknesses. Additionally, the mass loss due to dripping was found to remain approximately constant for all airflow velocities and samples. Finally, normalizing these dripping results to fractional mass loss by dripping showed that the conductance of the wire also had a significant reduction effect on the dripping.

Next, an analysis was performed examining the combined effects of reduced ambient pressure and low flow velocities on horizontal flame spread and dripping of copper-cored, LDPE-insulated wires. Through this analysis, it was found that, for the present wire characteristics and experimental conditions, the flame spread rate as well as the molten insulation dripping frequency decrease both with decreasing pressure and flow velocity. Contrarily, it was observed that the total mass that dripped increased with decreasing pressure and was not significantly affected by flow velocity. It was hypothesized that these results may be due to variations in heat transfer to the insulation from the flame as well as from the core to the insulation. Comparison with results from other studies with wires of different core materials and dimensions showed that the effect of the environmental parameters on the flame spread rate depends strongly on the core conductivity as well as core and insulation diameters.

The last set of experiments, although disrupted by lab closures caused by the COVID-19 pandemic, still showed interesting results and allowed for initial results regarding the combined effect of oxygen concentration, ambient pressure, and forced flow velocity to be obtained. Overall, these results showed that flame spread rate along the horizontal simulated electrical wires studied here tends to increase with increasing oxygen concentration, pressure, and flow velocity. However, the oxygen concentration appeared to have a greater effect on the flame spread rate than did the ambient pressure. From these experiments, it was also determined that the limiting oxygen concentration for burning thin copper-cored, LDPE-insulated wire samples was either slightly below or between the range of 18 to 21% oxygen concentration.

To increase the understanding of this problem, an artificial neural network was created and trained by a comprehensive database, which included over one thousand data points for flame spread rate results from both the literature and the experiments presented in this study. Through

this training process, the artificial neural network developed the capability to accurately predict flame spread rate for simulated electrical wires of different makeups in a variety of different environmental conditions which are important to SEAs, including varying oxygen concentration, ambient pressure, flow velocity, wire orientation, and gravitational strength.

ANN predictions showed that, with careful consideration for relevant input parameters, it is possible to unify the wire burning problem and accurately predict flame spread rate for varying wire types and ambient conditions. Using these ANN predictions, parametric surfaces were developed depicting the dependence of flame spread rate along electrical wires for various ambient conditions and wire compositions. These trends reinforced what was observed in the experimental results, such as the increase of flame spread rate with oxygen concentration, ambient pressure, and flow velocity. They also provided further insight into the wire burning problem by showing the effect of wire conductivity in combination with varying insulation thickness on flame spread rate for a range of wire compositions with granularity that is not practical experimentally.

Other ANN parametric surfaces were also used to compare predictions for flame spread rate in 1g environments versus 0g environments and showed that dripping observed in 1g, together with buoyant heat and mass transport effects, results in faster flame spread. It was also observed that larger discrepancies between flame spread rates subject to 0g versus 1g conditions occurred at higher pressures, due to increased strength of buoyancy-induced flows, which are not present in microgravity. While these initial results are interesting, it must be remembered that these surfaces were developed by training the ANN with the limited microgravity data that is currently available in the field. Once the future planned analogous experiments on the ISS are completed and the data is returned, those results can also be incorporated into the ANN training process to strengthen the network and increase the accuracy of its predictions.

Overall, these parametric trends as well as comparison of experimental results with those from other external studies with different wire samples show that the effect of environmental parameters on flame spread rate depends strongly on wire composition and insulation dripping. Consequently, care should be taken in extending results obtained from specific wire tests conducted in normal gravity to other wires and reduced gravity environments.

# References


[1] L. S. Olson, A. G. Ruff and J. F. Miller, "Microgravity Flame Spread in Exploration Atmospheres: Pressure Oxygen, and Velocity Effects on Opposed and Concurrent Flame Spread," National Aeronautics and Space Administration, Glenn Research Center, Cleveland, Ohio, 2008.

[2] K. E. Lange, A. T. Perka, B. E. Duffield, B. E. Duffield and F. F. Jeng, "Bounding the Spacecraft Atmosphere Design Space for Future Exploration Missions," NASA, Houston, Texas, 2005.

[3] P. D. Campbell, "Recommendations for Exploration Spacecraft Internal Atmospheres: The Final Report of the NASA Exploration Atmospheres Working Group," NASA Exploration, 2010.

[4] National Aeronautics and Space Administration, "Constellation Program: America's Spacecraft for a New Generation of Explorers," Lyndon B. Johnson Space Center, Houston, TX, 2008.

[5] National Aeronautics and Space Administration, "Constellation," JSC2006-E-43965, October 2006. [Online]. Available: https://www.nasa.gov/mission_pages/constellation/multimedia/orion_contract_images.html. [Accessed 2021].

[6] S. Graham and T. Reckart, "FLARE - Flammability Limits At Reduced-g Experiment (FLARE)," NASA Glenn Research Center, 14 August 2019. [Online]. Available: https://www1.grc.nasa.gov/space/iss-research/iss-fcf/cir/flammability-limits-at-reduced-g-experiment-flare/. [Accessed July 2021].

[7] O. Fujita, "Solid combustion research in microgravity as a basis of fire safety in space," *Proceedings of the Combustion Institute,* vol. 35, no. 3, pp. 2487-2502, 2015.

[8] R. Friedman, "Fire Safety in the Low-Gravity Spacecraft Environment," NASA Glenn Research Center, Denver, CO, 1999.

[9] S. Link, X. Huang, C. Fernandez-Pello, S. Olson and P. Ferkul, "The Effect of Gravity on Flame Spread over PMMA Cylinders," *Scientific Reports,* vol. 8, no. 1, 2018.

[10] M. Thomsen, C. Fernandez-Pello, D. L. Urban, G. A. Ruff and S. L. Olson, "On Simulating Concurrent Flame Spread in Reduced Gravity by Reducing Ambient Pressure," *Proceedings of the Combustion Institute,* vol. 37, no. 3, pp. 3793-3800, 2018.

[11] M. Thomsen, C. Fernandez-Pello, G. A. Ruff and D. L. Urban, "Buoyancy Effects on Concurrent Flame Spread Over Thick PMMA," *Combustion and Flame,* vol. 199, pp. 279-291, 2019.

[12] Y. Nakamura, N. Yoshimura, T. Matsumura, H. Ito and O. Fujita, "Flame Spread over Polymer-Insulated Wire in Sub-Atmospheric Pressure: Similarity to Microgravity Phenomena," in *Progress in Scale Modeling*, Springer, Dordrecht, 2008, pp. 17-27.

[13] V. Babrauskas, Ignition Handbook, Fire Science Publishers, 2003.

[14] FEMA and U.S. Fire Administration, "Fire Estimate Summaries: Residential Building Fires," National Fire Data Center, Emmitsburg, MD, 2020.

[15] M. Ahrens, Home Structure Fires, 2016.

[16] A. Fernandez-Pello, H. Hasegawa, K. Staggs, A. Lipska-quinn and N. Alvares, "A Study of the Fire Performance of Electrical Cables," in *IAFSS*, 1991.

[17] IRENA, "Global Energy Transformation: A roadmap to 2050," International Renewable Energy Agency, Abu Dhabi, 2018.

[18] M. Kikuchi, O. Fujita, K. Ito, A. Sato and T. Sakuraya, "Experimental Study on Flame Spread over Wire Insulation in Microgravity," *Symposium (International) on Combustion,* vol. 27, no. 2, pp. 2507-2514, 1998.

[19] O. Fujita, M. Kikuchi, K. Ito and K. Nishizawa, "Effective mechanisms to determine flame spread rate over ethylene-tetrafluoroethylene wire insulation: Discussion on dilution gas effect based on temperature measurements," *Proceedings of the Combustion Institute,* vol. 28, no. 2, pp. 2905-2911, 2000.

[20] O. Fujita, K. Nishizawa and K. Ito, "Effect of low external flow on flame spread over polyethylene-insulated wire in microgravity," *Proceedings of the Combustion Institute,* vol. 29, no. 2, pp. 2545-2552, 2002.

[21] S. Takahashi, H. Takeuchi, H. Ito, Y. Nakamura and O. Fujita, "Study on unsteady molten insulation volume change during flame spreading over wire insulation in microgravity," *Proceedings of the Combustion Insitute,* vol. 34, no. 2, pp. 2657-2664, 2013.

[22] C. H. Leung, J. E. J. Staggs, J. Brindley, A. C. Mcintosh and R. H. Whiteley, "The effects of an inert central core on the thermal pyrolysis of an electrical cable," *Fire Safety Journal,* vol. 34, no. 2, pp. 143-168, 2000.

[23] Y. Nakamura, N. Yoshimura, H. Ito, K. Azumaya and O. Fujita, "Flame spread over electric wire in sub-atmospheric pressure," *Proceedings of the Combustion Institute,* vol. 32, no. 2, pp. 2559-2566, 2009.

[24] Y. Nakamura, N. Yoshimura, T. Matsumura, H. Ito and O. Fujita, "Opposed-wind Effect on Flame Spread of Electric Wire in Sub-atmospheric Pressure," *Journal of Thermal Science and Technology,* vol. 3, no. 3, pp. 430-441, 2008.

[25] K. Miyamoto, X. Huang, N. Hashimoto, O. Fujita and C. Fernandez-Pello, "Limiting Oxygen Concentration (LOC) of Burning Polyethylene Insulated Wires under External Radiation," *Fire Safety Journal,* vol. 86, pp. 32-40, 2016.

[26] Y. Konno, Y. Kobayashi, Fernandez-Pello, Carlos, N. Hashimoto, S. Nakaya, M. Tsue and O. Fujita, "Opposed-Flow Flame Spread and Extinction in Electric Wires: The Effects of Gravity, External Radiant Heat Flux, and Wire Characteristics on Wire Flammability," *Fire Technology,* vol. 56, no. 1, pp. 131-148, 2020.

[27] Y. Kobayashi, Y. Konno, X. Huang, S. Nakaya, M. Tsue, N. Hashimoto, O. Fujita and C. Fernandez-Pello, "Laser piloted ignition of electrical wire in microgravity," *Proceedings of the Combustion Institute,* vol. 37, no. 3, pp. 4211-4219, 2018.

[28] K. Miyamoto, X. Huang, N. Hashimoto, F. Osamu and C. Fernandez-Pello, "Opposed Flame Spread over Polyethylene Insulated Wires under Varying External Radiations and Oxygen Concentrations," in *46th International Conference on Environmental Systems*, Vienna, Austria, 2016.

[29] X. Huang, Y. Nakamura and F. A. Williams, "Ignition-to-spread transition of externally heated electrical wire," *Proceedings of the Combustion Institute,* vol. 34, no. 2, pp. 2505-2512, 2013.

[30] A. F. Osorio, K. Mizutani, C. Fernandez-Pello and F. Osamu, "Microgravity flammability limits of ETFE insulated wires exposed to external radiation," *Proceedings of the Combustion Institute,* vol. 35, no. 3, pp. 2683-2689, 2015.

[31] Z. Wang, T. Zhou, R. Wei and J. Wang, "Experimental study of flame spread over PE-insulated single copper core wire under varying pressure and electric current," *Fire and Materials,* vol. 44, no. 6, pp. 835-843, 2020.

[32] S. J. Lim, S. H. Park, J. Park, O. Fujita, S. I. Keel and H. S. Chung, "Flame spread over inclined electrical wires with AC electric fields," *Combustion and Flame,* vol. 185, no. November, pp. 82-92, 2017.

[33] S. Takahashi, H. Ito, Y. Nakamura and O. Fujita, "Effect of Conductor on Spreading Flames over Wire in Microgravity," in *43rd International Conference on Environmental Systems*, Vail, Colorado, US, 2013.

[34] O. Fujita, T. Kyono, Y. Kido, H. Ito and Y. Nakamura, "Ignition of electrical wire insulation with short-term excess electric current in microgravity," *Proceedings of the Combustion Institute,* vol. 33, no. 2, pp. 2517-2623, 2011.

[35] M. Nagachi, M. Fumiya, J.-M. Citerne, H. Dutilleul, A. Guibaud, G. Jomaas, G. Legros, N. Hashimoto and O. Fujita, "Can a spreading flame over electric wire insulation in concurrent flow achieve steady propagation in microgravity?," *Fire Technology,* vol. 55, pp. 193-209, 2019.

[36] Y. Kobayashi, Y. Konno, X. Huang, S. Nakaya, M. Tsue, N. Hashimoto, O. Fujita and C. Fernandez-Pello, "Effect of insulation melting and dripping on opposed flame spread over laboratory simulated electrical wires," *Fire Safety Journal,* vol. 95, no. January, pp. 1-10, 2018.

[37] Y. Konno, N. Hashimoto and O. Fujita, "Downward flame spreading over electric wire under various oxygen concentrations," *Proceedings of the Combustion Institute,* vol. 37, no. 3, pp. 3817-3824, 2019.

[38] Y. Konno, N. Hashimoto and O. Fujita, "Role of wire core in extinction of opposed flame spread over thin electric wires," *Combustion and Flame,* vol. 220, no. October, pp. 7-15, 2020.

[39] Y. Lu, X. Huang, L. Hu and C. Fernandez-Pello, "The interaction between fuel inclination and horizontal wind: Experimental study using thin wire," *Proceedings of the Combustion Institute,* vol. 37, no. 3, pp. 3809-3816, 2019.

[40] L. Zhao, Q. Zhang, R. Tu, J. Fang, J. Wang and Y. Zhang, "Effects of electric current and sample orientation of flame spread over electrical wires," *Fire Safety Journal,* vol. 112, 2020.

[41] L. Hu, Y. Zhang, K. Yoshioka, H. Izumo and O. Fujita, "Flame spread over electric wire with high thermal conductivity metal core at different inclinations," *Proceedings of the Combustion Institute,* vol. 35, no. 3, pp. 2607-2614, 2015.

[42] Y. Ma, X. Zhang, Y. Lu, J. Lv, N. Zhu and L. Hu, "Effect of transverse flow on flame spread and extinction over polyethylene-insulated wires," *Proceedings of the Combustion Institute,* vol. In Press, 2020.

[43] Y. Kobayahsi, X. Huang, S. Nakaya, M. Tsue and C. Fernandez-Pello, "Flame spread over horizontal and vertical wires: The roll of dripping and core," *Fire Safety Journal,* vol. 91, no. 5, pp. 112-122, 2017.

[44] T. Gong, Q. Xie and X. Huang, "Fire behaviors of flame-retardant cables part I: Decomposition, swelling and spontaneous ignition," *Fire Safety Journal,* vol. 35, no. 3, pp. 113-121, 2017.

[45] X. Huang, "Critical Drip Size and Blue Flame Shedding of Dripping Ignition in Fire," *Scientific Reports,* vol. 8, pp. 1-13, 2018.

[46] M. Thomsen, D. Murphy, C. Fernandez-Pello, D. L. Urban and G. A. Ruff, "Flame spread limits (LOC) of fire resistant fabrics," *Fire Safety Journal,* vol. 921, no. 2017, pp. 259-265, 2017.

[47] Y. Lu, L. Hu, X. Huang and C. Fernandez-Pello, "Concurrent Flame Spread and Blow-off Over Horizontal Thin Electrical Wires," *Fire Technology,* vol. 55, pp. 193-209, 2019.

[48] X. Huang, "Ignition and spread of electrical wire fires," University of California, San Diego, San Diego, CA, 2012.

[49] A. C. Fernandez-Pello, "The Solid Phase," in *Combustoin Fundamentals of Fire*, 1995, pp. 31-100.

[50] R. A. Seban and R. Bond, "Skin-Friction and Heat-Transfer Characteristics of Laminar Boundary Layer on a Cylinder in Axial Incompressible Flow," *Journal of the Aeronautical Sciences,* vol. 18, no. 10, pp. 671-675, 1951.

[51] Y. Zhao, J. Chen, X. Chen and S. Lu, "Pressure effect on flame spread over polyethylene-insulated copper core wire," *Applied Thermal Engineering,* vol. 123, pp. 1042-1049, 2017.

[52] L. Hu, K. Zhu and X. Zhang, "An experimental study on flame spread over electrical wire with high conductivity copper core and controlling heat transfer mechanism under sub-atmospheric pressures," *International Journal of Thermal Sciences,* vol. 141, pp. 141-149, 2019.

[53] L. Gagnon, C. Fernandez-Pello, J. L. Urban, V. P. Carey, Y. Konno and O. Fujita, "Effect of reduced ambient pressures and opposed airflows on the flame," *Fire Safety Journal,* vol. 120, no. March, 2021.

[54] J. Fang, Xue Yan, J. Wang, X. He, Y. Zhang, S. Zhao and Y. Zhang, "PE and ETFE wire insulation flame morphologies and spread rates under subatmospheric pressures," *Journal of Thermoplastic Composite Materials,* 2020.

[55] J. Fang, Y. Zhang, X. Huang, Y. Xue, J. Want, S. Zhao, X. He and L. Zhao, "Dripping and Fire Extinction Limits of Thin Wire: Effect of Pressure and Oxygen," *Combustion Science and Technology,* vol. 193, no. 3, pp. 437-452, 2019.

[56] M. Thomsen, C. Fernandez-Pello, X. Huang, S. L. Olson and P. V. Ferkul, "Opposed Flow Burning of PMMA Cylinders in Normoxic," *Fire Safety Journal,* vol. 110, no. December, 2019.

[57] Y. Kobayashi, S. Nakaya, M. Tsue and S. Takahashi, "Flame spread over polyethylene-insulated copper and stainless-steel wires at high pressure," *Fire Safety Journal,* vol. In Press, 2020.

[58] J. G. Quintiere, Fundamentals of Fire Phenomena, New York City: John Wiley & Sons, Ltd, 2006.

[59] Z. Wang and J. Wang, "Experimental study on flame propagation over horizontal electrical wires under varying pressure," *International Journal of Thermal Sciences,* vol. 156, 2020.

[60] L. Gagnon, V. P. Carey and C. Fernandez-Pello, "Using an Artificial Neural Network to Predict Flame Spread across Electrical Wires," *ASME Journal of Energy Resources Technology,* Vols. In-Press, 2021.

[61] V. J. A. Krose and P. van der Smagt, An Introduction to Neural Networks, Amsterdam: University of Amsterdam, 1996.

[62] F. Chollet, "Keras," 2015. [Online]. Available: https://keras.io/.

[63] Z. Boger and H. Guterman, "Knowledge extraction from artificial neural network models," in *EEE International Conference on Systems, Man, and Cybernetics. Computational Cybernetics and Simulation*, Orlando, Florida, 1997.

[64] G. S. Linoff and M. J. A. Berry, Data Mining Techniques: For Marketing, Sales, and Customer Relationship Management, New York, New York: John Wiley & Sons, 1997.

[65] A. Blum, Neural Networks in C++: An Object-Oriented Framework for Building Connectionist Systems, New York, New York: John Wiley & Sons, 1992.

[66] G. Hinton, N. Srivastava and K. Swersky, "Neural Networks for Machine Learning - Overview of mini-batch gradient descent," 2012. [Online]. Available: http://www.cs.toronto.edu/~hinton/coursera/lecture6/lec6.pdf. [Accessed 2020].

[67] A. C. Fernandez-Pellp and C. P. Mao, "A Unified Analysis of Concurrent Modes of Flame Spread," *Combustion Science and Technology,* vol. 26, no. 3-4, pp. 147-156, 1981.

# Appendix – Artificial Neural Network Code

In [3]:

```
#IMPORT USEFUL PACKAGES
import sys
import numpy
import pandas
import keras
from keras.models import Sequential
import keras.backend as kerasbackend
import tensorflow
import matplotlib.pyplot as plt
from matplotlib import cm
import statistics

numpy.set_printoptions(threshold=sys.maxsize)
```

In [4]:

```
#FUNCTIONS FOR PROGRAM

##############################################################################################
##############################################################################################
#IMPORT DATA THAT WILL BE USED FOR NN TRAINING (NOTE: Excel file being imported must be in
very specific format)
##############################################################################################
##############################################################################################

def import_data_from_excel(file_path):
    #Give titles to columns in data sheet and designate which columns are needed for analy
sis. This is specifically formatted to match my data sheet.
    data_sheet_column_names = ["Test_Number","Core_Material", "Insulation_Material", "Core
_Outer_Diameter_mm", "Core_Inner_Diameter_mm", "Insulation_Outer_Diameter_mm", "Insulation
_Inner_Diameter_mm", "Oxygen_Concentration_percentage", "Forced_Flow_x_Velocity_m_per_s",
"Forced_Flow_y_Velocity_m_per_s", "Forced_Flow_z_Velocity_m_per_s", "Gravity_x_Vector_gs",
"Gravity_y_Vector_gs", "Average_Pressure_kPa", "Spread_Occurrence", "Flame_Spread_Rate_mm_
per_s", "Bad_Test_Occurrence", "Video_Analyzed_Occurrence"]
    used_columns_in_data_sheet = "A,D:I,O,S:W,AB,AF:AG,AJ:AK"

    return pandas.read_excel(file_path,header=1,usecols=used_columns_in_data_sheet,names=d
ata_sheet_column_names)

##############################################################################################
##############################################################################################



##############################################################################################
##############################################################################################
#REMOVE INVALID DATA
##############################################################################################
##############################################################################################

def remove_invalid_data_from_dataframe(data_file):
    #Determine which rows have incomplete data
    [rows_in_data_file,ColumnsInDataFile] = data_file.shape

    first_invalid_test = 0

    for row_in_data_file in range(0,rows_in_data_file):
        if not numpy.isnan(data_file.Spread_Occurrence.iloc[row_in_data_file]): #Spread_Oc
currence will not be NaN (will be FALSE) if there was no spread
            if first_invalid_test == 0:
                rows_of_invalid_tests_to_analyze = [row_in_data_file]
                first_invalid_test = 1
            else:
                rows_of_invalid_tests_to_analyze = numpy.append(rows_of_invalid_tests_to_a
nalyze,[row_in_data_file])
        elif not numpy.isnan(data_file.Bad_Test_Occurrence.iloc[row_in_data_file]): #Bad_T
est_Occurrence will not be NaN (will be TRUE) if the test was bad
            if first_invalid_test == 0:
                rows_of_invalid_tests_to_analyze = [row_in_data_file]
```

```
                first_invalid_test = 1
            else:
                rows_of_invalid_tests_to_analyze = numpy.append(rows_of_invalid_tests_to_a
nalyze, [row_in_data_file])
        elif numpy.isnan(data_file.Video_Analyzed_Occurrence.iloc[row_in_data_file]): #Vid
eo_Analyzed_Occurrence will be NaN if video wasn't analyzed (otherwise will be TRUE)
            if first_invalid_test == 0:
                rows_of_invalid_tests_to_analyze = [row_in_data_file]
                first_invalid_test = 1
            else:
                rows_of_invalid_tests_to_analyze = numpy.append(rows_of_invalid_tests_to_a
nalyze, [row_in_data_file])
        elif data_file.Insulation_Material.iloc[row_in_data_file] == "PMMA": #these tests
 were weird, and I don't want to consider them right now
            if first_invalid_test == 0:
                rows_of_invalid_tests_to_analyze = [row_in_data_file]
                first_invalid_test = 1
            else:
                rows_of_invalid_tests_to_analyze = numpy.append(rows_of_invalid_tests_to_a
nalyze, [row_in_data_file])

    if first_invalid_test == 0: #i.e. If no bad tests were found
        rows_of_invalid_tests_to_analyze = []

    #Remove rows with incomplete data
    valid_tests_to_analyze = data_file.drop(rows_of_invalid_tests_to_analyze)

    valid_tests_to_analyze = valid_tests_to_analyze.reset_index(drop = True)

    return valid_tests_to_analyze

##########################################################################################
##########################################################################################



##########################################################################################
##########################################################################################
#INSERT COLUMNS FOR NEEDED DATA (E.G. MATERIAL PROPERTIES) THAT WASN'T IN ORIGINAL DATA SH
EET (THIS WILL GET ADDED LATER)
##########################################################################################
##########################################################################################

def add_empty_columns_to_dataframe(valid_tests_to_analyze):
    #Add empty columns for more parameters to add to data
    [rows,columns] = valid_tests_to_analyze.shape
    empty_column0 = [None]*rows
    empty_column1 = [None]*rows
    empty_column2 = [None]*rows
    empty_column3 = [None]*rows
    empty_column4 = [None]*rows
    empty_column5 = [None]*rows
    empty_column6 = [None]*rows
    empty_column7 = [None]*rows
    empty_column8 = [None]*rows
    empty_column9 = [None]*rows
```

```
    #Name the new columns that were added (these are more parameters of interest)
    valid_tests_to_analyze.insert(3,"Core_Material_Density_kg_per_m3",empty_column0,True)
    valid_tests_to_analyze.insert(4,"Core_Material_Thermal_Conductivity_W_per_mK",empty_co
lumn1,True)
    valid_tests_to_analyze.insert(5,"Core_Material_Specific_Heat_J_per_kgK",empty_column2,
True)
    valid_tests_to_analyze.insert(7,"Insulation_Material_Density_kg_per_m3",empty_column3,
True)
    valid_tests_to_analyze.insert(8,"Insulation_Material_Thermal_Conductivity_W_per_mK",em
pty_column4,True)
    valid_tests_to_analyze.insert(9,"Insulation_Material_Specific_Heat_J_per_kgK",empty_co
lumn5,True)
    valid_tests_to_analyze.insert(12,"Core_XSectional_Area_m2",empty_column6,True)
    valid_tests_to_analyze.insert(15,"Insulation_XSectional_Area_m2",empty_column9,True)

    return valid_tests_to_analyze

##########################################################################################
##########################################################################################



##########################################################################################
##########################################################################################
#SELECT WHICH DATA TO ANALYZE
##########################################################################################
##########################################################################################

def select_valid_data_for_training(valid_tests_to_analyze,set_of_test_numbers_to_analyze,t
est_numbers_list):
    if set_of_test_numbers_to_analyze == 1: #To analyze a select number of tests pick 1
        if test_numbers_list == []:
            ("There was no subset of tests specified. Please include a non-empty list of t
ests as an input.")

        else:
            print("Selecting a subset of the tests.")
            test_numbers_to_analyze_array = test_numbers_list

    elif set_of_test_numbers_to_analyze == 2: #To analyze all the valid tests pick 2
        print("Selecting all the tests.")
        test_numbers_to_analyze_array = numpy.array(valid_tests_to_analyze.Test_Number)

    elif set_of_test_numbers_to_analyze == 3: #To analyze half the tests (and use the othe
r half for training) pick 3
        print("Selecting half the tests for training (and the other half for validation)."
)
        test_numbers_to_analyze_array = numpy.array(valid_tests_to_analyze.Test_Number)

    return test_numbers_to_analyze_array

##########################################################################################
##########################################################################################
```

```
##########################################################################################
##########################################################################################
#GO THROUGH VALID DATA AND REMOVE TEST YOU DON'T WANT TO ANALYZE WHILE FILLING IN DATA MIS
SING FROM ORIGINAL DATA SHEET (E.G. MATERIAL PROPERTIES)
##########################################################################################
##########################################################################################

def finalize_dataset(valid_tests_to_analyze,test_numbers_to_analyze_array,set_of_test_numb
ers_to_analyze): #dataframe, list of test numbers to be analyzed, list-type of tests selec
ted (1, 2, or 3)
    #From all of the valid tests in the data set, determine which tests I do NOT want to a
nalyze and which parameters I'm NOT currently
    #interested in.  Also add the missing data to the columns that were previously added.
    [rows_in_valid_tests_to_analyze,columns_in_valid_tests_to_analyze] = valid_tests_to_an
alyze.shape

    first_nonincluded_test = 0
    count = 0

    #First compile a set of test numbers that I don't currently want to analyize
    for row_in_valid_tests_to_analyze in range(0,rows_in_valid_tests_to_analyze):

        if valid_tests_to_analyze.Test_Number.iloc[row_in_valid_tests_to_analyze] not in t
est_numbers_to_analyze_array:
            if first_nonincluded_test == 0:
                nonincluded_tests_to_analyze = [row_in_valid_tests_to_analyze]
                first_nonincluded_test = 1
            else:
                nonincluded_tests_to_analyze = numpy.append(nonincluded_tests_to_analyze,[
row_in_valid_tests_to_analyze])

        #only add data into the new columns if I want to keep that row for analysis
        else:
            #print("This wire's core material is: " + valid_tests_to_analyze.Core_Materia
l.iloc[row_in_valid_tests_to_analyze] + ".")
            if valid_tests_to_analyze.Core_Material.iloc[row_in_valid_tests_to_analyze] ==
'Copper' or valid_tests_to_analyze.Core_Material.iloc[row_in_valid_tests_to_analyze] == 'C
u Yong':
                valid_tests_to_analyze.Core_Material_Density_kg_per_m3.iloc[row_in_valid_t
ests_to_analyze] = 8880 #[kg/m3]
                valid_tests_to_analyze.Core_Material_Thermal_Conductivity_W_per_mK.iloc[ro
w_in_valid_tests_to_analyze] = 398 #[W/mK]
                valid_tests_to_analyze.Core_Material_Specific_Heat_J_per_kgK.iloc[row_in_v
alid_tests_to_analyze] = 390 #[J/kgK]
                #print("Therefore, it will be given the material properties of COPPER.")
            elif valid_tests_to_analyze.Core_Material.iloc[row_in_valid_tests_to_analyze]
== 'NiCr' or valid_tests_to_analyze.Core_Material.iloc[row_in_valid_tests_to_analyze] ==
'NiCr TC-K':
                valid_tests_to_analyze.Core_Material_Density_kg_per_m3.iloc[row_in_valid_t
ests_to_analyze] = 7800 #[kg/m3]
                valid_tests_to_analyze.Core_Material_Thermal_Conductivity_W_per_mK.iloc[ro
w_in_valid_tests_to_analyze] = 21.5 #[W/mK]
                valid_tests_to_analyze.Core_Material_Specific_Heat_J_per_kgK.iloc[row_in_v
alid_tests_to_analyze] = 440 #[J/kgK]
                #print("Therefore, it will be given the material properties of NICKEL CHRO
```

```
MIUM.")
            elif valid_tests_to_analyze.Core_Material.iloc[row_in_valid_tests_to_analyze]
== 'Steel tube':
                valid_tests_to_analyze.Core_Material_Density_kg_per_m3.iloc[row_in_valid_t
ests_to_analyze] = 8650 #[kg/m3]
                valid_tests_to_analyze.Core_Material_Thermal_Conductivity_W_per_mK.iloc[ro
w_in_valid_tests_to_analyze] = 17.4 #[W/mK]
                valid_tests_to_analyze.Core_Material_Specific_Heat_J_per_kgK.iloc[row_in_v
alid_tests_to_analyze] = 500 #[J/kgK]
                #print("Therefore, it will be given the material properties of STEEL TUB
E.")
            elif valid_tests_to_analyze.Core_Material.iloc[row_in_valid_tests_to_analyze]
== '-': #properties of air at 1 atm and room temp (this is for no-core wires)
                valid_tests_to_analyze.Core_Material_Density_kg_per_m3.iloc[row_in_valid_t
ests_to_analyze] = 1.225 #[kg/m3]
                valid_tests_to_analyze.Core_Material_Thermal_Conductivity_W_per_mK.iloc[ro
w_in_valid_tests_to_analyze] = 1.4#[W/mK]
                valid_tests_to_analyze.Core_Material_Specific_Heat_J_per_kgK.iloc[row_in_v
alid_tests_to_analyze] = 1000 #[J/kgK]
                # https://www.ohio.edu/mechanical/thermo/property_tables/air/air_Cp_Cv.htm
l
                #print("Therefore, it will be given the material properties of AIR.")
            elif valid_tests_to_analyze.Core_Material.iloc[row_in_valid_tests_to_analyze]
== 'Fe':
                valid_tests_to_analyze.Core_Material_Density_kg_per_m3.iloc[row_in_valid_t
ests_to_analyze] = 7897 #[kg/m3]
                valid_tests_to_analyze.Core_Material_Thermal_Conductivity_W_per_mK.iloc[ro
w_in_valid_tests_to_analyze] = 71.8#[W/mK]
                valid_tests_to_analyze.Core_Material_Specific_Heat_J_per_kgK.iloc[row_in_v
alid_tests_to_analyze] = 452 #[J/kgK]
                #https://www.engineersedge.com/properties_of_metals.htm
                #print("Therefore, it will be given the material properties of IRON.")

            if valid_tests_to_analyze.Insulation_Material.iloc[row_in_valid_tests_to_analy
ze] == "LDPE":
                valid_tests_to_analyze.Insulation_Material_Density_kg_per_m3.iloc[row_in_v
alid_tests_to_analyze] = 923 #[kg/m3] average of Fang2019, Fang2020, Kobayashi2018, Kobaya
shi2020, Konno2020[2], Miyamoto2016, Takahashi2013, Wang2020[2]
                valid_tests_to_analyze.Insulation_Material_Thermal_Conductivity_W_per_mK.i
loc[row_in_valid_tests_to_analyze] = 0.272 #[W/mK]
                valid_tests_to_analyze.Insulation_Material_Specific_Heat_J_per_kgK.iloc[ro
w_in_valid_tests_to_analyze] = 1993 #[J/kgK]
            elif valid_tests_to_analyze.Insulation_Material.iloc[row_in_valid_tests_to_ana
lyze] == "HDPE":
                valid_tests_to_analyze.Insulation_Material_Density_kg_per_m3.iloc[row_in_v
alid_tests_to_analyze] = 946 #[kg/m3]
                valid_tests_to_analyze.Insulation_Material_Thermal_Conductivity_W_per_mK.i
loc[row_in_valid_tests_to_analyze] = 0.338 #[W/mK]
                valid_tests_to_analyze.Insulation_Material_Specific_Heat_J_per_kgK.iloc[ro
w_in_valid_tests_to_analyze] = 2075 #[J/kgK]
            elif valid_tests_to_analyze.Insulation_Material.iloc[row_in_valid_tests_to_ana
lyze] == "ETFE":
                valid_tests_to_analyze.Insulation_Material_Density_kg_per_m3.iloc[row_in_v
alid_tests_to_analyze] = 1700 #[kg/m3] Fang2020
                valid_tests_to_analyze.Insulation_Material_Thermal_Conductivity_W_per_mK.i
loc[row_in_valid_tests_to_analyze] = 0.238 #[W/mK] https://www.fluorotherm.com/technical-i
nformation/materials-overview/etfe-properties/
```

```
                valid_tests_to_analyze.Insulation_Material_Specific_Heat_J_per_kgK.iloc[ro
w_in_valid_tests_to_analyze] = 1800 #[J/kgK] Fang2020
            elif valid_tests_to_analyze.Insulation_Material.iloc[row_in_valid_tests_to_ana
lyze] == "PMMA":
                valid_tests_to_analyze.Insulation_Material_Density_kg_per_m3.iloc[row_in_v
alid_tests_to_analyze] = 1185 #[kg/m3] https://designerdata.nl/materials/plastics/thermo-p
lastics/poly(methyl-methacrylate)
                valid_tests_to_analyze.Insulation_Material_Thermal_Conductivity_W_per_mK.i
loc[row_in_valid_tests_to_analyze] = 0.2085 #[W/mK]
                valid_tests_to_analyze.Insulation_Material_Specific_Heat_J_per_kgK.iloc[ro
w_in_valid_tests_to_analyze] = 1466 #[J/kgK]


            #Calculate and populate surface area and volume for core and insulation
            valid_tests_to_analyze.Core_XSectional_Area_m2.iloc[row_in_valid_tests_to_anal
yze] = 0.25*numpy.pi*((valid_tests_to_analyze.Core_Outer_Diameter_mm.iloc[row_in_valid_tes
ts_to_analyze]**2) - (valid_tests_to_analyze.Core_Inner_Diameter_mm.iloc[row_in_valid_test
s_to_analyze]**2))
            valid_tests_to_analyze.Insulation_XSectional_Area_m2.iloc[row_in_valid_tests_t
o_analyze] = 0.25*numpy.pi*((valid_tests_to_analyze.Insulation_Outer_Diameter_mm.iloc[row_
in_valid_tests_to_analyze]**2) - (valid_tests_to_analyze.Insulation_Inner_Diameter_mm.iloc
[row_in_valid_tests_to_analyze]**2))
            #NOTE: X-SECTIONAL AREA UNIT IS ACTUALLY mm^2


    #Remove from the data set the tests that I'm not interested in, leaving tests I am int
erested in
    #If only a subset of data was looked at, remove all other tests
    if first_nonincluded_test > 0:
        tests_to_analyze = valid_tests_to_analyze.drop(nonincluded_tests_to_analyze)
        tests_to_analyze = tests_to_analyze.reset_index(drop = True)
    else:
        tests_to_analyze = valid_tests_to_analyze
        nonincluded_tests_to_analyze = []


    #Make opposed flow rates negative (switching from speed and direction parameters to si
ngle velocity parameter)
    [rows_tests_to_analyze,columns] = tests_to_analyze.shape


    #IF TRAINING AND VALIDATION DATA SETS DESIRED, SELECT HALF FOR TRAINING AND HALF FOR V
ALIDATION
    if set_of_test_numbers_to_analyze == 3:
        first_test_number_to_analyze = 0
        first_test_number_to_validate = 0
        pick_every_other_test = 0

        for row_in_valid_tests_to_analyze in range(0,rows_in_valid_tests_to_analyze):
            if pick_every_other_test == 0:
                if first_test_number_to_analyze == 0:
                    test_numbers_to_analyze_array = tests_to_analyze.Test_Number.iloc[row_
in_valid_tests_to_analyze]
                    first_test_number_to_analyze = 1
                else:
                    test_numbers_to_analyze_array = numpy.append(test_numbers_to_analyze_a
rray,tests_to_analyze.Test_Number.iloc[row_in_valid_tests_to_analyze])
```

```
                pick_every_other_test = 1

            elif pick_every_other_test == 1:
                if first_test_number_to_validate == 0:
                    test_numbers_to_validate_array = tests_to_analyze.Test_Number.iloc[row
_in_valid_tests_to_analyze]
                    first_test_number_to_validate = 1
                else:
                    test_numbers_to_validate_array = numpy.append(test_numbers_to_validate
_array,tests_to_analyze.Test_Number.iloc[row_in_valid_tests_to_analyze])
                pick_every_other_test = 0

        #Create copy of valid tests - one will be pruned for training tests and the other
 for validation tests
        valid_tests_for_validation = tests_to_analyze

        first_nonincluded_test_for_training = 0
        first_nonincluded_test_for_validation = 0
        for row_in_valid_tests_to_analyze in range(0,rows_in_valid_tests_to_analyze):

            if valid_tests_to_analyze.Test_Number.iloc[row_in_valid_tests_to_analyze] not
in test_numbers_to_analyze_array:
                if first_nonincluded_test_for_training == 0:
                    nonincluded_tests_to_analyze = [row_in_valid_tests_to_analyze]
                    first_nonincluded_test_for_training = 1
                else:
                    nonincluded_tests_to_analyze = numpy.append(nonincluded_tests_to_analy
ze,[row_in_valid_tests_to_analyze])

            if valid_tests_for_validation.Test_Number.iloc[row_in_valid_tests_to_analyze]
not in test_numbers_to_validate_array:
                if first_nonincluded_test_for_validation == 0:
                    nonincluded_tests_for_validation = [row_in_valid_tests_to_analyze]
                    first_nonincluded_test_for_validation = 1
                else:
                    nonincluded_tests_for_validation = numpy.append(nonincluded_tests_for_
validation,[row_in_valid_tests_to_analyze])


        #Use one array for training and remove all the validation tests
        tests_to_analyze = tests_to_analyze.drop(nonincluded_tests_to_analyze)
        tests_to_analyze = tests_to_analyze.reset_index(drop = True)

        #Use the other array for validation and remove all the training tests as well as t
he flame spread rate data
        tests_for_validation = valid_tests_for_validation.drop(nonincluded_tests_for_valid
ation)
        tests_for_validation = tests_for_validation.reset_index(drop = True)

        return tests_to_analyze, tests_for_validation

    elif set_of_test_numbers_to_analyze == 1:
        tests_for_validation = []
        return tests_to_analyze

    elif set_of_test_numbers_to_analyze == 2:
        tests_for_validation = []
```

```
        return tests_to_analyze

##########################################################################################
##########################################################################################



##########################################################################################
##########################################################################################
#RUN COMBINATION OF ABOVE FUNCTIONS TO CREATE A DIMENSIONAL DATASET
##########################################################################################
##########################################################################################

def create_dimensonal_dataset(FLARE_data_sheet,set_of_tests_to_analyze,test_numbers_list):
    excel_data_as_dataframe = import_data_from_excel(FLARE_data_sheet)

    valid_data_for_analysis = remove_invalid_data_from_dataframe(excel_data_as_dataframe)
    list_of_tests_to_use = select_valid_data_for_training(valid_data_for_analysis,set_of_t
ests_to_analyze,test_numbers_list)

    valid_data_with_extra_columns = add_empty_columns_to_dataframe(valid_data_for_analysis
)

    if set_of_tests_to_analyze == 3:
        [dimensional_data_for_NN, validation_dimensional_data_for_NN] = finalize_dataset(v
alid_data_with_extra_columns,list_of_tests_to_use,set_of_tests_to_analyze)
        return dimensional_data_for_NN, validation_dimensional_data_for_NN
    else:
        dimensional_data_for_NN = finalize_dataset(valid_data_with_extra_columns,list_of_t
ests_to_use,set_of_tests_to_analyze)
        return dimensional_data_for_NN

##########################################################################################
##########################################################################################



##########################################################################################
##########################################################################################
#NORMALIZE DATA AND RETURN NORMALIZED DATA ARRAYS + CONSTANT USED TO NORMALIZE FSR
##########################################################################################
##########################################################################################

def calculate_normalizing_values(tests_to_analyze,normalizing_variable):

    #To get a normalizing value for the vectors, must first weed out zero-values and take
 absolute value of negative values
    rows_in_vector = tests_to_analyze.Forced_Flow_x_Velocity_m_per_s.size #just using this
vector - all should be the same shape
    first_xVel_value = 0
    first_yVel_value = 0
    first_zVel_value = 0
    first_xGrav_value = 0
    first_yGrav_value = 0
```

```
    for row_in_vector in range(0,rows_in_vector):

        if tests_to_analyze.Forced_Flow_x_Velocity_m_per_s.iloc[row_in_vector] < 0:
            if first_xVel_value == 0:
                x_Velocity_values = [(tests_to_analyze.Forced_Flow_x_Velocity_m_per_s.iloc
[row_in_vector]*-1)]
                first_xVel_value = 1
            else:
                x_Velocity_values = numpy.append(x_Velocity_values,[(tests_to_analyze.Forc
ed_Flow_x_Velocity_m_per_s.iloc[row_in_vector]*-1)])
        elif tests_to_analyze.Forced_Flow_x_Velocity_m_per_s.iloc[row_in_vector] > 0:
            if first_xVel_value == 0:
                x_Velocity_values = [tests_to_analyze.Forced_Flow_x_Velocity_m_per_s.iloc[
row_in_vector]]
                first_xVel_value = 1
            else:
                x_Velocity_values = numpy.append(x_Velocity_values,[tests_to_analyze.Force
d_Flow_x_Velocity_m_per_s.iloc[row_in_vector]])

        if tests_to_analyze.Forced_Flow_y_Velocity_m_per_s.iloc[row_in_vector] < 0:
            if first_yVel_value == 0:
                y_Velocity_values = [(tests_to_analyze.Forced_Flow_y_Velocity_m_per_s.iloc
[row_in_vector]*-1)]
                first_yVel_value = 1
            else:
                y_Velocity_values = numpy.append(y_Velocity_values,[(tests_to_analyze.Forc
ed_Flow_y_Velocity_m_per_s.iloc[row_in_vector]*-1)])
        elif tests_to_analyze.Forced_Flow_y_Velocity_m_per_s.iloc[row_in_vector] > 0:
            if first_yVel_value == 0:
                y_Velocity_values = [tests_to_analyze.Forced_Flow_y_Velocity_m_per_s.iloc[
row_in_vector]]
                first_yVel_value = 1
            else:
                y_Velocity_values = numpy.append(y_Velocity_values,[tests_to_analyze.Force
d_Flow_y_Velocity_m_per_s.iloc[row_in_vector]])

        if tests_to_analyze.Forced_Flow_z_Velocity_m_per_s.iloc[row_in_vector] < 0:
            if first_zVel_value == 0:
                z_Velocity_values = [(tests_to_analyze.Forced_Flow_z_Velocity_m_per_s.iloc
[row_in_vector]*-1)]
                first_zVel_value = 1
            else:
                z_Velocity_values = numpy.append(z_Velocity_values,[(tests_to_analyze.Forc
ed_Flow_z_Velocity_m_per_s.iloc[row_in_vector]*-1)])
        elif tests_to_analyze.Forced_Flow_z_Velocity_m_per_s.iloc[row_in_vector] > 0:
            if first_zVel_value == 0:
                z_Velocity_values = [tests_to_analyze.Forced_Flow_z_Velocity_m_per_s.iloc[
row_in_vector]]
                first_zVel_value = 1
            else:
                z_Velocity_values = numpy.append(z_Velocity_values,[tests_to_analyze.Force
d_Flow_z_Velocity_m_per_s.iloc[row_in_vector]])

        if tests_to_analyze.Gravity_x_Vector_gs.iloc[row_in_vector] < 0:
            if first_xGrav_value == 0:
                x_Gravity_values = [(tests_to_analyze.Gravity_x_Vector_gs.iloc[row_in_vect
or]*-1)]
```

```
                first_xGrav_value = 1
            else:
                x_Gravity_values = numpy.append(x_Gravity_values,[(tests_to_analyze.Gravit
y_x_Vector_gs.iloc[row_in_vector]*-1)])
        elif tests_to_analyze.Gravity_x_Vector_gs.iloc[row_in_vector] > 0:
            if first_xGrav_value == 0:
                x_Gravity_values = [tests_to_analyze.Gravity_x_Vector_gs.iloc[row_in_vecto
r]]
                first_xGrav_value = 1
            else:
                x_Gravity_values = numpy.append(x_Gravity_values,[tests_to_analyze.Gravity
_x_Vector_gs.iloc[row_in_vector]])

        if tests_to_analyze.Gravity_y_Vector_gs.iloc[row_in_vector] < 0:
            if first_yGrav_value == 0:
                y_Gravity_values = [(tests_to_analyze.Gravity_y_Vector_gs.iloc[row_in_vect
or]*-1)]
                first_yGrav_value = 1
            else:
                y_Gravity_values = numpy.append(y_Gravity_values,[(tests_to_analyze.Gravit
y_y_Vector_gs.iloc[row_in_vector]*-1)])
        elif tests_to_analyze.Gravity_y_Vector_gs.iloc[row_in_vector] > 0:
            if first_yGrav_value == 0:
                y_Gravity_values = [tests_to_analyze.Gravity_y_Vector_gs.iloc[row_in_vecto
r]]
                first_yGrav_value = 1
            else:
                y_Gravity_values = numpy.append(y_Gravity_values,[tests_to_analyze.Gravity
_y_Vector_gs.iloc[row_in_vector]])

    if normalizing_variable == "mean":
        print("Input parameters normalized by mean values.")

        #Determine the averages of the parameters of interest
        normalizing_value_core_density = tests_to_analyze.Core_Material_Density_kg_per_m3.
mean()
        normalizing_value_core_thermal_conductivity = tests_to_analyze.Core_Material_Therm
al_Conductivity_W_per_mK.mean()
        normalizing_value_core_specific_heat = tests_to_analyze.Core_Material_Specific_Hea
t_J_per_kgK.mean()

        normalizing_value_core_xsectional_area = tests_to_analyze.Core_XSectional_Area_m2.
mean()

        normalizing_value_insulation_density = tests_to_analyze.Insulation_Material_Densit
y_kg_per_m3.mean()
        normalizing_value_insulation_thermal_conductivity = tests_to_analyze.Insulation_Ma
terial_Thermal_Conductivity_W_per_mK.mean()
        normalizing_value_insulation_specific_heat = tests_to_analyze.Insulation_Material_
Specific_Heat_J_per_kgK.mean()

        normalizing_value_insulation_xsectional_area = tests_to_analyze.Insulation_XSectio
nal_Area_m2.mean()

        normalizing_value_oxygen_concentration = tests_to_analyze.Oxygen_Concentration_per
centage.mean()
        normalizing_value_pressure = tests_to_analyze.Average_Pressure_kPa.mean()
```

```
        normalizing_value_x_velocity = statistics.mean(x_Velocity_values)
        normalizing_value_y_velocity = statistics.mean(y_Velocity_values)
        normalizing_value_z_velocity = statistics.mean(z_Velocity_values)

        normalizing_value_x_gravity = statistics.mean(x_Gravity_values)
        normalizing_value_y_gravity = statistics.mean(y_Gravity_values)

        normalizing_value_flame_spread_rate = tests_to_analyze.Flame_Spread_Rate_mm_per_s.
mean()


    elif normalizing_variable == "median":
        print("Input parameters normalized by median values.")

        #Determine the medians of the parameters of interest
        normalizing_value_core_density = tests_to_analyze.Core_Material_Density_kg_per_m3.
median()
        normalizing_value_core_thermal_conductivity = tests_to_analyze.Core_Material_Therm
al_Conductivity_W_per_mK.median()
        normalizing_value_core_specific_heat = tests_to_analyze.Core_Material_Specific_Hea
t_J_per_kgK.median()

        normalizing_value_core_xsectional_area = tests_to_analyze.Core_XSectional_Area_m2.
median()

        normalizing_value_insulation_density = tests_to_analyze.Insulation_Material_Densit
y_kg_per_m3.median()
        normalizing_value_insulation_thermal_conductivity = tests_to_analyze.Insulation_Ma
terial_Thermal_Conductivity_W_per_mK.median()
        normalizing_value_insulation_specific_heat = tests_to_analyze.Insulation_Material_
Specific_Heat_J_per_kgK.median()

        normalizing_value_insulation_xsectional_area = tests_to_analyze.Insulation_XSectio
nal_Area_m2.median()

        normalizing_value_oxygen_concentration = tests_to_analyze.Oxygen_Concentration_per
centage.median()
        normalizing_value_pressure = tests_to_analyze.Average_Pressure_kPa.median()

        normalizing_value_x_velocity = statistics.median(x_Velocity_values)
        normalizing_value_y_velocity = statistics.median(y_Velocity_values)
        normalizing_value_z_velocity = statistics.median(z_Velocity_values)

        normalizing_value_x_gravity = statistics.median(x_Gravity_values)
        normalizing_value_y_gravity = statistics.median(y_Gravity_values)

        normalizing_value_flame_spread_rate = tests_to_analyze.Flame_Spread_Rate_mm_per_s.
median()

        normalizing_values = [normalizing_value_core_density,normalizing_value_core_therma
l_conductivity,normalizing_value_core_specific_heat,normalizing_value_core_xsectional_area
,normalizing_value_insulation_density,normalizing_value_insulation_thermal_conductivity,no
rmalizing_value_insulation_specific_heat,normalizing_value_insulation_xsectional_area,norm
alizing_value_oxygen_concentration,normalizing_value_pressure,normalizing_value_x_velocity
,normalizing_value_y_velocity,normalizing_value_z_velocity,normalizing_value_x_gravity,nor
malizing_value_y_gravity]
```

```
    return normalizing_values, normalizing_value_flame_spread_rate

#########################################################################################
#########################################################################################



#########################################################################################
#########################################################################################
#NORMALIZE DATA AND RETURN NORMALIZED DATA ARRAYS + CONSTANT USED TO NORMALIZE FSR
#########################################################################################
#########################################################################################

def normalize_dataset(tests_to_analyze,normalizing_values,normalizing_value_flame_spread_r
ate,parameters_of_interest):

    normalized_core_density = tests_to_analyze.Core_Material_Density_kg_per_m3/normalizing
_values[0]
    normalized_core_thermal_conductivity = tests_to_analyze.Core_Material_Thermal_Conducti
vity_W_per_mK/normalizing_values[1]
    normalized_core_specific_heat = tests_to_analyze.Core_Material_Specific_Heat_J_per_kgK
/normalizing_values[2]

    normalized_core_xsectional_area = tests_to_analyze.Core_XSectional_Area_m2/normalizing
_values[3]

    normalized_insulation_density = tests_to_analyze.Insulation_Material_Density_kg_per_m3
/normalizing_values[4]
    normalized_insulation_thermal_conductivity = tests_to_analyze.Insulation_Material_Ther
mal_Conductivity_W_per_mK/normalizing_values[5]
    normalized_insulation_specific_heat = tests_to_analyze.Insulation_Material_Specific_He
at_J_per_kgK/normalizing_values[6]

    normalized_insulation_xsectional_area = tests_to_analyze.Insulation_XSectional_Area_m2
/normalizing_values[7]

    normalized_oxygen_concentration = tests_to_analyze.Oxygen_Concentration_percentage/nor
malizing_values[8]
    normalized_pressure = tests_to_analyze.Average_Pressure_kPa/normalizing_values[9]

    normalized_x_velocity = tests_to_analyze.Forced_Flow_x_Velocity_m_per_s/normalizing_va
lues[10]
    normalized_y_velocity = tests_to_analyze.Forced_Flow_y_Velocity_m_per_s/normalizing_va
lues[11]
    normalized_z_velocity = tests_to_analyze.Forced_Flow_z_Velocity_m_per_s/normalizing_va
lues[12]

    normalized_x_gravity = tests_to_analyze.Gravity_x_Vector_gs/normalizing_values[13]
    normalized_y_gravity = tests_to_analyze.Gravity_y_Vector_gs/normalizing_values[14]

    normalized_flame_spread_rate = tests_to_analyze.Flame_Spread_Rate_mm_per_s/normalizing
_value_flame_spread_rate
    normalized_flame_spread_rate_array = numpy.array(tests_to_analyze.Flame_Spread_Rate_mm
_per_s/normalizing_value_flame_spread_rate).astype(numpy.float32)
```

```
    #CREATE AN ARRAY OF NORMALIZED PARAMETERS (FOR THE PARAMETERS OF INTEREST)
    normalized_input_data_not_yet_created = 1

    if "Core_Material_Density_kg_per_m3" in parameters_of_interest:
        if normalized_input_data_not_yet_created == 1: #if normalized_input_data doesn't e
xist yet
            normalized_input_data = normalized_core_density
            normalized_input_data_not_yet_created = 0
        else: #if normalized_input_data already exists
            normalized_input_data = pandas.concat([normalized_input_data,normalized_core_d
ensity],axis = 1)

    if "Core_Material_Thermal_Conductivity_W_per_mK" in parameters_of_interest:
        if normalized_input_data_not_yet_created == 1: #if normalized_input_data doesn't e
xist yet
            normalized_input_data = normalized_core_thermal_conductivity
            normalized_input_data_not_yet_created = 0
        else: #if normalized_input_data already exists
            normalized_input_data = pandas.concat([normalized_input_data,normalized_core_t
hermal_conductivity],axis = 1)

    if "Core_Material_Specific_Heat_J_per_kgK" in parameters_of_interest:
        if normalized_input_data_not_yet_created == 1: #if normalized_input_data doesn't e
xist yet
            normalized_input_data = normalized_core_specific_heat
            normalized_input_data_not_yet_created = 0
        else: #if normalized_input_data already exists
            normalized_input_data = pandas.concat([normalized_input_data,normalized_core_s
pecific_heat],axis = 1)

    if "Core_XSectional_Area_m2" in parameters_of_interest:
        if normalized_input_data_not_yet_created == 1: #if normalized_input_data doesn't e
xist yet
            normalized_input_data = normalized_core_xsectional_area
            normalized_input_data_not_yet_created = 0
        else: #if normalized_input_data already exists
            normalized_input_data = pandas.concat([normalized_input_data,normalized_core_x
sectional_area],axis = 1)

    if "Insulation_Material_Density_kg_per_m3" in parameters_of_interest:
        if normalized_input_data_not_yet_created == 1: #if normalized_input_data doesn't e
xist yet
            normalized_input_data = normalized_insulation_density
            normalized_input_data_not_yet_created = 0
        else: #if normalized_input_data already exists
            normalized_input_data = pandas.concat([normalized_input_data,normalized_insula
tion_density],axis = 1)

    if "Insulation_Material_Thermal_Conductivity_W_per_mK" in parameters_of_interest:
        if normalized_input_data_not_yet_created == 1: #if normalized_input_data doesn't e
xist yet
            normalized_input_data = normalized_insulation_thermal_conductivity
            normalized_input_data_not_yet_created = 0
        else: #if normalized_input_data already exists
            normalized_input_data = pandas.concat([normalized_input_data,normalized_insula
tion_thermal_conductivity],axis = 1)
```

```
    if "Insulation_Material_Specific_Heat_J_per_kgK" in parameters_of_interest:
        if normalized_input_data_not_yet_created == 1: #if normalized_input_data doesn't e
xist yet
            normalized_input_data = normalized_insulation_specific_heat
            normalized_input_data_not_yet_created = 0
        else: #if normalized_input_data already exists
            normalized_input_data = pandas.concat([normalized_input_data,normalized_insula
tion_specific_heat],axis = 1)

    if "Insulation_XSectional_Area_m2" in parameters_of_interest:
        if normalized_input_data_not_yet_created == 1: #if normalized_input_data doesn't e
xist yet
            normalized_input_data = normalized_insulation_xsectional_area
            normalized_input_data_not_yet_created = 0
        else: #if normalized_input_data already exists
            normalized_input_data = pandas.concat([normalized_input_data,normalized_insula
tion_xsectional_area],axis = 1)

    if "Oxygen_Concentration_percentage" in parameters_of_interest:
        if normalized_input_data_not_yet_created == 1: #if normalized_input_data doesn't e
xist yet
            normalized_input_data = normalized_oxygen_concentration
            normalized_input_data_not_yet_created = 0
        else: #if normalized_input_data already exists
            normalized_input_data = pandas.concat([normalized_input_data,normalized_oxygen
_concentration],axis = 1)

    if "Average_Pressure_kPa" in parameters_of_interest:
        if normalized_input_data_not_yet_created == 1: #if normalized_input_data doesn't e
xist yet
            normalized_input_data = normalized_pressure
            normalized_input_data_not_yet_created = 0
        else: #if normalized_input_data already exists
            normalized_input_data = pandas.concat([normalized_input_data,normalized_pressu
re],axis = 1)

    if "Forced_Flow_x_Velocity_m_per_s" in parameters_of_interest:
        if normalized_input_data_not_yet_created == 1: #if normalized_input_data doesn't e
xist yet
            normalized_input_data = normalized_x_velocity
            normalized_input_data_not_yet_created = 0
        else: #if normalized_input_data already exists
            normalized_input_data = pandas.concat([normalized_input_data,normalized_x_velo
city],axis = 1)

    if "Forced_Flow_y_Velocity_m_per_s" in parameters_of_interest:
        if normalized_input_data_not_yet_created == 1: #if normalized_input_data doesn't e
xist yet
            normalized_input_data = normalized_y_velocity
            normalized_input_data_not_yet_created = 0
        else: #if normalized_input_data already exists
            normalized_input_data = pandas.concat([normalized_input_data,normalized_y_velo
city],axis = 1)

    if "Forced_Flow_z_Velocity_m_per_s" in parameters_of_interest:
        if normalized_input_data_not_yet_created == 1: #if normalized_input_data doesn't e
```

```
xist yet
            normalized_input_data = normalized_z_velocity
            normalized_input_data_not_yet_created = 0
        else: #if normalized_input_data already exists
            normalized_input_data = pandas.concat([normalized_input_data,normalized_z_velo
city],axis = 1)

    if "Gravity_x_Vector_gs" in parameters_of_interest:
        if normalized_input_data_not_yet_created == 1: #if normalized_input_data doesn't e
xist yet
            normalized_input_data = normalized_x_gravity
            normalized_input_data_not_yet_created = 0
        else: #if normalized_input_data already exists
            normalized_input_data = pandas.concat([normalized_input_data,normalized_x_grav
ity],axis = 1)

    if "Gravity_y_Vector_gs" in parameters_of_interest:
        if normalized_input_data_not_yet_created == 1: #if normalized_input_data doesn't e
xist yet
            normalized_input_data = normalized_y_gravity
            normalized_input_data_not_yet_created = 0
        else: #if normalized_input_data already exists
            normalized_input_data = pandas.concat([normalized_input_data,normalized_y_grav
ity],axis = 1)

    normalized_input_data = numpy.array(normalized_input_data).astype(numpy.float32)

    return normalized_input_data, normalized_flame_spread_rate_array

#########################################################################################
#########################################################################################



#########################################################################################
#########################################################################################
#Create a results matrix comparing NN predicted FSR data vs measured FSR data
#########################################################################################
#########################################################################################

def create_NN_results_matrix(tests_to_analyze,predicted_flame_spread_rate):
    results = pandas.concat([tests_to_analyze.Test_Number],axis = 1)

    #Add the original experimental values to the results matrix
    results['Flame_Spread_Rate_mm_per_s'] = tests_to_analyze.Flame_Spread_Rate_mm_per_s

    #Add the predicted results from the neural network to the results matrix
    results['Predicted_FSR_mm_per_s'] = predicted_flame_spread_rate

    #Calculate the percent error between the measured and predicted values of flame spread
rate and add this to the results matrix
    percent_error = (abs(results.Flame_Spread_Rate_mm_per_s - results.Predicted_FSR_mm_per
_s)/results.Flame_Spread_Rate_mm_per_s)*100

    #Add the calculated percent error to the results matrix
    results['Percent_Predicted_FSR_Error'] = percent_error
```

```
    #Convert the results to an array
    results_array = numpy.array(results).astype(numpy.float32)

    return results, results_array

#############################################################################################
#############################################################################################
```

In [5]:

```
#CHOOSE PARAMETERS THAT I'M INTERESTED IN ANALYSING/USING FOR TRAINING THE NETWORK
#Current parameters that I'm interested in using to train the neural network to predict fl
ame spread
#Currently: commented out core/insulation surface area and igniter on length from the prev
ious list (dripping parameters commented out indefinitely)

parameters_of_interest = ["Test_Number"] #doesn't end up being used

parameters_of_interest += ["Core_Material_Density_kg_per_m3"]
parameters_of_interest += ["Core_Material_Thermal_Conductivity_W_per_mK"]
parameters_of_interest += ["Core_Material_Specific_Heat_J_per_kgK"]
#parameters_of_interest += ["Core_Volume_m3"]
#parameters_of_interest += ["Core_Surface_Area_m2"]
parameters_of_interest += ["Core_XSectional_Area_m2"]

parameters_of_interest += ["Insulation_Material_Density_kg_per_m3"]
parameters_of_interest += ["Insulation_Material_Thermal_Conductivity_W_per_mK"]
parameters_of_interest += ["Insulation_Material_Specific_Heat_J_per_kgK"]
#parameters_of_interest += ["Insulation_Volume_m3"]
#parameters_of_interest += ["Insulation_Surface_Area_m2"]
parameters_of_interest += ["Insulation_XSectional_Area_m2"]

parameters_of_interest += ["Oxygen_Concentration_percentage"]
parameters_of_interest += ["Average_Pressure_kPa"]
parameters_of_interest += ["Forced_Flow_x_Velocity_m_per_s"]
parameters_of_interest += ["Forced_Flow_y_Velocity_m_per_s"]
parameters_of_interest += ["Forced_Flow_z_Velocity_m_per_s"]

parameters_of_interest += ["Gravity_x_Vector_gs"]
parameters_of_interest += ["Gravity_y_Vector_gs"]
```

In [6]:

```
#GET MEDIAN TO USE FOR FUTURE NETWORK TRAINING/VALIDATION

#Location of data sheet - change this to wherever you save this file
#Selected "FLARE Master Data V4 (including external data)" to train the network using all
 the data
FLARE_data_sheet = r"D:\File_Path\Data_Sheet.xlsx"

#choose 2 for selecting all the tests in the selected excel file (use empty brackets inste
ad of a list of test numbers)
set_of_tests_to_analyze = 2
test_numbers_list = []
complete_dataset = create_dimensonal_dataset(FLARE_data_sheet,set_of_tests_to_analyze,test
_numbers_list) #returns dataframe


#CALCULATE CONSTANTS TO NORMALIZE INPUT AND FSR DATA
#Pick normalization type
#normalizing_variable = "mean"
normalizing_variable = "median"

[normalizing_input_constants,normalizing_FRS_constant] = calculate_normalizing_values(comp
lete_dataset,normalizing_variable)
```

```
Selecting all the tests.

Input parameters normalized by median values.
```

In [7]:

```
#GET NORMALIZED DATA TO TRAIN/VALIDATE THE NEURAL NETWORK

#choose 3 for selecting half of the tests for training and half for validation (use empty
 brackets instead of a list of test numbers)
set_of_tests_to_analyze = 3
test_numbers_list = []

#Have two outputs from create_dimensonal_dataset because will return training and validati
on data
[NN_training_dataset,NN_validation_dataset] = create_dimensonal_dataset(FLARE_data_sheet,s
et_of_tests_to_analyze,test_numbers_list) #returns dataframes

[normalized_input_training_data,normalized_flame_spread_rate_training_array] = normalize_d
ataset(NN_training_dataset,normalizing_input_constants,normalizing_FRS_constant,parameters
_of_interest)
```

```
Selecting half the tests for training (and the other half for validation).
```

In [8]:

```
#DEFINE THE NEURAL NETWORK MODEL

#As seen below, we have created three dense layers each with just one neuron.
#A dense layer is a layer in neural network that's fully connected.
#In other words, all the neurons in one layer are connected to all other neurons in the ne
xt layer.
#In the first layer, we need to provide the input shape, which is 3 in this case.
#The activation function we have chosen is ReLU, which stands for rectified linear unit.

#Currently using three layers with one neuron per layer and initial weights with values be
tween 0 and 1
initializer = tensorflow.keras.initializers.RandomUniform(minval=0.01, maxval=0.04)

#define three layer model with a number of neurons in each layer

input_shape_value = len(parameters_of_interest) - 1 #equal to the number of parameters of
 interest minus 1 because not including "Test Number"
input_layer_number_of_neurons = input_shape_value #this is a rule of thumb I've been going
by
layer2_number_of_neurons = input_shape_value - 3 #this is just an estimation of the rule o
f thumb I've been going by; can be adjusted
layer3_number_of_neurons = layer2_number_of_neurons
output_layer_number_of_neurons = 1 #only predicting one parameter: flame spread rate

#print("input layer #")
#print(input_layer_number_of_neurons)
#print("layer 2 #")
#print(layer2_number_of_neurons)
#print("layer 3 #")
#print(layer3_number_of_neurons)

model = keras.Sequential([
    keras.layers.Dense(input_layer_number_of_neurons, activation=kerasbackend.tanh, kernel
_initializer=initializer, input_shape=[input_shape_value]),
    keras.layers.Dense(layer2_number_of_neurons, activation=kerasbackend.tanh, kernel_init
ializer=initializer),
    keras.layers.Dense(layer3_number_of_neurons, activation=kerasbackend.tanh, kernel_init
ializer=initializer),
    keras.layers.Dense(output_layer_number_of_neurons, kernel_initializer=initializer)
  ])
```

In [9]:

```
#RUN THE NEURAL NETWORK

#RMSprop (Root Mean Square Propagation) is used as the optimizer. It's one of the most pop
ular gradient descent optimization algorithms
#for deep learning networks.
#Note: running model.fit successive times extends the calculation to addtional epochs.

sgd = tensorflow.keras.optimizers.RMSprop(0.00070) #input is the learning rate, usually ab
out 0.001
model.compile(loss='mean_absolute_error',optimizer='sgd')

#The fit method takes three parameters; namely, x, y, and number of epochs.
#During model training, if all the batches of data are seen by the model once,
#we say that one epoch has been completed.

model.fit(normalized_input_training_data,normalized_flame_spread_rate_training_array,epoch
s=5000)
```

```
Epoch 1/5000
18/18 [==============================] - 0s 781us/step - loss: 1.1776
Epoch 2/5000
18/18 [==============================] - 0s 664us/step - loss: 1.0473
Epoch 3/5000
18/18 [==============================] - 0s 605us/step - loss: 0.9799
Epoch 4/5000
18/18 [==============================] - 0s 610us/step - loss: 0.9426
Epoch 5/5000
18/18 [==============================] - 0s 555us/step - loss: 0.9217

                                    .

                                    .

                                    .

Epoch 4995/5000
18/18 [==============================] - 0s 609us/step - loss: 0.0940
Epoch 4996/5000
18/18 [==============================] - 0s 665us/step - loss: 0.0919
Epoch 4997/5000
18/18 [==============================] - 0s 609us/step - loss: 0.0952
Epoch 4998/5000
18/18 [==============================] - 0s 610us/step - loss: 0.0874
Epoch 4999/5000
18/18 [==============================] - 0s 665us/step - loss: 0.0979
Epoch 5000/5000
18/18 [==============================] - 0s 610us/step - loss: 0.1056
```

Out[9]:

```
<tensorflow.python.keras.callbacks.History at 0x199243c60a0>
```

In [13]:

```
#OBTAIN RESULTS FROM TRAINING THE NEURAL NETWORK AND FROM VALIDATION DATA SET

#Obtain results from neural network
predicted_flame_spread_rate = model.predict(normalized_input_training_data)*normalizing_FR
S_constant

#Obtain results from neural network
[normalized_input_validation_data,_] = normalize_dataset(NN_validation_dataset,normalizing
_input_constants,normalizing_FRS_constant,parameters_of_interest)
validation_predicted_flame_spread_rate = model.predict(normalized_input_validation_data)*n
ormalizing_FRS_constant
```